



Ejector-boosted Transcritical CO₂ Refrigeration System

Dissertation Thesis

Study programme: P2301 Mechanical Engineering
Study branch: Applied Mechanics

Author: **M.Eng. Anas F. A. Elbarghthi**
Thesis Supervisor: prof. Ing. Václav Dvořák, Ph.D.
Department of Engineering Mechanics



Declaration

I hereby certify, I, myself, have written my dissertation as an original and primary work using the literature listed below and consulting it with my thesis supervisor and my thesis counsellor.

I acknowledge that my dissertation is fully governed by Act No. 121/2000 Coll., the Copyright Act, in particular Article 60 – School Work.

I acknowledge that the Technical University of Liberec does not infringe my copyrights by using my dissertation for internal purposes of the Technical University of Liberec.

I am aware of my obligation to inform the Technical University of Liberec on having used or granted license to use the results of my dissertation; in such a case the Technical University of Liberec may require reimbursement of the costs incurred for creating the result up to their actual amount.

At the same time, I honestly declare that the text of the printed version of my dissertation is identical with the text of the electronic version uploaded into the IS/STAG.

I acknowledge that the Technical University of Liberec will make my dissertation public in accordance with paragraph 47b of Act No. 111/1998 Coll., on Higher Education Institutions and on Amendment to Other Acts (the Higher Education Act), as amended.

I am aware of the consequences which may under the Higher Education Act result from a breach of this declaration.

October 26, 2021

M.Eng. Anas F. A. Elbarghthi

ABSTRACT

Recently, the field of refrigeration and air conditioning has come under immense scrutiny as a result of their indirect contribution to global warming and climate change. This is due to the imminent danger posed on the globe by greenhouse gas emissions. This field is continually increasing, experiencing high-grade energy consumption, and calls for the developing of innovative alternative technologies for saving energy. The use of ejector allows overcoming the significant exergy destruction lays on the expansion processes of the cooling systems and led to spark improvement in the system performance by recovering some of the expansion work.

The thesis focused on two things: investigate detailed experimental work on the ejector supplied R744 transcritical cooling system and the impact of the ejector profile on the system performance. The experiment was implemented on the commercial ejector cartridge type (032F7045 CTM ELP60 by Danfoss). The effect of different operating conditions determined by exit gas cooler pressure and temperature, evaporation temperature, and liquid separator pressure was examined. The ejector performance of the pressure lift, mass entrainment ratio, work rate recovery and efficiency were evaluated. In addition, exergy efficiency and the variation of exergy produced, consumed, and destructed related to the ejector profile were assessed based on the transiting exergy. The result revealed better overall performance when the ejector operated at transcritical conditions. The ejector was able to recover up to 36.9% of the available work rate and provided a maximum pressure lift of 9.51 bar.

Moreover, it was found out that the overall available work recovery potential increased by raising the gas cooler pressure. Out of the findings, the ejector could deliver maximum exergy efficiency of 23% when working at higher motive nozzle flow temperatures along with providing lower exergy destruction. The experiment results show that the amount of the ejector exergy consumed and destructed were gradually increased with higher gas cooler pressure and, in contrast, decreasing with higher motive nozzle flow temperature. The ejector-supported system was theoretically compared with the parallel compression concept

as the baseline system and carried out at different pressure lifts and exit gas cooler properties. The result indicated a COP and exergy efficiency improvement up to 2.05% and 1.92% for the set conditions, respectively, while the COP could be improved to a maximum of 11.22% when the system cooling load is minimized.

Additionally, the ejector played a vital role in the system input power. Up to 3.46% of the energy consumption was reduced at subcritical heat rejection conditions. Operating the system with an ejector at a lower cooling capacity allows further overall power consumption reduction to 18%. In addition, the exergy analysis revealed a prominent lack of total system exergy destruction by employing the ejector in parallel with the high-pressure valve, which recovered 21% of the expansion work and saved 46% of the HPV exergy losses. Furthermore, the result exhibited a maximum system exergy loss of 7.8% that could be saved at the set condition and a maximum of 13.2% total system exergy destruction rate recovered by the ejector depending on the cooling load.

Keywords: Natural fluid, CO₂, Ejector, Transcritical system, Pressure lift, Efficiency, Work recovery, COP, Exergy destruction, Power consumption.

PREFACE

Through my years of studying, I became fascinated by the research field. My enthusiasm and passion for technology represented the driving force and source of my excitement. Being a student at the Technical University of Liberec has taught me that there is no limit to challenges, and I should keep the creative thinking leading me. Thanks to this prestigious institution of learning. I had wanted to get an international education experience. Fortunately, destiny brought me to the Czech Republic, where I was captivated by the serenity, multicultural nature, and the caliber of erudite professors that are not only authorities in their respective fields but equally versatile in the areas of cordiality, kindness and more importantly, their untiring spirit with which they imparted knowledge to me.

It is really hard to eloquently express my gratitude and appreciation to my supervisor Professor Václav Dvořák for his patience, motivation, enthusiasm, and immense knowledge. His expertise and understanding added considerably to my graduate experience. I thank him for the systematic guidance and great effort he put into my study since the day I started my doctoral study. The thesis was completed through his guidance and tremendous assistance. My sincere gratitude is extended to the Faculty of Mechanical Engineering/Department of Mechanics, Elasticity, and Strength (KMP), especially the head of the department doc. Ing. Iva Petříková Ph.D. and all the staff members as well as the international Office, Mrs. Marcela Valkova, and the study office Mgr. Radka Dvořáková and Ing. Dana Semotjuková for their help during my study process. Most importantly, my greatest pleasure is cordially extended to my parents upon whose shoulders I stand and my siblings who paved the path before me for their tremendous contribution and support towards completing my dissertation.

I am profoundly grateful to Prof. Armin Hafner, Krzysztof Banasiak, and all Department of Energy and Process Engineering members at the Norwegian University of Science and Technology (NTNU), who facilitated my internship and permitted me to use their test rig to conduct the experiments. I would also like to acknowledge the financial support I gained throughout the Student Grant Competition project No. SGS-2021-5063 of TUL. A huge thanks to my friends and university colleagues for their unconditional support and encouragement. This is also dedicated to my colleagues in Arabian Gulf Oil Company for unlimited support and valuable contributions towards the successful completion of my study. A lot of names to mention, but you are all deeply appreciated.

I am committed to reaching my goal and hope to excel in all parts of life; then, as a researcher, I wish to apply my knowledge in such a way that provides the greatest benefit to my field and the wider public.

Table of contents

ABSTRACT	3
PREFACE	5
1 INTRODUCTION.....	14
1.1 CONTEXTUALIZATION OF THE THESIS	14
1.2 MAIN OBJECTIVES OF THE THESIS	15
1.3 MOTIVATIONS FOR THE PROPOSED RESEARCH WORK.....	15
1.4 STRUCTURE OF THE THESIS.....	16
2 LITERATURE REVIEW.....	17
2.1 BRIEF HISTORICAL BACKGROUND.....	17
2.2 OVERVIEW OF COMMERCIAL CO ₂ SYSTEMS.....	19
2.3 R744 TWO-PHASE EJECTOR TECHNOLOGY	22
2.3.1 <i>Ejector control strategy</i>	22
2.3.2 <i>Description of the multi-ejector pack</i>	24
2.4 CO ₂ AS A REFRIGERANT.....	26
2.5 EJECTOR-SUPPORT R744 TRANSCRITICAL REFRIGERATION SYSTEM.....	29
2.6 SUMMARY	38
3 THEORY AND DATA ANALYSIS	39
3.1 EJECTOR THEORY AND WORKING PRINCIPLE.....	39
3.2 EJECTOR VAPOR COMPRESSION CYCLE	40
3.3 EJECTOR PERFORMANCE CHARACTERISTICS	41
3.4 ENERGY AND EXERGY ANALYSIS.....	44
4 EXPERIMENTAL METHOD.....	49
4.1 TEST FACILITY SET-UP.....	49
4.2 SYSTEM COMPONENTS DESCRIPTION	51
4.2.1 <i>The compressors rack</i>	51
4.2.2 <i>The ejector profile</i>	54
4.2.3 <i>Heat exchangers</i>	55
4.2.4 <i>Valves and tanks</i>	55
4.2.5 <i>Data acquisition and monitoring system</i>	56
4.3 UNCERTAINTY ANALYSIS	57
5 RESULTS AND DISCUSSION	59

5.1 EFFECT OF THE OPERATION CONDITIONS	61
5.2 EJECTOR EFFICIENCY INVESTIGATIONS	66
5.3 EJECTOR EXERGY ANALYSIS	70
5.4 SYSTEM PERFORMANCE CALCULATIONS	74
5.4.1 <i>Ejector characteristic functions</i>	75
5.4.2 <i>Test of the ejector performance</i>	78
5.4.3 <i>Ejector system performance improvement</i>	80
5.4.4 <i>System exergy analysis</i>	88
6 CONCLUSIONS AND FUTURE WORK	93
6.1 CONCLUSIONS	93
6.2 ASSESSMENT OF OBJECTIVES	95
6.3 FUTURE WORKS	95
BIBLIOGRAPHY	97
COURSEWORK AND EXAMINATIONS	105
LIST OF PUBLICATIONS.....	106
AUTHOR CURRICULUM VITAE	107
APPENDIX 1 PID FOR R744 TEST RIG	108

LIST OF TABLES

TABLE 2.1 ODP AND GWP COMPARISON OF DIFFERENT REFRIGERANTS.	27
TABLE 2.2 CHARACTERISTICS AND PROPERTIES OF CO ₂ AND OTHER REFRIGERANTS	29
TABLE 4.1 DORIN COMPRESSORS POLYNOMIAL COEFFICIENTS.	52
TABLE 4.2 EJECTOR CARTRIDGE CTM ELP 60 MAIN GEOMETRY PARAMETERS.	54
TABLE 4.3 THE SET OF THE INSTRUMENTATIONS USED FOR EXPERIMENTAL INVESTIGATION	57
TABLE 4.4 THE UNCERTAINTY VALUES FOR THE MAIN COLLECTED DATA AND DERIVED FUNCTIONS.	58
TABLE 5.1 EXERGY METRICS OF THE EXPERIMENT FOR DIFFERENT EVAPORATION TEMPERATURES AND LIQUID SEPARATOR PRESSURE.	73
TABLE 5.2 COEFFICIENT VALUES IN EQUATION (5-4) FOR THE EJECTOR PROFILE.	78

LIST OF FIGURES

FIGURE 2.1 TWO-PHASE EJECTOR PATENT BY GAY	18
FIGURE 2.2 PRINCIPLES OF GENERATIONS OF CO ₂ CIRCUIT ARCHITECTURE OF THE BOOSTER REFRIGERATION SYSTEM	19
FIGURE 2.3 ANNUAL ENERGY CONSUMPTION OF THREE DIFFERENT GENERATIONS R744 SUPERMARKET REFRIGERATION SYSTEM COMPARED WITH R404A DIRECT EXPANSION UNIT IN THE EUROPEAN CLIMATE CONTEXT	22
FIGURE 2.4 TWO-PHASE EJECTOR MODULAR PROTOTYPE WITH AN INTEGRATED NEEDLE MECHANISM PROPOSED BY ELBEL ET AL. ON THE LEFT SIDE [32] AND LIU ET AL. ON THE RIGHT SIDE	23
FIGURE 2.5 THE ELECTRONIC EJECTOR MODULE BY CAREL INDUSTRIES	23
FIGURE 2.6 THE MULTI-EJECTOR BLOCK FROM DANFOSS	24
FIGURE 2.7 SKETCH OF THE MULTI-EJECTOR BLOCK	25
FIGURE 2.8 CO ₂ PHASE DIAGRAM	28
FIGURE 2.9 CO ₂ P-H DIAGRAMS TO REPRESENT (A) SUBCRITICAL CYCLE AND (B) TRANSCRITICAL CYCLE FROM	28
FIGURE 2.10 VAPOR-COMPRESSSION CYCLE WITH ISENTHALPIC EXPANSION SHOWN ON TEMPERATURE VS. SPECIFIC ENTROPY DIAGRAM FOR R744 (CO ₂), R410A AND R134A (HFCs). THE THROTTLING LOSSES OF EACH REFRIGERANT ARE VISUALIZED AS VERTICAL BARS ON THE SPECIFIC ENTROPY AXIS	30
FIGURE 2.11 COMMON USED R744 EJECTOR CYCLE	32
FIGURE 2.12 SCHEMATICS OF THE MULTI-EJECTOR R744 CIRCUIT TEST FACILITY FOR BANASIAK ET AL.....	34
FIGURE 2.13 COMPARISON IN TERMS OF COP AMONG THE INVESTIGATED SOLUTIONS	36
FIGURE 2.14 INNOVATIVE SOLUTIONS FOR INTEGRATING THE AC PRODUCTION WITH CONVENTIONAL EVAPORATION AND EJECTOR-SUPPORTED EVAPORATION	37
FIGURE 3.1 THE PRESSURE PROFILE ALONG THE EJECTOR AXIS ADAPTED FROM DANFOSS ..	39
FIGURE 3.2 SCHEMATIC OF A SIMPLE R744 VAPOR-COMPRESSSION SYSTEM EQUIPPED WITH A TWO-PHASE EJECTOR (LEFT-HAND SIDE) AND ITS P-H DIAGRAM (RIGHT-HAND SIDE) ...	41
FIGURE 3.3 EXPANSION AND COMPRESSION OF THE MOTIVE AND SUCTION NOZZLE FLOW INSIDE A TWO-PHASE EJECTOR. ADAPTED FROM ELBEL AND HRNJAK.	43
FIGURE 4.1 THE TEST RIG EQUIPPED WITH A MULTI-EJECTOR PACK.	50

FIGURE 4.2 R744 PISTON-TYPE COMPRESSORS PACK. BASE-LOAD COMPRESSOR (DORIN CD1400H) AT THE LEFT AND PARALLEL COMPRESSORS (DORIN CD1000H AND DORIN CD380H) AT THE RIGHT.....	52
FIGURE 4.3 THE SIMPLIFIED PROCESS AND INSTRUMENTATION DIAGRAM OF THE EXPERIMENTAL TEST FACILITY, INCLUDING THE R744 REFRIGERANT AND THE GLYCOL LOOP.....	53
FIGURE 4.4 SKETCH OF THE MULTI-EJECTOR BLOCK AND THE USED CARTRIDGE FROM DANFOSS (FOR INTERNAL USE ONLY)	54
FIGURE 5.1 R744 EJECTOR OVERALL CONDUCTED EXPERIMENTS, (A) P-H DIAGRAM REPRESENTING MN FLOW INLET CONDITIONS, (B) P-H DIAGRAM REPRESENTING SN FLOW INLET CONDITIONS, (C) P-H DIAGRAM REPRESENTING THE OUTLET MIXED FLOW TO THE LIQUID SEPARATOR, (D) THE CALCULATED COEFFICIENT OF LIQUID MASS BALANCE FOR DIFFERENT LIQUID SEPARATOR PRESSURE.....	60
FIGURE 5.2 PRESSURE LIFT AS A FUNCTION OF MOTIVE NOZZLE INLET PRESSURE.....	61
FIGURE 5.3 VARIATION OF EJECTOR EFFICIENCY WITH PRESSURE LIFT AT DIFFERENT MOTIVE NOZZLE PRESSURE.	62
FIGURE 5.4 VARIATION OF EJECTOR MASS ENTRAINMENT RATIO WITH LIQUID SEPARATOR PRESSURE (RECEIVER PRESSURE) AND PRESSURE LIFT AS A FUNCTION OF MOTIVE FLOW CONDITIONS.....	65
FIGURE 5.5 POTENTIAL WORK RECOVERY RATE VS. LIQUID SEPARATOR PRESSURE AT $T_{MN} = 20$ °C, $T_{EVAP} = -6$ °C.....	68
FIGURE 5.6 EXPERIMENTAL EJECTOR EFFICIENCY FOR DIFFERENT MOTIVE NOZZLE FLOW PRESSURE AT $T_{MN} = 20$ °C AND $T_{EVAP} = -6$ °C.....	68
FIGURE 5.7 COOLING COP, H_{EJE} , P_{LIFT} , \dot{W}_{RECV} , AND ER VS. DIFFERENT P_{MN} AT $P_{REC} = 34.6$ BAR, $T_{MN} = 20$ °C AND $T_{EVAP} = -6$ °C.	69
FIGURE 5.8 COOLING COP, H_{EJE} , P_{LIFT} , \dot{W}_{RECV} , AND ER VS. DIFFERENT P_{REC} AT $P_{MN} = 90$ BAR, $T_{MN} = 20$ °C AND $T_{EVAP} = -6$ °C.	70
FIGURE 5.9 EJECTOR EXERGY EFFICIENCY AND EXERGY DESTRUCTION VS. LIQUID SEPARATOR PRESSURE P_{REC} , (A) AT DIFFERENT MOTIVE PRESSURE, (B) AT DIFFERENT MOTIVE TEMPERATURES.	71
FIGURE 5.10 EJECTOR EXERGY METRICS AT DIFFERENT MOTIVE NOZZLE FLOW TEMPERATURES AND PRESSURE AT $T_{EVAP} = -6$ °C, (A) $P_{REC} \approx 35.4$ BAR AND $P_{MN} = 34.5$ BAR, (B) $P_{REC} \approx 34.6$ BAR AND $T_{MN} = 20$ °C.....	72
FIGURE 5.11 P-H DIAGRAM OF THE CONVENTIONAL PARALLEL R744 TRANSCRITICAL REFRIGERATION CYCLES AND THE EJECTOR SUPPORT CYCLE.	75
FIGURE 5.12 THE RELATIVE ERROR BETWEEN MEASURED (HORIZONTAL AXIS) AND THE PREDICTED RESULT (VERTICAL AXIS) FOR MOTIVE NOZZLE MASS FLOW RATE (TOP),	

SUCTION NOZZLE MASS FLOW RATE (MIDDLE), AND MASS ENTRAINMENT RATIO (BOTTOM).....	77
FIGURE 5.13 CALCULATION OF THE EJECTOR PROFILE CHARACTERISTICS DEPENDING ON THE PRESSURE LEFT AND THE INLET MOTIVE NOZZLE TEMPERATURE.....	79
FIGURE 5.14 SYSTEM COP CHARACTERISTICS VS. PRESSURE LIFT FOR THE PARALLEL SYSTEM LAYOUT AND EJECTOR SUPPORTED SYSTEM AT DIFFERENT GAS COOLER OUTLET TEMPERATURES.	81
FIGURE 5.15 SYSTEM COP CHARACTERISTICS VS. PRESSURE LIFT FOR THE PARALLEL SYSTEM LAYOUT AND EJECTOR SUPPORTED SYSTEM AT DIFFERENT GAS COOLER PRESSURE LEVELS.	82
FIGURE 5.16 SYSTEM EXERGY EFFICIENCY CHARACTERISTICS VS. PRESSURE LIFT FOR THE PARALLEL SYSTEM AND (VEJ_1) EJECTOR SYSTEM LAYOUT AT DIFFERENT GAS COOLER OUTLET TEMPERATURES.	84
FIGURE 5.17 THE IMPACT OF THE EJECTOR PROFILE ON THE COMPRESSOR POWER-SAVING AS A FUNCTION OF THE DIFFERENT PRESSURE LIFT AND EXIT GAS COOLER TEMPERATURES.	85
FIGURE 5.18 TOTAL POWER CONSUMPTION OF THE COMPRESSORS AS A FUNCTION OF THE DIFFERENT EXIT GAS COOLER PRESSURE AND TEMPERATURE WITH AND WITHOUT EJECTOR SUPPORTED SYSTEM.	86
FIGURE 5.19 CONTRIBUTION OF THE EJECTOR ON THE SYSTEM COP IMPROVEMENT AND COMPRESSOR POWER REDUCTION VERSUS DIFFERENT SYSTEM COOLING CAPACITIES. .	87
FIGURE 5.20 EXERGY DESTRUCTION OF THE TOTAL SYSTEM AND EACH COMPONENT FOR BOTH PARALLEL AND EJECTOR SUPPORTED SYSTEMS AT DIFFERENT EXIT GAS COOLER TEMPERATURES AND PRESSURE LIFT OF 5 BAR.....	88
FIGURE 5.21 BREAKDOWN OF THE EXERGY DESTRUCTION RATE OF EACH SYSTEM COMPONENT CONTRIBUTION AT $T_{GC,OUT} = 20\text{ }^{\circ}\text{C}$, $P_{LIFT} = 5\text{ BAR}$ AND 90 BAR GAS COOLER PRESSURE (A) WITHOUT EJECTOR. (B) WITH EJECTOR.	90
FIGURE 5.22 TOTAL EXERGY DESTRUCTION RATE OF THE BASELINE PARALLEL SYSTEM AND EJECTOR SUPPORTED SYSTEM VIA DIFFERENT COOLING CAPACITIES AT TWO DIFFERENT EXIT GAS COOLER TEMPERATURES.....	91

LIST OF ABBREVIATIONS AND ACRONYMS

List of abbreviations

<i>Abbreviation</i>	Description
<i>COP</i>	Coefficient of performance
<i>FGV</i>	Flash gas valve
<i>HFC</i>	Hydrofluorocarbon
<i>HFOs</i>	Hydrofluoroolefins
<i>HP</i>	High pressure
<i>HPV</i>	High pressure valve
<i>LEJ</i>	Liquid ejector
<i>LP</i>	Low pressure
<i>MFM</i>	Mass flow meter
<i>VEJ</i>	Vapour ejector

List of variables

<i>Variable</i>	Description
<i>A</i>	Area (m ²)
\dot{D}	Exergy destruction rate (kW)
<i>e</i>	Specific exergy (kJ/kg)
\dot{E}	Exergy rate (kW)
<i>ER</i>	Mass Entrainment Ratio (-)
<i>h</i>	Specific enthalpy (kJ/kg)
\dot{m}	Mass flow rate (kg/s)
<i>P</i>	Pressure (bar)
<i>s</i>	Specific entropy (kJ/kg.K)
<i>T</i>	Temperature (°C)
\dot{W}	Work rate (kW)
<i>x</i>	Mass fraction (-)

Greek letters

<i>Variable</i>	Description
β	Coefficient of liquid mass balance
∇	Consumed
Δ	Produced
η	Efficiency
ρ	Density (kg/m ³)

List of subscripts

<i>Subscript</i>	Description
<i>comp</i>	Compressor
<i>cr</i>	Critical
<i>ej</i>	Ejector
<i>evap</i>	Evaporator
<i>ex</i>	Exergy
<i>GC</i>	Gas cooler
<i>in</i>	Inlet of component
<i>incr</i>	Increment
<i>MN</i>	Motive nozzle
<i>o</i>	Dead state
<i>out</i>	Outlet of component
<i>rec</i>	Liquid separator
<i>recv</i>	Recovery
<i>SN</i>	Suction nozzle
<i>tr</i>	Transiting

1 INTRODUCTION

1.1 Contextualization of the thesis

Refrigeration is identified as an indispensable method that is widely used in many applications, including food storage, providing thermal comfort, and in the health care industry. The conventional vapor-compression refrigeration systems are mainly driven by electricity and are usually characterized by high energy consumption [1]. R744 Transcritical refrigeration systems have proven to be very energy efficient, reliable, and more attractive, especially as the world becomes more energy conscious. Therefore, the use of an ejector allows overcoming the significant exergy destruction that lies in the expansion processes of the cooling systems. It also led to spark improvement in the system performance by recovering some of the expansion work in the transcritical CO₂ system [2]. The ejector comes with advantages such as simple mode of function, lack of moving parts in construction, low cost, long lifespan.

Owing to the increasing levels of parameters influencing global warming, high GWP refrigerants have been replaced by eco-friendly and neutral impact alternatives such as the natural working fluid CO₂ (denoted as R744) [3, 4]. The properties of CO₂ have made the transcritical refrigeration systems to be cost-effective and efficient. This is based on the thermophysical advantages that CO₂ offers, such as high thermal conductivity, high vapor density, and low viscosity. These advantages allow smaller dimensions of pipelines and valves to be produced with 3 – 10 times the refrigeration capacity of CFC, HCFC, and HFC refrigerants with a remarkable reduction in investment costs [5]. Furthermore, CO₂ has an A1 safety classification based on ASHRAE. It is also an odourless and colourless gas with a slightly pungent taste of acid as well as being non-flammable and non-toxic [6]. Based on the exceptional characteristics of CO₂ as a refrigerant, it is currently being used in the development of refrigeration and heat pumps, such as booster systems for commercial applications.

The market is witnessing an increase in commercial CO₂ refrigeration systems worldwide. In the recent years, the performance of R744 transcritical booster systems has been improved by introducing the multi-ejector block with parallel compression. The performance of the transcritical CO₂ systems has been shown to be greatly influenced by the ejector efficiency and the achieved pressure lift. On the other hand, the advantages of using the ejector have resulted in many research works for its significant energy reduction. The investigations

have been classified based on the impact of the working fluid properties, the ejector geometries, and the refrigeration system purposes (cooling, freezing, or air conditions). As a result of this, further improvements are necessary, possible, and desired.

1.2 Main objectives of the thesis

The research aims to study the usage of the small-size ejector in refrigeration systems utilizing CO₂ as the natural fluid and environmentally friendly refrigerant. The principal research objectives will be as following:

1. Accomplish a literature review on the CO₂ refrigeration system and ejector technology.
2. Conduct a comprehensive test campaign to investigate the effect of different operation conditions on the ejector profile performance experimentally.
3. Investigate the exergy distributions in the ejector profile and their effect on the rate of work recovery.
4. Assess the potential impact of the equipped expansion ejector profile on the R744 vapor compression system operational characteristics (COP and exergy efficiency improvement, power consumption).
5. Determine the contribution of the ejector to improve the exergy destruction of the total system and each component based on the second law of thermodynamics.

1.3 Motivations for the proposed research work

Fortunately, the industry is now facing a devoted development of utilizing cleaner technologies to replace all the harmful fluids used as refrigerants with more eco-friendly alternatives like natural refrigerants. For instance, the Coca-Cola Company has decided to phase out HFCs by adapting to CO₂ technology as the leading solution [7]. In the beginning, when CO₂ was first introduced as a working fluid, the scientific community met plenty of skepticism within the investigated application [8]. The reason lies in the high pressure levels, low theoretical cycle efficiency, and the need to develop new system components that introduce technological challenges. Recently, these objections have been conquered through better system design which led to boost the main advantages of using CO₂ cooling systems and allow the transition to energy-efficient solutions. As a result, both the input energy needs and greenhouse gas emissions will be reduced. Based on the preceding research, the ejector could improve the

supercritical R744 refrigeration system performance by recovering the expansion work losses and reduce the exergy reduction rate. Therefore, the motivation of this work is to investigate and evaluate the individual use of ejector profile performance and further illuminate the impact of various operation conditions experimentally on the advanced test facility. In addition, promote the influence of the ejector profile as relatively representing the smallest cartridge geometry manufactured by Danfoss using the gathered knowledge throughout this field.

1.4 Structure of the thesis

This thesis comprises six chapters and one appendix. This section summarizes the structure and the content of each chapter to serve as a road map. The up-to-date and the previous research study on R744 transcritical system technology were given in Chapter 2. It provides the development of the transcritical system and the essential research area and gaps related to the ejector, supporting the thesis objectives. After that, the method and the data analysis used in the study evaluation are described in Chapter 3. In addition, the ejector working principle, characteristics, and integration into the transcritical CO₂ system are illustrated. In chapter four, the test rig facility and the experimental methodology are defined. This includes the ejector geometry and setting of the test boundary conditions. The main component of the system, process and installation diagram, and instruments used together with the uncertainty analysis are reported. The result and discussion are provided in Chapter 5. The main findings are classified based on the ejector performance map through a sensitive analysis of different variables and the impact of this ejector profile on the system performance and energy consumption. The last chapter sums up the presented research with the most critical conclusion, including the assessment of the thesis objectives and some suggestions for future work. The thesis finishes with one appendix revealed the P&ID of the tested system.

2 LITERATURE REVIEW

This section will summarize the current and the previous research study on R744 transcritical system technology. The purpose is to provide the reader with an update of the essential research area and function as a reference to the discussion and conclusion for the fundamental refrigeration cycle with expansion ejector supported. The chapter includes why CO₂ is classified as a suitable refrigerant and the most pertinent research related to this thesis.

Today, there is still a need for an approach adopted by the scientific community regarding the most efficient ejector for refrigeration applications. Nonetheless, the novel processes and methods developed in the last five years seem to be more addressed to the design of low impact, energy safe, and eco-friendly systems. The International Energy Agency observed in 2018 that the demand for air-conditioners worldwide is predicted to soar, resulting in an increase in the number of air-conditioners from 1.6 billion units today to 5.6 billion units by mid-century [9]. Therefore, there is a growing concern that the amount of electricity needed to power them will overload the electrical grids. Even though the need to reduce the cost associated with the high energy consumption of conventional refrigerators has resulted in many developments in refrigeration systems such as more energy-efficient compressors, there is a limit to which this can be achieved. In addition, there is an increase in global-warming emissions caused by refrigeration systems relying on fossil fuels and the use of harmful substances such as chlorofluorocarbons (CFCs) as refrigerants. In fact, the emissions from these systems also contribute to global warming, which is most likely to increase the demand for air-conditioning, especially for thermal comfort.

2.1 Brief historical background

Henry Giffard has first invented ejector technology in condensing applications, where it solved the problem of replenishing the reservoir by feeding the water into the steam engine boilers in 1858 [10]. Ever since the ejector occupied many applications intensively. In 1901 the ejector was used by Parsons as the pumping device due to the ability to remove the existing vapor portion from the steam condensers [11]. Then the ejector was presented in the first steam jet refrigeration cycle by Maurice Leblanc in 1910. Consequently, the ejector cycle was

invented by Gay in 1931 to be derived in commercial refrigeration systems, as represented in Figure 2.1 [12]. Gay's patent introduced the two-phase ejector as a solution to increase the system efficiency and reduce the inherent throttling losses in the expansion process. CO₂ is not specified in the patent as a refrigerant, but it contributes to the recovery of the transcritical system losses at later stages.

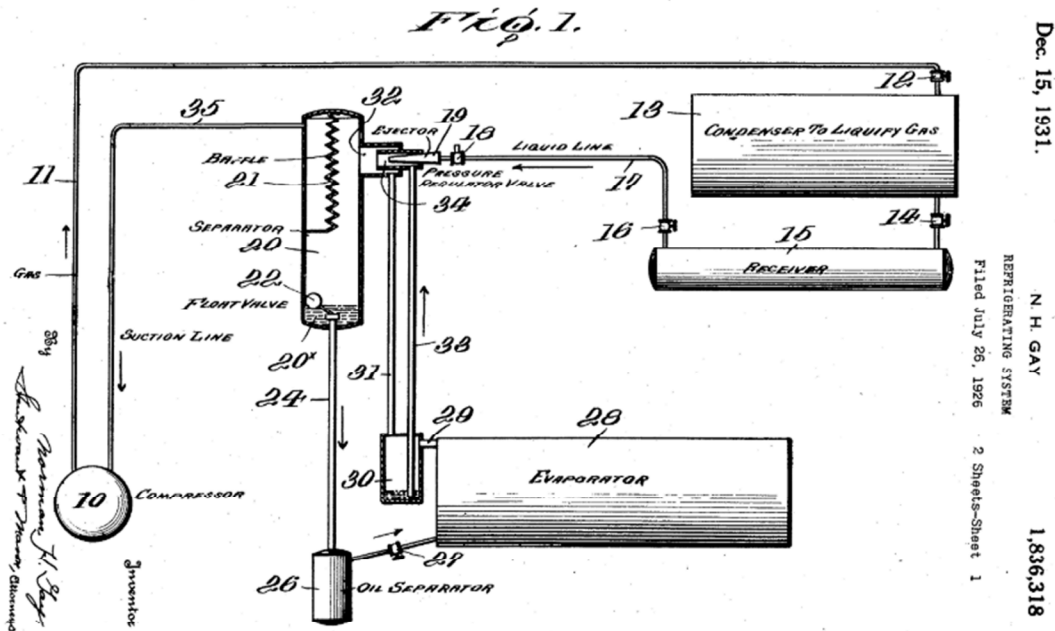


Figure 2.1 Two-phase ejector patent by Gay [12].

In the nuclear reactors, water steam ejectors were used in the emergency cooling water, which represents the fundamental passive feature of the steam-driven jet pumps where no moving parts exist in the second half of the 20th century [13]. Recently, the ejector is used in many chemical industries for harsh pressure and temperature conditions or to pump hazardous substances, as reported by Power [14]. In addition, the multi-stage ejector is being used as the largest ejector ever built to decrease the pressure in the test chamber of aerospace engineering applications [15]. Furthermore, the ejector took place in the aircraft propulsion system for the thrust augmentation and reduce the thermal signature by mixing the exhaust gases with fresh air [15, 16]. The ejector also proved the eligibility of high energy chemical lasers or for the food and medical drugs drying processes in the evaporative cooling applications, as pointed out by ASHRAE and Addy et al. [17].

2.2 Overview of Commercial CO₂ Systems

A considerable evolution in CO₂ refrigeration systems has been experienced in the last 10 years. This development has focused on the enhancement of energy efficiency and unit locations [2]. The CO₂ system undergoes a huge pressure difference between the heat absorption and rejection level, which corresponds to the transcritical operation. As a result, the expansion process is a major part of the exergy destruction in the system. Therefore, the leading solutions for driving the commercial CO₂ system has passed through three generations. The 1st generation, developed in June 2006 at Danish Technological Institute, represented the basic booster plant layout containing the heat recovery unit and flash gas removal. This layout improved the system and saved 4% of the energy consumption compared with a similar R404A system, and laid the groundwork for further research and improvements. The first generation layout is representing on the left side in Figure 2.2. The CO₂ leaves the gas cooler and expands through the high pressure valve to produce a vapor/liquid mixture, which is then separated in the liquid receiver. The liquid portion is supplied to the low and medium temperature evaporators, whereas the pressure of vapor portion is reduced to the compressor medium pressure suction line via the flash gas valve.

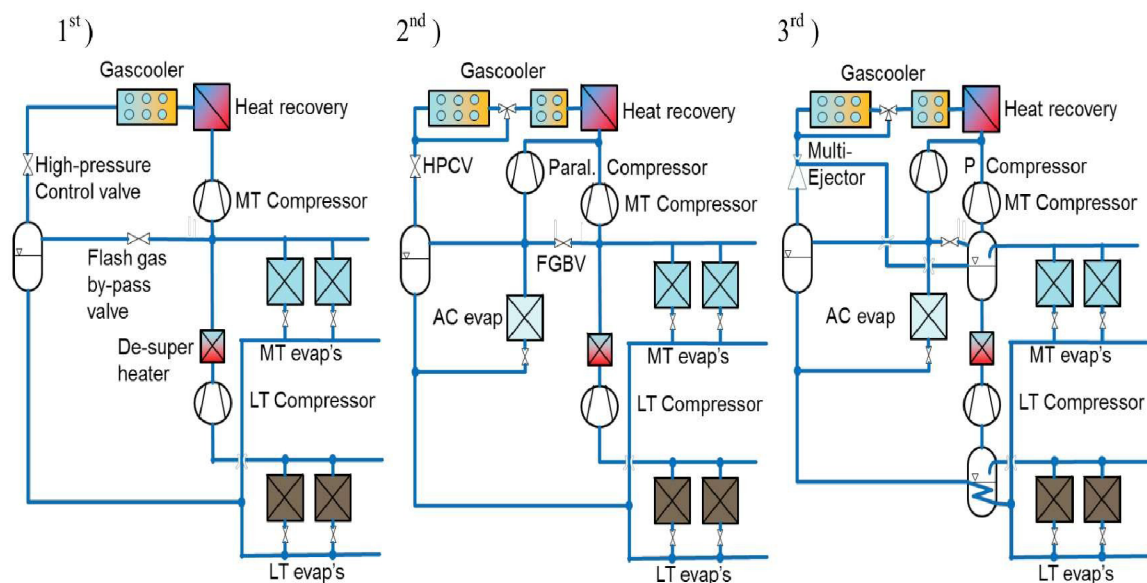


Figure 2.2 Principles of CO₂ circuit architecture generations of the booster refrigeration system [18].

This approach plays a dominant improvement mechanism for reducing the pressure drop in the evaporators by feeding them with liquid and improve the refrigerant distribution in the

cycle [19]. In addition, the system provides a great heat recovery potential for the heating demands in the supermarkets for the transcritical operations [20]. Many types of research have been accomplished to approve the advantages of R744 transcritical system configuration over other kinds of refrigerants used. For instance, the result reported by Gullo et al. indicated up to 17% lower energy consumption for the R744 conventional booster compared with similar R404a units, as represented in Figure 2.3 for the first generation [21].

The operation of the system in warmer climates causing an increase in the exit gas cooler temperature, which brought to the light the rise in the quantity of the flashed gas. The flash gas amount in the transcritical operations represents 45% of the total mass flow rate while it could increase to 50% at an ambient temperature higher than 40°C [22]. In this stage, the researchers emphasized the need to use the available flashed gas.

The adaptation of a supplementary compressor to draw part or the whole amount of the vapor from the liquid separator and to compress it to the gas cooler pressure represented the main solution. This method together with the flash gas removal is denoted by a parallel compressor layout representing the 2nd generation of the CO₂ refrigeration system architecture, as shown in the middle of Figure 2.2. The second generation allowed to unload the base-load compressor providing a drop in the receiver pressure level; therefore, the parallel compressor will consume more power input, but the total system cooling capacity will be increased simultaneously [23, 24]. Because of this optimization, many researches have been highlighted in this generation. It was declared by Chesi et al. [25] that the system COP could be improved by higher than 30% experimentally depending on the working conditions, and the improvement could reach over 65% in special cases according to the cooling load and pressure loss. Gullo et al. [26] compared the parallel compressor configuration system efficiency and the final cost with the basic solution through energetic, exergetic, and exergoeconomic analysis. The result indicated a reduction of the total input power by 18.7%, followed by a 6.7% lower final cost of the product, and about 50% decrease of the throttling valve irreversibilities compared with the conventional solution. In the calculation conducted by Karampour et al. [27], from 3% to 7% of the annual energy used was saved based on the location of the system in the globe using a parallel compressor. Nowadays, the combination of flash removal and the parallel compression equipped unit representing the indispensable base of the CO₂ transcritical refrigeration technology.

The major exergy destruction in commercial CO₂ systems lies in the expansion of the gas during the throttling process. The throttling losses have led to a sparked interest in developing new techniques on the recovery and reduction of expansion work and, consequently, the increase in the overall performance of the system [28]. Using the expanders was one of the solutions to recover the available exergy. However, the researchers have repeatedly shown their low efficiency, pressure and heat leakage, and the erosion risk due to the liquid impingement with the possibility to break at a high liquid level [29, 30]. Therefore, the researchers signified the ejector to be the most efficient solution as it is rugged with simple constructions, has low cost besides long lifespan, and can handle an enormous volume of gas [31]. On the contrary to the expanders, the ejector is easy to manufacture and control with the capability of handling two-phase flow under various operation conditions.

Several experiments on the R744 ejector have been conducted to illustrate the potential impact of the ejector on the transcritical system. The result of the experiment on the prototype ejector by Elbel and Hrnjak revealed 8% and 7% improvement in the system cooling capacity and COP, respectively [32]. Higher COP improvement of 15% in the system was obtained experimentally using the two-phase ejector compared to the conventional system that was recorded by Lee et al. [33]. Moreover, the experimental work performed by Nakagawa et al. indicated COP improvement of up to 27% employing the ejector in the cycle [34]. Furthermore, the literature showed that utilizing the ejector could recover from 20% to 30% of the expansion work [35]. The individual fixed geometry ejector will not be able to control the discharge pressure together with the effective work recovery for different cooling loads. Therefore, a control strategy is imperative since R744 systems come mostly with high throttling losses to control the heat rejection accurately. Therefore, a multi-ejector block composed of parallel arrangements of different geometry cartridges is implemented in the system and was first tested in 2013 [36]. This system is entitled as CO₂ integrated ejector supported parallel compression (IESPC), denoted by the 3rd booster system generation and represented on the right side of Figure 2.2. The adaption of the multi-ejector concept recorded several aspects of refrigeration system improvement. For example, in a study on the R744 multi-ejector supermarket refrigeration system by *Hafner et al.* [37], a single-stage and multi-ejector system with flash gas bypass and heat recovery was analyzed for four days in 3 different European countries. Each day corresponded to a typical season. The systems, equipped with a controllable ejector was assessed for different fixed geometries. The results depicted a 30% increase in the energy

performance of the multi-ejector setup over the reference booster system. Recovery of potential work with ejectors has been addressed and proven in several studies to significantly increase the COP of cooling and heating modes in supermarket refrigeration and heat recovery systems. It is evident in Figure 2.3 that the third generation layout has the minimum annual energy consumption compared with the other booster generations and the R404A system at similar locations. For instance, in Oslo and Athens the 2nd generation offers between 1% to 5.7% energy saving over the 1st generation while the 3rd generation with multi-ejector concept obtains from 17.8% to 26.7% energy saving compared with 1st generation. Furthermore, the multi-ejector concept allows to reduce the annual energy consumption from 16.9% in London to 23.4% in Oslo over the second generation [38].

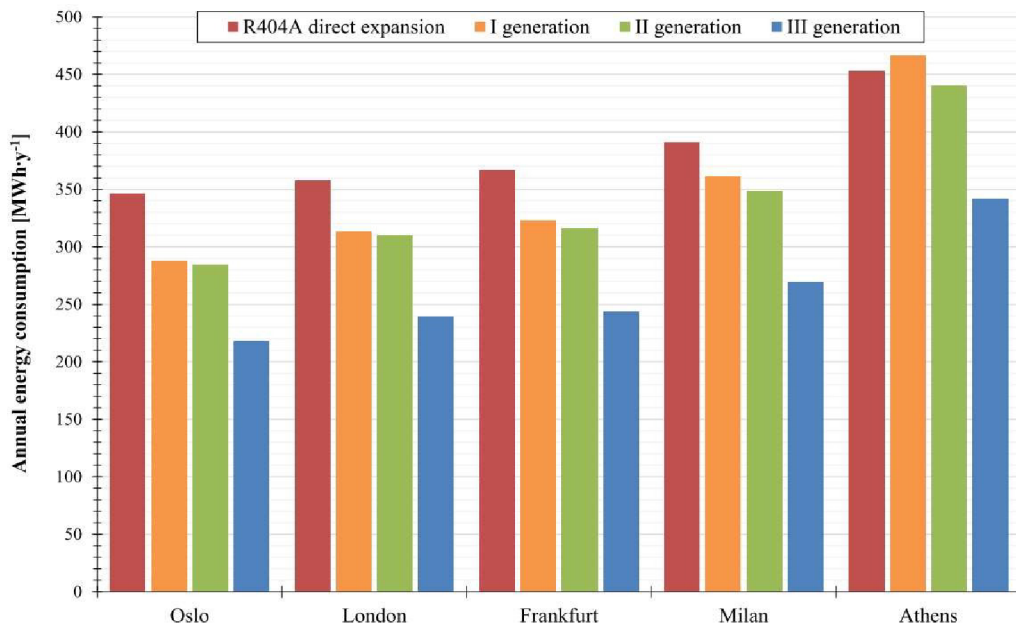


Figure 2.3 Annual energy consumption of three different generations R744 supermarket refrigeration system compared with R404A direct expansion unit in the European climate context [38].

2.3 R744 two-phase ejector technology

2.3.1 Ejector control strategy

The two-phase ejector used for the CO₂ refrigeration system had many obstacles related to the single-fixed geometries. The main issue was the absence of high pressure control in the heat rejection process. One of the control strategy solutions proposed is an integrated movable needle for the ejector inlet high-side pressure [10]. This mechanism allows to vary the area of

the motive nozzle throat. The prototype ejector is shown on the left side of Figure 2.4. Liu et al. also represent a controllable ejector with a similar mechanism to control the suction and the motive nozzle flow areas, as illustrated on the right side of Figure 2.4 [39]. Both needle-based ejector prototypes concluded satisfactory results via different operation conditions from the performed experiments.

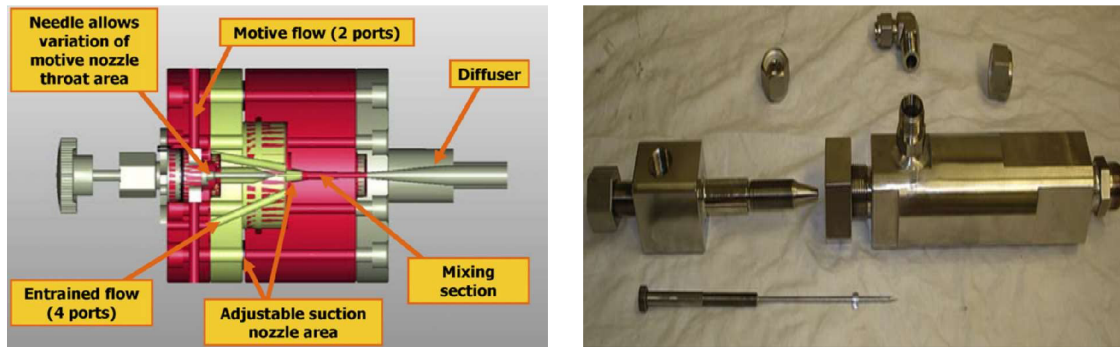


Figure 2.4 Two-phase ejector modular prototype with an integrated needle mechanism proposed by Elbel et al. on the left side [32] and Liu et al. on the right side [39].

Alternatively, an electronic ejector module was introduced by Carel Industries using the previous approach and represented in Figure 2.5 [40]. The producer claimed that the ejector could manage to operate at the different conditions of the system requirements in an optimal way. However, the researchers inferred a limited ejector efficiency, especially in the off-design operation, and further clarified that the needle-based ejectors are adequate only for specific cooling capacity [41, 42]. Therefore, the research based on this solution is still in the first phase facing uncertainty associated with the reliability and the performance of the heat rejection pressure controlling mechanism.



Figure 2.5 The electronic ejector module by Carel Industries [40].

An up-to-date control strategy is a multi-ejector concept based on various ejector cartridges located in parallel arrangement introduced by Hafner et al. [37]. In this approach, the active ejector combination changes based on the required system capacity to keep the optimum

work recovery and maintain the gas cooler pressure level accurately. The multi-ejector block is represented in Figure 2.6. There are several research investigations to cover each actuating aspect in the multi-ejector block. For example, Banasiak et al. used a cartridge with four different ejector sizes and mapped the performance for each profile [43]. The authors asserted the ability of the multi-ejector to control the heat rejection pressure and reach the greater extent of the work recovery with a significant overall energy performance improvement. In addition, a computational field was devoted to modeling the two-phase ejector profile, investigating the irreversibility, and predicting the experimental results for ejector design and geometry optimization [44–51].

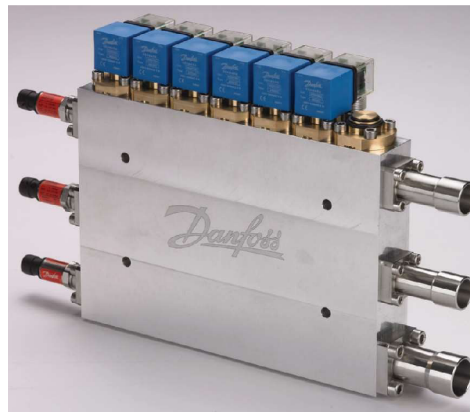


Figure 2.6 The multi-ejector block from Danfoss [52]

2.3.2 Description of the multi-ejector pack

Carbon dioxide systems have been modified with the inclusion of multi-ejector systems to increase its efficiency as well as widen the range of applicability of the CO₂ technology. In these systems, a control strategy is imperative since R744 systems come mostly with high throttling losses to control the heat rejection accurately. The commercial multi-ejector block manufactured by Danfoss is composed of parallel arrangements of different geometry cartridges, as depicted in Figure 2.7.

The desired ejector cartridge is activated by the ordinary coil (solenoid shut-off valves) located at the motive nozzle inlet. There are built-in check valves in each ejector at the suction nozzle to regulate the flow with preventing back flow which can create pressure instability. The block has a discharge port for the mixed elevated pressure fluid and a low-pressure and high-pressure side suction ports for suction of entrained fluid and motive fluid, respectively. The side of each flow port (motive, suction, and discharge) is equipped with pressure sensors to measure

the pressure level in each port. The flow enters the multi-ejector through the strainer/filter in front of the high-pressure inlet which is placed in a separate port.

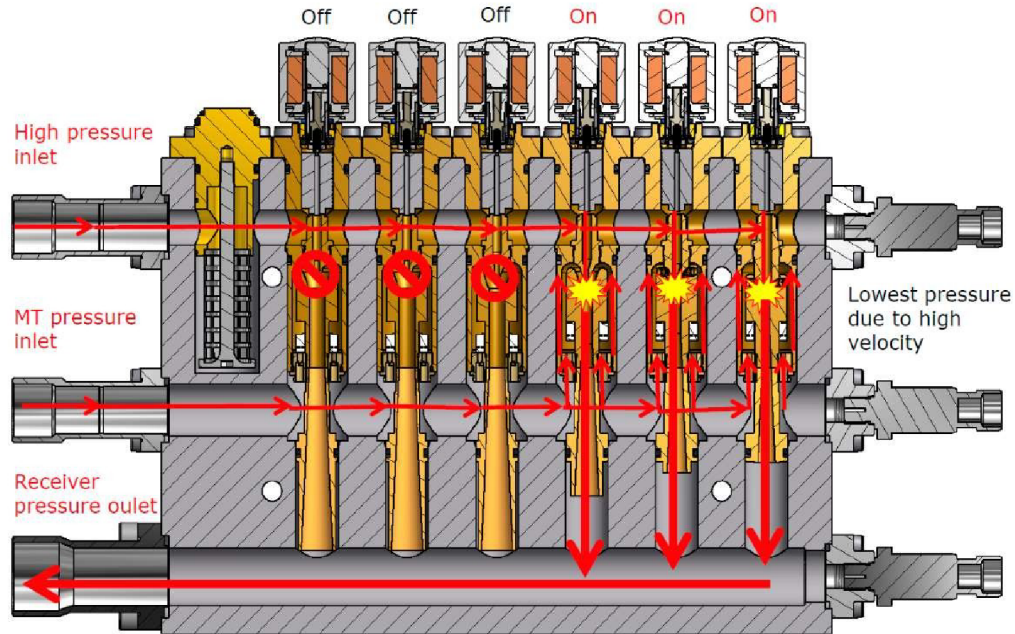


Figure 2.7 Sketch of the multi-ejector block [2]

However, there exists a high pressure valve (HPV) which is arranged in parallel to the block as a form of safety measure and serves as a pressure regulator for the gas coolers. The multi-ejector block is implemented due to three major advantages. The first being the fact that, due to the pre-compression of CO₂ from the evaporator pressure level to an intermediate pressure, there is a significant reduction of compressor power input needed. Moreover, the refrigerating effect is highly increased with the refrigerant entering the evaporator at a much lower vapor quality. Lastly, the possibility of overfeeding of the evaporators increases the effectiveness of the overall heat exchange process. Consequently, the work can be reduced by elevating the evaporation pressure to higher suction pressure, hence reducing defrosting cycles demand in the evaporators. There are two kinds of ejectors based on the application; the low-pressure ejectors (LP) and the high-pressure ejectors (HP). The low-pressure ejectors are used for low lift applications such as pumping gas from the evaporators back to the receiver as well as ensuring low-pressure lift for suction mass flow. A high-pressure ejector system lifts the pressure of a liquid or vapor from the medium temperature suction level in a system with parallel compression. From the receiver, it then moves to the parallel compressor and the main purpose of this is to ensure high-pressure lift for lower suction mass flow. Relative to the low-

pressure ejectors, flash formation is high and the system significantly benefits from pre-compression of the gas.

2.4 CO₂ as a refrigerant

Carbon dioxide (R744) represents one of the initial naturally occurring compounds collectively substance used as a refrigerant together with air, water, and Ammonia [53]. CO₂ was first proposed by Alexander Twining in a British patent as a refrigerant from 1850; then, it turns out to be the best choice for different refrigeration applications [8]. The properties of R744 were tested and studied in cooling systems since 1860 and established in freezing and food transportation in 1890 to cover over 300 refrigerated ships for meat products deliver around the world by 1900. CO₂ gained dominance in the marine refrigeration application in the following year because the refrigerant provided a fundamental safety and thus representing a reliable solution for rapid fresh food distribution globally, which allowed to grow in exporting and importing food products by 1935. Once the synthetic refrigerants were developed in 1940 and became available, the CO₂ popularity was reduced, and the majority of land-based refrigeration systems shifted to halocarbons working fluids. When the researchers highlighted the effect of the chlorofluorocarbons (CFC) emission then hydrochlorocarbons (HCFCs) on the atmosphere, a great concern from the governments and the societies pointed toward the limitation of these types of refrigerants in 1970 [53]. Therefore, the hydrofluorocarbon (HFC) refrigerants were developed due to the high rate of other refrigerants groups ozone-depleting potential (ODP). Furthermore, the negative impact of these working fluids shifted the attention on climate change. The effect of working fluids on climate change is known as the global warming potential (GWP). Recently, R744 taking the lead and become a refrigerant of great interest again because it provides more energy-efficient and environmentally friendly solution, especially when adapting the cycle components to the specific properties of this refrigerant. Today, several refrigerant groups based on chemical compounds have a different impact on the environment represented in Table 2.1, together with their safety class. The data were obtained from ASHRAE [53] and Handbook for the Montreal Protocol [54].

CO₂ properties are quite different from other conventional refrigerants. The phase diagram of CO₂ can be seen in Figure 2.8. The triple point where the three phases co-exist in equilibrium is represented at 5.18 bar and -56.57°C. There is an uncleared condition to

distinguish between the liquid and the vapor at temperature and pressure above the critical point of 31.06°C and 73.8 bar. This region is called supercritical, and the boundaries at this region do not represent the fluid phase change. The upper and the lower limit of the evaporation and the condensation process, respectively, occurs between the triple and the critical points. At the atmospheric pressure, the solid form of the CO₂ sublimates to vapor at a temperature higher than -78.5°C, while the gas form deposits to the solid state below the mentioned temperature.

Table 2.1 ODP and GWP comparison of different refrigerants.

Refrigerant number	Refrigerant group	Chemical formula	ODP	GWP	Safety group
R12	CFC	CCl ₂ F ₂	1	10900	A1
R22	HCFC	CHClF ₂	0.055	1810	A1
R134a	HFC	CF ₃ CH ₂ F	0	1430	A1
R410A	HFC blend	HFC-32/125 (50/50)	0	2088	A1
R1234yf	HFO	C ₃ H ₂ F ₄	0	4	A2L
R717	Natural	NH ₃	0	0	B2
R744	Natural	CO ₂	0	1	A1

- ODP relative to R-11 (as defined in Montreal Protocol [54]).
- R410A is a binary mixture of R-32/125 (50/50, %).
- GWP [54]: the ratio of the warming caused by a substance compared to the warming caused by a similar mass of CO₂.
- Safety classification [53]: (A/B: Low/high toxicity), (1/2/3: No/low/high flammability), (L: maximum burning velocity of ≤ 10 cm/s).

Most refrigerants reject heat below the critical point in conventional applications, unlike CO₂, which often operates transcritical because the critical point is very low. In this regard, the CO₂ refrigeration system can operate in two different modes, subcritical and transcritical, as illustrated in the thermodynamic cycles for a conventional system in Figure 2.9. In the transcritical operation, the heat is rejected in the supercritical region, and the refrigerant temperature decreased through the process by interacting with a cooling media at ideally constant pressure without phase change as no saturation condition exists. Because of the high temperature, the system can be applied in many heating applications such as domestic hot water and space heating very efficiently. In contrast, heat absorption occurs below the critical point at a constant temperature. In the subcritical operation, all processes took place below the critical point with a maximum condensation temperature of 28 °C, preferably much lower. Therefore, the heat rejection can be characterized by desuperheating and condensation with the possibility of subcooling too.

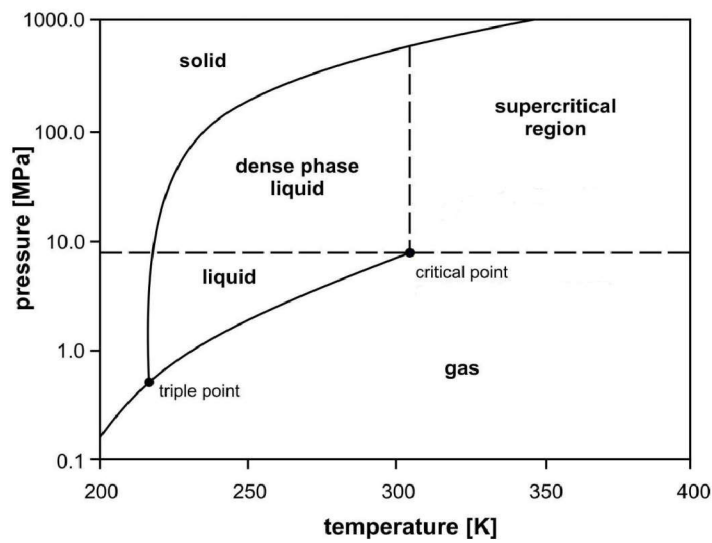


Figure 2.8 CO₂ phase diagram [55]

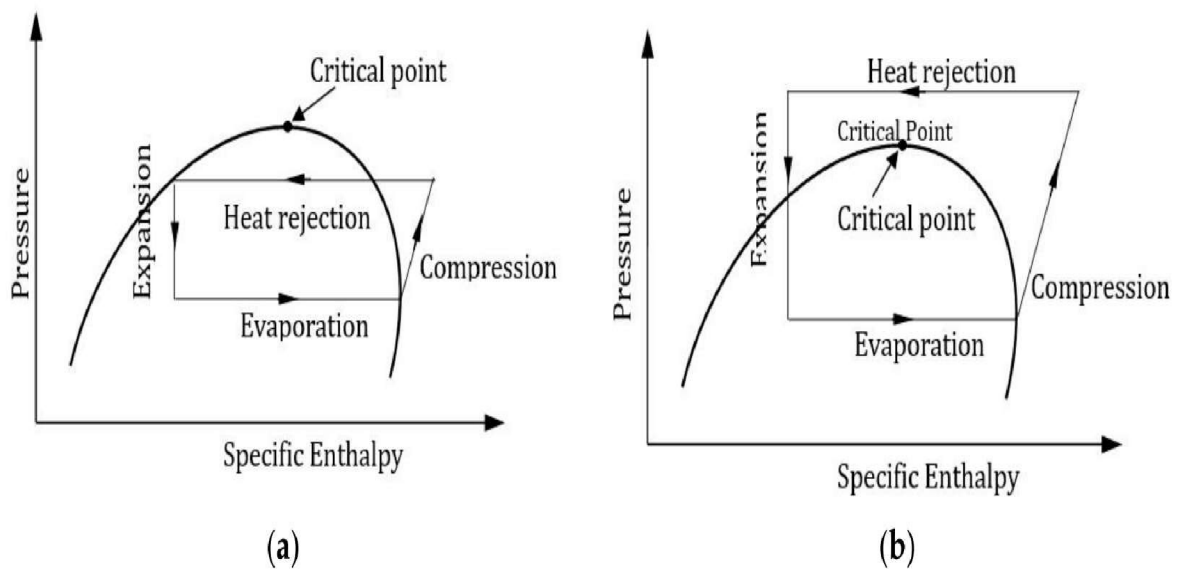


Figure 2.9 CO₂ P-h diagrams to represent (a) Subcritical cycle and (b) Transcritical cycle from [56].

CO₂ as a refrigerant provides many positive features and advantages over other refrigerants; for example, it is an odourless and colourless gas with a slightly pungent taste of acid as well as being non-flammable (Hydrocarbons) and non-toxic (Ammonia) with no known carcinogenic, mutagenic effects [6]. Despite operating transcritical in most cases, CO₂ offers significant benefits to the cooling systems with its peculiar and exceptional transport properties with minimal safety risks. Moreover, R744 carries many thermophysical advantages, such as high thermal conductivity, high vapor density, and low viscosity. Table 2.2 representing the comparison of CO₂ characteristics and properties with other refrigerants.

Table 2.2 Characteristics and properties of CO₂ and other refrigerants [5, 57, 58].

	R12	R22	R134a	R410A	R1234yf	R717	R744
Molecular mass [kg/kmol]	120.9	86.5	102.0	72.6	114.0	17.0	44.0
Normal boiling point [°C]	-29.8	-40.8	-26.2	-52.6	-29.5	-33.3	-78.5
Critical pressure [Mpa]	4.11	4.97	4.07	4.79	3.38	11.42	7.38
Critical temperature [°C]	112.0	96.0	101.1	70.2	94.7	133.0	31.06
Refrigeration capacity [kJ/m ³]	2734	4356	2868	6763	3528	4382	22545
Saturation pressure at 0°C [Mpa]	0.308	0.498	0.293	0.801	0.316	0.429	3.485
Kinematic viscosity [mm ² /s]	0.176	0.169	0.141	-	0.177	0.266	0.107
Thermal conductivity [W/m.K]	0.076	0.095	0.015	-	0.071	0.559	0.110
C _p at 0°C [kJ/kg.K]	0.934	1.17	1.50	1.52	1.29	4.62	2.54
h _{fg} at -30°C [kJ/kg.K]	166.3	226.8	219.5	253.6	180.5	1359.7	303.5
First commercial use	1931	1936	1990	1998	2010	1859	1869

- Refrigeration capacity, kinematic viscosity, and thermal conductivity are represented at 0°C.

It can be observed that the natural working fluids (R717 and R744) has superior advantages over other refrigerants with respect to the heat transfer properties. For instance, they are representing the highest thermal conductivity and specific heat capacity with the large latent heat of vaporization implementing to achieve more efficient heat transfer within the evaporator. On the other hand, CO₂ is characterized by a high volumetric refrigeration capacity among all mentioned refrigerants, which significantly influences the heat transfer coefficient based on the mass flux [59]. The low viscosity of this natural working fluid reduces the initial investment cost since small dimensions of the valves, pipelines, and other components can be made. In contrast, CO₂ has a 4-12 times higher saturation pressure of than other refrigerants and therefore requires special care for equipment manufacturing. As a result, due to the excellent properties of this refrigerant, it is nominated as a preferred working fluid [60].

2.5 Ejector-support R744 Transcritical Refrigeration System

Refrigeration and its applications held a prominent position as an essential service in modern society. R744 transcritical cooling systems have proven their high efficiency within outstanding performance, energy savings, and adhering to the fulfillment of the EU F-Gas Regulation 517/2014 [61] using eco-friendly and neutral-environmental-impact refrigerant. CO₂ refrigeration systems are characterized by a considerable pressure difference between the heat absorption and heat rejection pressure level due to operating transcritical in most cases. Therefore, the energy content is lost as the heat of friction when the refrigerant is expanded

(throttling losses) [62]. This generally connotes that higher gas cooler outlet temperatures result in a greater drawback for vapor-compression systems. This drawback can be seen in Figure 2.10, where CO₂ is compared to two different low-pressure HFCs. In other words, the expansion devices in the cycles do not recover the supplied mechanical energy, leading to significant exergy destruction that lies in the throttling process, which negatively impacts the system's overall efficiency [63].

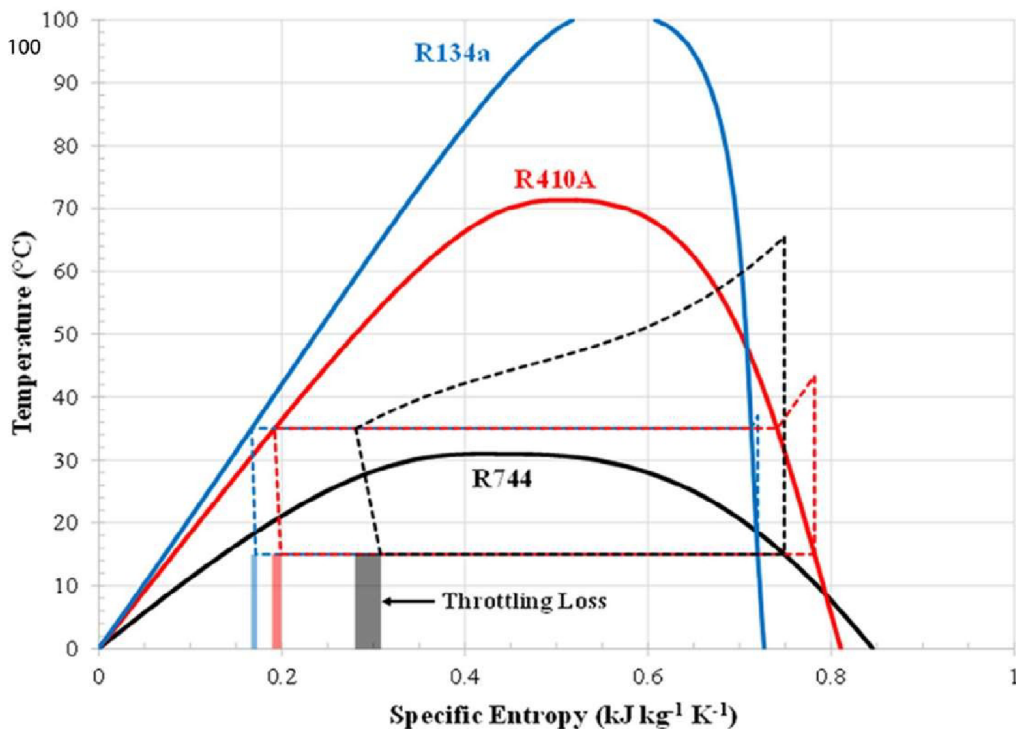


Figure 2.10 Vapor-compression cycle with isenthalpic expansion shown on temperature vs. specific entropy diagram for R744 (CO₂), R410A and R134a (HFCs). The throttling losses of each refrigerant are visualized as vertical bars on the specific entropy axis [65].

Implementing an ejector to the cycle will assist to drive the refrigerant pre-compression from the evaporator pressure level to an intermediate pressure, causing a reduction in the compressor power input needed and contributing to a higher coefficient of performance. In addition, the ejector provides a high refrigerating effect due to much lower vapor quality refrigerant after the separation at the exit [64].

The basic schematic of the ejector conventional refrigeration cycle can be seen in Figure 2.11. The advantages of applying a single ejector for expansion in refrigeration systems design with optimization of operating conditions have been explored widely in several experimental

approaches to reveal an 8% to 27% increase in COP. For example, an experiment performed by Elbel [10] showed significant benefits of using a transcritical ejector system to overcome large losses occurring due to throttling. COP and cooling capacity were simultaneously increased for a range of test conditions of internal heat exchanger up to 7% and 8%, respectively. Lucas et al. [66] investigated the maximum COP of the refrigeration system of both expansion valve and ejector cycles without an internal heat exchanger. At maximum ejector efficiencies of 22%, COP was observed to reach a 17% improvement over the expansion valve cycle. However, the performance of the two-phase ejector equipped systems was found not only to be sensitive to the efficiencies of the individual geometries but also to operating conditions.

In the application of the ejector to optimize the COP of the heat pump system, a significant improvement was reported by Sarkar et al. [68]. Ejector refrigeration systems function differently based on the form of refrigerant. When used as a vapor ejector, compression of R744 vapor is easily done without external work input from the medium-temperature evaporator [32]. In contrast, in flood mode, the liquid ejector pumps out the liquid from the medium-temperature evaporator in the CO₂ refrigeration system [4].

Several experimental approaches on the R744 ejector-based transcritical refrigeration cycles have explored potential increase in system coefficient of performance. For example, Banasiak et al. [69] compared the COP using a classic valve and ejector for expansion. The result reported an 8% higher COP for the ejector-equipped system over the traditional valve. Since different geometries of ejectors generally tend to influence the balance of overall system performance, Boccardi et al. [70] analyzed its effect on the heat pump applied in air-conditioning. The analysis explored the ejector configuration best suited to achieve maximum efficiency of the ejectors, heating capacity, and COP by comparing the system performances of the proposed concept to the basic throttling valve configuration equipped with a regenerator cycle. Although a refrigeration multi-ejector system was used, it was possible to obtain an optimal ejector configuration that produced better exergy efficiency over the regenerative cycle system. However, the mismatched system does not correlate with the energy performance; hence, a more accurate design was proposed for future investigations to improve the R744 multi-ejector system [71].

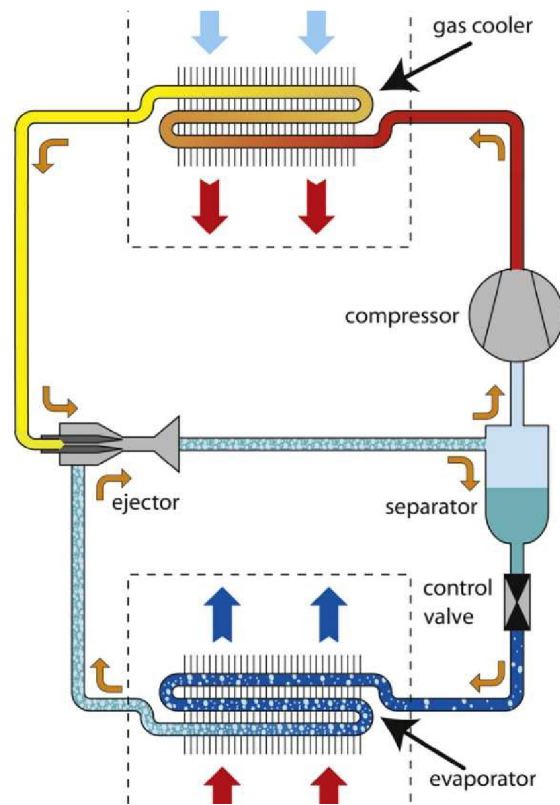


Figure 2.11 Common used R744 ejector cycle [67].

He et al. [72] tracked the dynamic responses of a transcritical CO₂ ejector refrigeration system to predict the ejector efficiency and system performance with a virtual online cascade controller. The controller tracks the optimal pressure of the gas cooler and analyses the performance based on the control of the variable area of the nozzle throat, which verified an increase to optimal performance with the tracker incorporated. Nonetheless, the working conditions for optimal performance do not indicate a maximum ejector cooling capacity or efficiency in simulation. However, the system performance was improved in the experimental system using the controller, although great variations in performance occur for different operating conditions. For a variable compressor speed, a multivariable controller according to studies is necessary to drive an increase in performance in the transcritical state of the ejector. This concept was simulated by Yang et al. [73] on the R744 refrigeration system equipped with a controllable ejector and was verified for improving the energy performance by predicting the optimal gas cooler pressure.

An additional configuration setup to enhance the performance of the parallel-compression R744 system is to replace the high-pressure expansion valve with a block of parallel ejectors to sustain the discharge pressure through a discrete opening feature. This study was performed by

Banasiak et al. [43] with a thoroughly designed and experimentally verified four different cartridge multi-ejector pack. The schematic of the test facility related to the CO₂ circuit can be seen in Figure 2.12. In the test, the performance of the individual cartridge is assessed. The whole ejector pack was evaluated for the possibility of maintaining the discharge pressure as the main expansion component, as well as its improvement of COP. The results depicted higher individual ejector efficiencies than those previously gathered with an overall improvement in energy performance. The multi-ejector pack was also verified to work efficiently in adapting and retaining precise discharge pressure under variable loads, even with a simple controlling method. Although the estimation method used to evaluate the COP and exergy efficiencies yielded results partly comparable to the real applications, up to 8%, and 13% of improvement was indicated.

Based on the effect of the geometries and operating conditions on efficiency, several experimental works have been conducted in that focus [74]. In XU et al. [75], an adjustable ejector was used to change the nozzle throat area at a distributed ejector efficiency within the range of 20 to 30% to maximize the system COP by increasing high-side pressure. Each geometric configuration gives a potential solution on which performance can be assessed. Smolka et al. [76] studied the parallel arrangement of ejectors for both fixed and adjustable geometries to provide an incremental or flexible mass flow of refrigerant with different nozzle configurations. The approach was simulated for transcritical parameters at various sizes for each geometric concept. For a range of operating conditions considered, the fixed-geometry ejector design produced high efficiency, whereas the controllable-geometry ejector design produced higher efficiency of up to approximately 35% when the motive nozzle throat area is reduced after which the efficiency gradually decreases. Palacz et al. [77] optimized the shape of a CO₂ ejector by six geometry parameters which enhanced the ejector efficiency by 6%. Consequently, different operating conditions and geometries were experimentally studied by Liu et al. [78] to provide correlations between the motive and suction nozzle efficiency, including the mixing section efficiency. On this account, Liu et al. [79] developed and validated experimentally the model of a two-phase ejector with a variable throat area and exit point for the motive nozzle to observe which optimized range of geometries produced better performance in transcritical CO₂ cycles. The study directly regulated the capacity of the ejector and depicted the influence of the efficiencies of the individual ejector components and system. The outcome of this simulated model showed that for a high inlet pressure of the motive stream, better ejector performance

could be achieved with higher motive and suction nozzle efficiencies. Additionally, Nakagawa et al. [80] studied how the mixing length altered the ejector performance in the cycle and concluded that COP could be lowered by 10% for improper sizing of the length of the mixing chamber as compared to conventional systems.

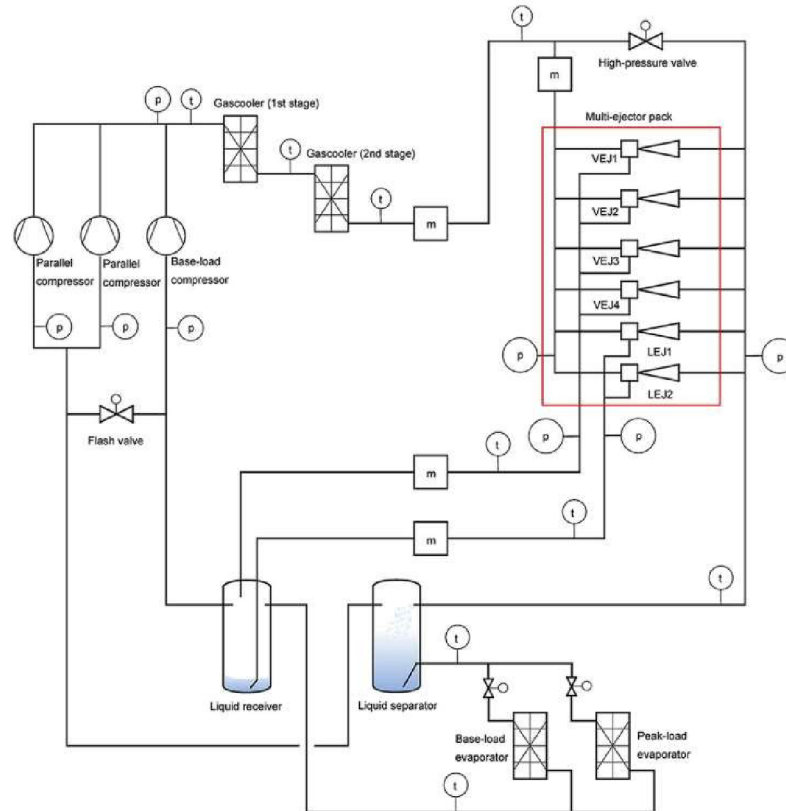


Figure 2.12 Schematics of the multi-ejector R744 circuit test facility for Banasiak et al. [43].

The low critical temperature of R744 allows the system to operate in a transcritical state; however, this lowers the thermodynamic system performance compared to the subcritical condition based on the higher rates of exergy destruction from throttling the supercritical state to the subcritical [28]. Therefore, to spread its use, exergy performance, and exergy destruction, and efficiencies should be evaluated. Recent investigations use a CO₂ two-phase ejector analysis of exergy to obtain how ejector irreversibilities are affected by different operating conditions [81]. Boccardi et al. [70] reported a reduction of the throttling irreversibilities losses by 46% using multi-ejector for expansion with a maximum increase in exergy efficiency by 9%. Ersoy et al. [82] studied theoretically the performance of the transcritical CO₂ ejector cooling cycle. The results showed the possibility of 39.1% reduction of ejector irreversibility compared to the classic refrigeration cycle and 5.46% compare to turbine expander systems.

The performance of the CO₂ ejector can be evaluated through dynamic simulations of a non-dimensional model [83][84]. Theoretical models of transcritical CO₂ ejectors were proposed and the approach elaborated. Experimental data were used for validation as well as idealized assumptions to specify the system performance with a two-phase flow ejector [85][86]. Nonetheless, several thermodynamic models have been proposed to determine how the drop in pressure of the suction nozzle affects the cycle performance [87]. The results showed an improvement of 45% of COP and exergy losses of ejector reduced by 43%. Investigations by Ameer et al. [88] using proposed thermodynamic calculations based on the real gas model depicted a good correlation with the experimental values. The result assumed that at double choking of nozzles, mass flux is maximum with constant isentropic efficiencies. However, most previous models do not include a detailed method to evaluate the occurrence of shock waves, neither models with geometric parameters and adapting hypotheses to support the model with the detailed information about the calculation of shock waves. These details have been covered in the 1-D model by Taleghani et al. [89], evaluating the two-phase CO₂ ejector for single and double choking conditions using constant polytropic efficiencies to predict the overall performance. Latterly, Ameer et al. [90] presented a thermodynamic simulation to model R744 transcritical heat pump cycle with implicit ejector geometry under different boundary conditions. The conclusion illustrated a 9% enhancement of COP when the system was supported with an ejector. In addition, the ejector throat and the mixing chamber diameter need to be adjusted to take into account changes in capacity, especially at lower evaporating temperatures.

The performance of the transcritical CO₂ cooling system is predominantly evaluated via conventional energy-based methods. Nevertheless, applying a conventional exergy-based analysis to determine the inefficiencies plays a vital role as the most potent thermodynamic tool for the assessment. This investigation describes the maximum work obtained from the system and merely describes the energy quality used [91]. This technique has been used by Haida et al. [92] to evaluate the system performance experimentally. The research outcome showed an improvement of 13.7% exergy efficiency and 7% COP when the system was equipped with the multi-ejector pack. The in-depth investigation performed by Gullo et al. brought to light that the R744 multi-ejector outperform R513A-, R450A-, R134a-, R1234ze(E)-, R290-, and R404A-based solutions below the so-called “CO₂ equator” [93]. The analysis was applied to average-size supermarkets in different cities. The result revealed up to 90.9% reductions in

environmental impact within around 26.9% energy savings over conventional hydrofluorocarbon-based solution. Moreover, the multi-ejector block allows reducing the power input up to 50.3% over HFC-based units at low outdoor temperatures. In terms of COP comparison, the configuration of R744 multi-ejector supported parallel compression system including medium temperature (EJ) and low-temperature overfed evaporators (EJ_OV) could outstandingly offer COP increasing by 77.6% and 96.3% at subcritical conditions, respectively, as illustrated in Figure 2.13.

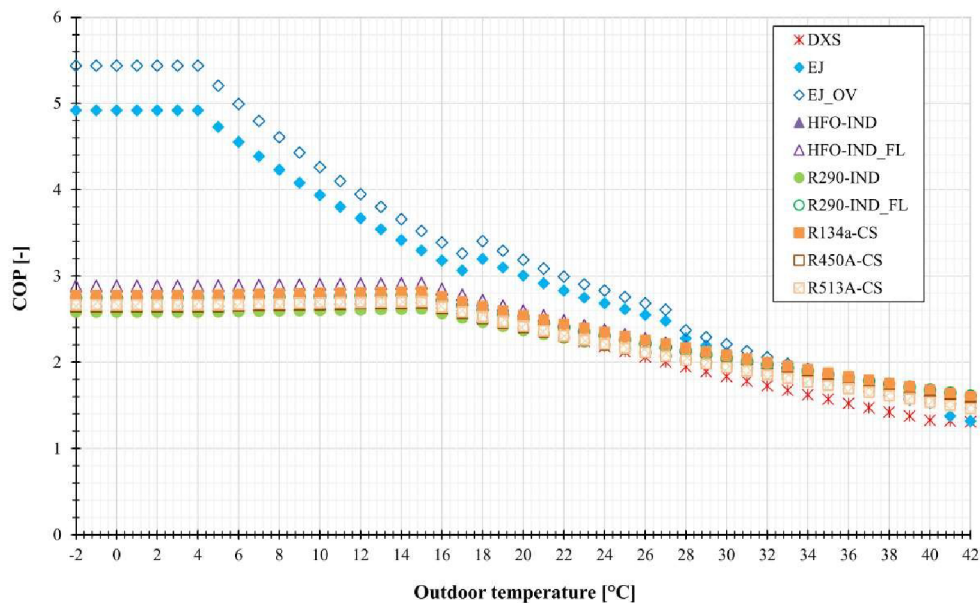


Figure 2.13 Comparison in terms of COP among the investigated solutions [93].

CO₂ systems have been implemented in the production of air conditioners (AC) in order to reduce overall investment and operating costs. However, this integration could be responsible for 4.2% to 15.1% system energy penalization [94]. Pardinás et al. [95] introduced novel feature solutions for the CO₂ vapor compression racks that utilized ejector-supported AC evaporation at two different pressure levels (EJ_{MT}+EJ_{AC}), as shown in Figure 2.14. The authors compared this solution with the conventional booster, parallel compression, and parallel compression with MT multi-ejector block configurations (EJ_{MT}). The first AC evaporator was located downstream of the liquid receiver and the second ac evaporator was placed between the liquid receiver and high-pressure control devices. The result proved a decrease in the total power consumption of the system by 8.3% at 30°C and 8.6% at 25°C when operating two groups of MT and AC multi-ejector blocks over other configurations.

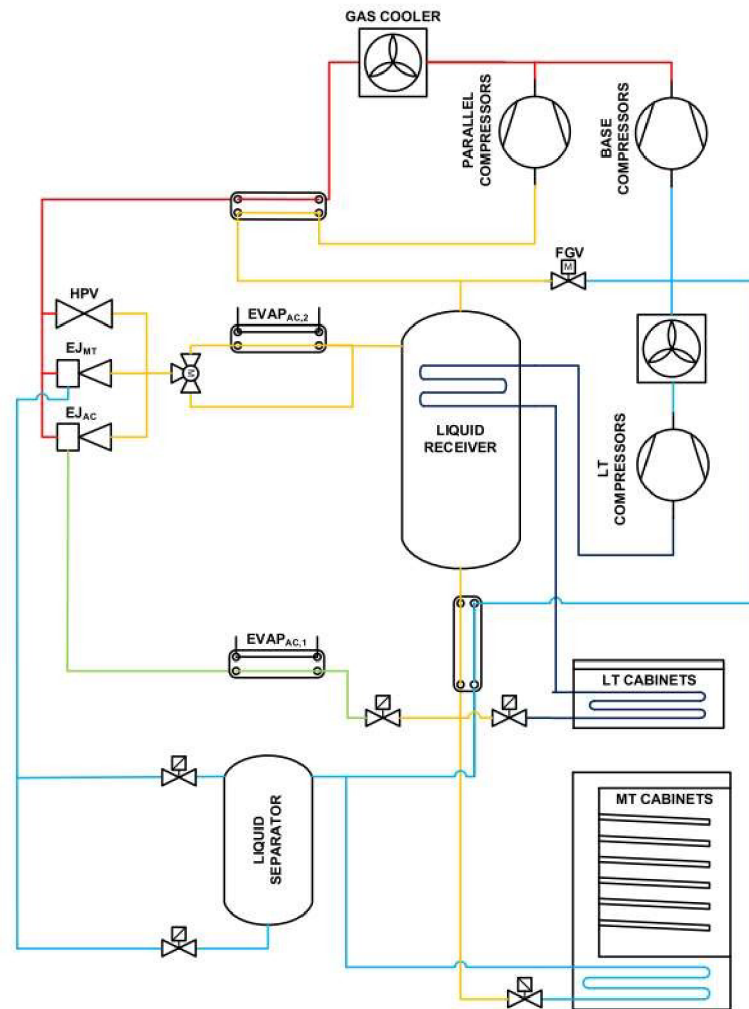


Figure 2.14 Innovative solutions for integrating the AC production with conventional evaporation and ejector-supported evaporation [95].

In general, the transcritical CO₂ refrigeration system exhibits relatively high exergy destruction. The overall exergy destruction can be reduced by 43.44% when the system components are improved, specifically the compressor which contribute to the largest destruction of exergy followed by the ejector, evaporator, and gas coolers [96]. Taslimi et al. [97] studied different transcritical CO₂ ejector systems at similar cooling capacity based on the laws of thermodynamics. The result illustrated that the evaporator exhibited major exergy destruction in the cycle by 33% followed by the compressor with 25.5% then the ejector at 24.4%. Fangtian and Yitai [98] concluded that utilizing ejector would decrease the exergy loss by 25% in a CO₂ transcritical cycle as compared to the conventional cycle. A current study by Gullo et al. [99] reported a 39% overall reduction of exergy destruction in multi-ejector supported CO₂ system compared to the conventional booster system.

2.6 Summary

The signs of climate change and the parameters that influenced global warming potential call for eco-friendly and neutral impact alternative refrigerants such as natural working fluids. CO₂ proved to be thermophysically suitable and environmentally friendly to held the lead as a working fluid over other refrigerants in the refrigeration sector. The development of transcritical R744 booster throughout different generations becomes a success and gaining market share, conquering the halocarbons-based systems worldwide. Some technical downsides of using R744 in the refrigeration systems, such as the high operating pressure and low critical point, have been addressed by designing the system components. The main issue is high irreversibilities in the expansion process, which produces a high destruction of exergy.

Operational measurements and the interest of the experiment led to introduce the ejector as a new technique for recovering the expansion losses and, consequently, increase the overall performance of the system compared with the standard layout. The open literature revealed the effect of the operation conditions and ejector geometry design to improve the ejector efficiency to a greater extent. Additionally, the contribution of the ejector in energy-saving was illustrated in many types of research, taking the variations of the climate into account together with the reduction in the total investment and working cost. Therefore, the research in the modern R744 transcritical refrigeration system equipped with an ejector expansion module has sparked interest for further possible and desired improvements.

3 THEORY AND DATA ANALYSIS

This section will describe the method of data analysis used to evaluate the study. The content will explain the ejector working principle and its integration into the R744 transcritical compression cycle. In addition, the main parameters to describe the characteristic of the ejector and appraise the system will be discussed, including the second law of thermodynamic analysis.

3.1 Ejector theory and working principle

Two-phase ejectors have gradually replaced expansion devices in the traditional vapor compression systems as a result of the high reduction in compression work needed. In vapor-compression units, expansion valves are used and lead to isenthalpic expansion causing large throttling losses rather than isentropic expansion. For these reasons, two-phase ejectors have attracted a lot of research in the scientific community. The ejector does not contain any moving parts and composes of the suction chamber, motive nozzle, diffuser and mixing chamber. Based on the two flow streams in the ejector, which are the entrained and the motive fluid flow, the basic working principle of this system is the conversion of pressure energy to kinetic energy isentropically, as shown in Figure 3.1.

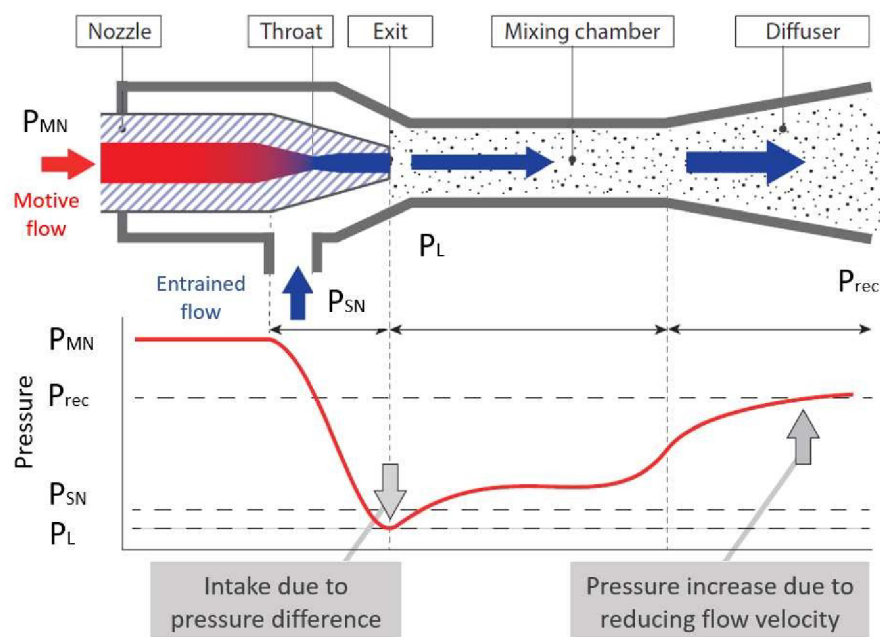


Figure 3.1 The pressure profile along the ejector axis adapted from Danfoss [100].

The driving force for the ejector is the primary fluid, which is usually termed as the motive fluid. The high-pressure primary fluid enters the converging-diverging nozzle and expansion occurs, causing an acceleration towards the motive nozzle. At this point, the pressure generated is very low and supersonic flow occurs at the exit. The motive flow is accommodated by a tangential force that develops at its edge. As a result, there is a pressure difference between the working fluid exiting the evaporator and the expanded refrigerant from the motive nozzle. Thus, the suction fluid is sucked toward the mixing chamber with high velocity. The entrained fluid is accelerated by the high-velocity motive fluid in the mixing section. The two flow streams start mixing in the pre-mixing section and there is a transmission of energy of the primary fluid in the form of kinetic energy to the entrained fluid (to increase its velocity), and part of the energy converted to pressure energy. Some of the energy is dissipated as heat due to the mixing and friction. The shock train phenomena also occur in the mixing chamber region, where oblique shock waves and expansions occur and diminish until they disappear.

Due to this momentum exchange, the mixed fluid is forced downstream. Furthermore, it is imperative for the mixing chamber section to have a specified length to prevent reverse flow [31]. As the mixed fluid enters the diffuser section, the pressure of the fluid begins to increase right to the end of the diffuser. The pressure of the outlet mixed-flow lies between that of the entrained fluid and the motive nozzle flow pressure. The changes in velocity (deceleration) in this section convert kinetic energy back to potential energy to obtain a high net pressure for the mixed fluid flow.

3.2 Ejector vapor compression cycle

Ejector devices can be used in different applications depending on the purpose and the functions. For example, in refrigeration systems, a compression ejector is utilized in conventional cooling systems with halocarbons as refrigerants using low-grade heat sources [101–104]. In this case, the ejector pressurizes the vapor working fluid from the evaporator level and discharges it to the condenser. This process usually falls within the vapor phase region and can be combined with any power cycle using heat rejection. On the other hand, the ejector can be used as an expansion device which is, for example, currently used in transcritical cooling systems. For this reason, the process happens to be at the transcritical and the two-phase (mixture) region. The simple sketch of the R744 vapor compression cycle supported with an

expansion ejector is shown in Figure 3.2. The refrigerant was discharged by the compressor (thermodynamic state 1-2) to the gas cooler, where the heat rejection took place at high pressure (thermodynamic state 2-3) then expanded isentropically through the ejector motive nozzle (thermodynamic state 3-4). Because of the pressure difference between the evaporator and the expanded primary flow, the refrigerant coming from the evaporator will be entrained, and the mixed stream (thermodynamic state 6) compress to the liquid separator pressure level (thermodynamic state 7). From the separator, the vapor portion will be compressed again and the liquid part will be feeding to the evaporator. By adding an expansion ejector in the cycle helps to reduce the compressor input power by suction flow stream pre-compression and ensures lower vapor quality fluid entering the evaporator (thermodynamic state 8).

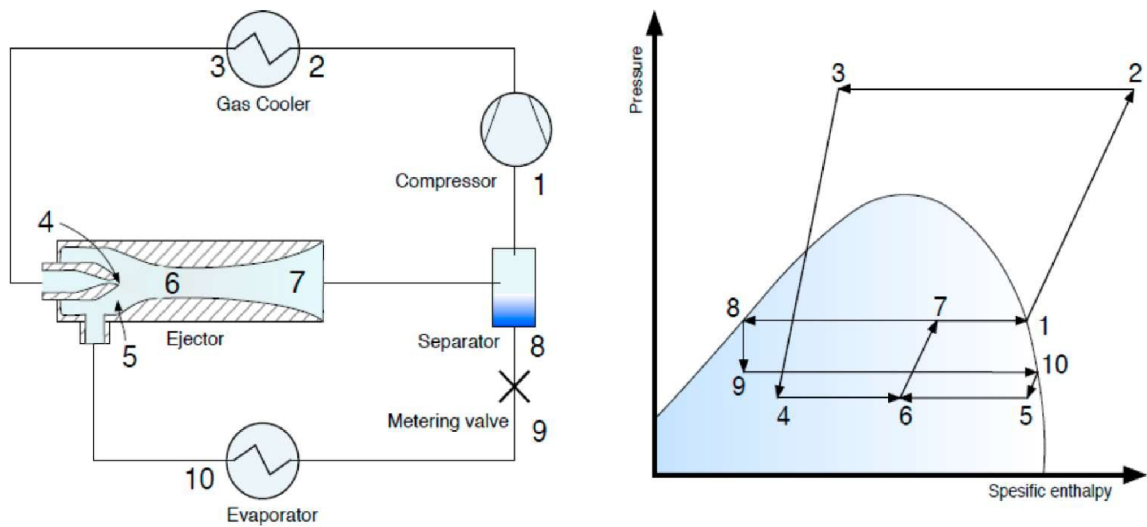


Figure 3.2 Schematic of a simple R744 vapor-compression system equipped with a two-phase ejector (left-hand side) and its p-h diagram (right-hand side) [105].

3.3 Ejector performance characteristics

The performance of the two-phase ejector, used for expansion work recovery in the refrigeration cycles, is commonly analyzed by several parameters. The main significant factors considered to evaluate the ejector are the pressure lift (P_{lift}), mass entrainment ratio (ER), ejector compression ratio, and the expansion work recovery, which is usually termed as the ejector efficiency (η_{eje}). The pressure lift represents the amount of pressure difference between the ejector discharged mixed-flow, (P_{rec}) the liquid separator receiver pressure level, and suction nozzle flow (P_{SN}), as shown in equation (3-1). Through the ejector, the refrigerant is being

pumped from the evaporator back to the separator and ensures a relatively low-pressure lift at a high suction nozzle mass flow rate. However, the mass entrainment ratio is determined as the ratio between the suction and the motive nozzle mass flow rates, as shown in equation (3-2). This ratio assesses the capability of the ejector to entrain the refrigerant from the evaporator through the suction accumulator tank back to the liquid separator receiver. Normally, the ejector ought to ensure large suction mass flow besides delivering a large pressure lift to obtain a good ejector performance.

$$P_{lift} = P_{rec} - P_{SN} \quad (3-1)$$

$$ER = \frac{\dot{m}_{SN}}{\dot{m}_{MN}} \quad (3-2)$$

Where MN and SN are representing the ejector motive nozzle and the suction nozzle. In fact, the ejector has two choking phenomena that impact the general performance. The first choking exists at the motive nozzle and the second occurs throughout the entrained flow. The ejector performance itself is divided into three operational modes according to the outlet mixed flow, critical, subcritical and backflow mode termed as double-choking, single choking, and malfunction mode, respectively. At the critical mode operation, both motive and suction nozzle flows are choked. The mass entrainment ratio reaches the maximum and remains constant with a further decrease in the range of the ejector discharge flow pressure (liquid separator receiver pressure). In sub-critical mode, only the motive flow is choked because the liquid separator pressure is higher than the ejector critical pressure value, which results in decreasing the mass entrainment ratio. If the liquid separator pressure continues to rise, the ejector experiences a backflow when the suction nozzle flow stream reverses and the entrainment ratio ends up as lower than zero. This operation mode also called stall condition and occurs as a result of the ejector being forced to give a pressure lift that is relatively higher than for which the ejector was designed for. Therefore, the motive flow utilized for pressure recovery will not be able to drive the entrained flow and the ejector will operate as a throttling valve only. The ratio between the ejector outlet pressure (P_{rec}) to the suction nozzle pressure (P_{SN}) is defined as the ejector compression ratio. It is also known as a pressure lift ratio or suction pressure ratio through the literature.

The ejector efficiency was first introduced by Köhler et al. [106]. The great advantage of this represented efficiency is that it can be calculated using only the external parameters that are

easy to measure. The same expression for the total ejector efficiency was presented by Elbel et al. deriving by different approaches as shown in equation (3-3) [32]. This formula was used in many literatures [49, 66, 107]. It was defined as the ratio of the amount of expansion work regenerated by the ejector over the maximum possible expansion work recovery potential, as seen in Figure 3.3.

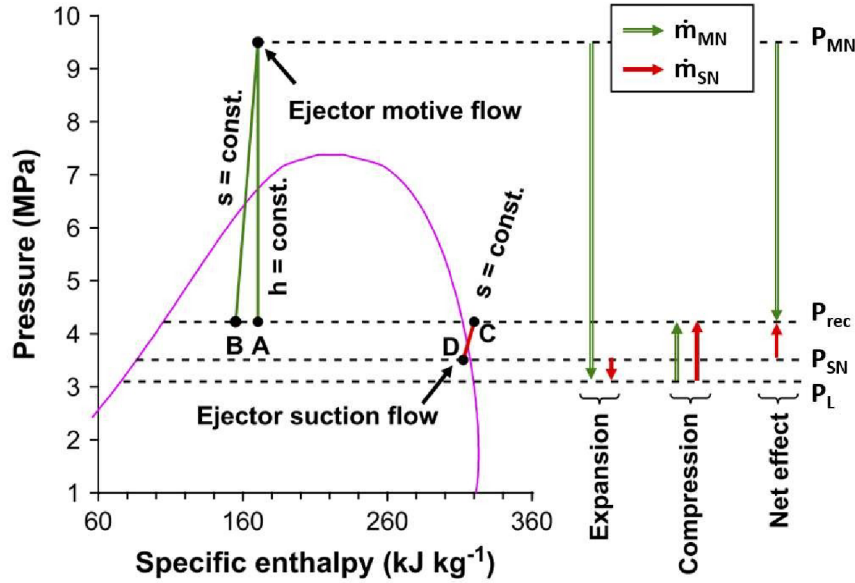


Figure 3.3 Expansion and compression of the motive and suction nozzle flow inside a two-phase ejector. Adapted from Elbel and Hrnjak [32].

The formula (as a dimensionless variable) can be interpreted as the amount of the total power applied to compress the entrained flow isentropically to the ejector outlet over the maximum theoretical work recovery potential. Additionally, the ejector efficiency is used as a universally accepted approach to assess the overall ejector energy performance by reflecting the total irreversibility that occurs inside the ejector passages. The efficiency can simply be calculated using the measured boundary operation conditions. From the formula, the liquid separator pressure (indicated as the ejector outlet pressure) plays a vital role in controlling the ejector efficiency.

$$\eta_{eje} = \frac{\dot{W}_{recv}}{\dot{W}_{recv,max}} = ER \frac{h_C - h_D}{h_A - h_B} = \frac{\dot{m}_{SN}}{\dot{m}_{MN}} \cdot \frac{h(P_{eje,out}, s_{SN}) - h_{SN}}{h_{MN} - h(P_{eje,out}, s_{MN})} \quad (3-3)$$

where the processes are:

A: isenthalpic throttling of the motive nozzle flow at the ejector outlet.

B: isentropic expansion of the motive nozzle flow at the same pressure level A.

C: isentropic compression of the suction nozzle flow at the same pressure level A and B.

D: suction nozzle flow at the inlet.

In this scope, Dvorak et al. has proposed the ejector efficiency based on the relation between the specific compression work acquired by the secondary stream and the specific work exerted by the primary flow [108]. Their formula has been used in many types of research [103, 109] and proposed a good agreement with the real equation (3-3) based on the ideal gas flow.

3.4 Energy and exergy analysis

In refrigeration systems, the energy efficiency of the cycle can be quantified by assessing the coefficient of performance (COP). It is defined as the ratio between the cooling capacities representing the heat transfer rate absorbed in the evaporator into the total compressor input power as the gross energy input to the cycle based on the first law of thermodynamic. The COP is described as:

$$COP = \frac{\dot{Q}_{evap}}{\dot{W}_{comp}} \quad (3-4)$$

where \dot{Q}_{evap} is the refrigeration capacity in kW, and \dot{W}_{comp} is the total internal compressors power in kW. It should be emphasized that the real system worked with many heat exchangers to control the exit gas cooler temperatures, maintain the requested degree of superheat, and provide a pure CO₂ vapor phase for the compressor suction line. However, the number of heat exchangers will not significantly affect the pressure drop compared with other refrigerants [5]. The advanced transcritical refrigeration systems usually operate with based and parallel compressors employing different evaporators for different applications (cooling, freezing, or air conditioning). Therefore, the cooling coefficient of performance can be calculated as follows:

$$COP = \frac{\sum_{i=1}^n \dot{Q}_{evap,i}}{\sum_{i=1}^n \dot{W}_{comp,i}} \quad (3-5)$$

When the ejector is integrated into the cycle, the performance of the refrigeration system could be evaluated by calculating the COP improvement ratio as follow:

$$COP_{improv} = \frac{COP_{ej} - COP}{COP} \cdot 100\% \quad (3-6)$$

Exergy efficiency is a very powerful parameter to assess the actual cooling system performance and individual thermodynamic process. The analysis compiles energy, mass conservation, and the second law of thermodynamics to analyze the system energy and improve the potential of each component. The specific exergy in any state is calculated as follows:

$$e_i(P, T) = (h_i - h_o) - T_o(s_i - s_o) \quad (3-7)$$

where e_i is the specific exergy in kJ/kg, h_o is a specific enthalpy at reference state in kJ/kg, s_o is a specific entropy at reference state in kJ/kg·K, T_o is reference state temperature in K.

Several methods are used to detect the location and magnitude of irreversible losses in energy conversion system, of which exergy analysis is the common method. This method detects losses in several ways. Conventionally, although irreversibility can be detected, the nature of the influence of individual components on each other in the system is not known as well as the possibility of eliminating individual inefficiencies. However, the advanced exergy model provides a comprehensive information on the exergetic performance of the system. The model quantitatively evaluates the interaction between the system components to determine the real system potential. The advanced exergy analysis is established based on the exergy destruction within a system based of constraints such as the system component under study and interaction with other components, manufacturing methods used and material costs and their influence on each other [96, 99].

The current thesis work considers a concept of the exergy initially proposed by Brodyansky et al. [110]. This method analyses the transiting exergy of the two-phase ejector to evaluate the ejector exergy efficiencies under different operating conditions. The transiting exergy of the material stream, which is the lowest exergy value, is characterized by the intensive parameters of the inlet and outlet parameters of the system. As a result of this approach, exergy consumed and produced can be clearly defined. Using this approach, the different pressure of the liquid separator from exergy destruction and efficiencies can be obtained to evaluate the performance under different working conditions of different motive pressure and temperatures as well as to characterize the behavior of three thermodynamic metrics that is, exergy produced, exergy consumed, and exergy destroyed. The transiting exergy efficiency used for the evaluation of a two-phase ejector is defined as follows;

$$\eta_{ej, tr} = \frac{\text{Exergy produced}}{\text{Exergy consumed}} = \frac{\Delta \dot{E}_{tr}}{\nabla \dot{E}_{tr}} \quad (3-8)$$

The exergy produced is the difference between the exergy flow rate at the outlet \dot{E}_{out} and the transiting exergy \dot{E}_{tr} as the lowest exergy value of a material stream, which is defined by the pressure and temperature at the inlet and outlet of a system along with the dead state temperature T_o (i.e., selected outdoor temperature). T_o was fixed to 20°C for all the exergy calculations. It is worth stating that the results associated with an exergy analysis are not substantially affected by the adopted dead state [111]. It is also assumed that the minimum velocity is equal to zero. The exergy consumed is the difference between the inlet exergy flow rate \dot{E}_{in} and the transiting exergy \dot{E}_{tr} . The exergy destruction or losses represent the difference between the exergy production and consumed or between the inlet and the outlet exergies. \dot{E}_{tr} is calculated as follows:

$$\text{if } (T_{in} > T_o \text{ and } T_{out} > T_o): \dot{E}_{tr} = \dot{E}(P_{min}, T_{min}, u_{min}) \quad (3-9)$$

$$\text{if } (T_{in} < T_o \text{ and } T_{out} < T_o): \dot{E}_{tr} = \dot{E}(P_{min}, T_{max}, u_{min}) \quad (3-10)$$

$$\begin{aligned} \text{if } (T_{in} > T_o \text{ and } T_{out} < T_o) \text{ or } (T_{in} < T_o \text{ and } T_{out} > T_o): \dot{E}_{tr} \\ = \dot{E}(P_{min}, T_o, u_{min}) \end{aligned} \quad (3-11)$$

$$\begin{aligned} \Delta \dot{E}_{tr} = \dot{m}_{MN} [e(P_{rec}, T_{rec}) - e(P_{rec}, T_o)] \\ + \dot{m}_{SN} [e(P_{rec}, T_{rec}) - e(P_{SN}, T_{rec})] \end{aligned} \quad (3-12)$$

$$\nabla \dot{E}_{tr} = \dot{m}_{MN} [e(P_{MN}, T_{MN}) - e(P_{rec}, T_o)] + \dot{m}_{SN} [e(P_{SN}, T_{SN}) - e(P_{SN}, T_{rec})] \quad (3-13)$$

The total exergies consumed and produced are linked with the motive and suction nozzle flow streams. The exergy production described by equation (3-12) emphasizes the increase of the specific thermal exergy. The temperature of the motive flow drops to the ejector outlet temperature caused by constant pressure addition at the mixing section. Likewise, the exergy of the suction fluid also increases towards the ejector outlet due to the same constant pressure addition. Furthermore, the first term in the exergy consumption shown in equation (3-13) characterizes the decrease in the specific thermo-mechanical exergy of the motive fluid due to expansion and temperature drop. The second term shows the decrease in the specific thermal exergy of the suction nozzle flow due to constant pressure and increase in temperature. Further

details can be seen in reference [81]. For the exergy calculations, all the thermodynamic properties of CO₂ are generated by using the NIST REFPROP 10 database.

The total exergy output of the cooling mode is determined as an exergy rate increment in the evaporator as follows:

$$\dot{E}_{out} = \dot{m}_{evap} \cdot e_{incr} \quad (3-14)$$

where \dot{E}_{out} represents the total exergy rate output in kW. According to Fang et al. [112], the exergy increment (e_{incr}) of the amount of heat (q) in kJ/kg, at which the temperature of the heat source or heat sink changed from T_1 to T_2 , is defined in equation (3-15) and the efficiency based on the second law is defined in equation (3-16). In addition, the performance of the refrigeration system supported with ejector could be evaluated by calculating the exergy improvement ratio as follows [92]:

$$e_{incr} = q \cdot \left| 1 - \frac{T_0 \cdot \ln(T_1/T_2)}{T_1 - T_2} \right| \quad (3-15)$$

$$\eta_{ex} = \dot{E}_{out} / \dot{W}_{comp} \quad (3-16)$$

$$\eta_{ex,improv} = \frac{\eta_{ex,ej} - \eta_{ex}}{\eta_{ex}} \cdot 100\% \quad (3-17)$$

The Energy balance equations and the exergy destruction rate (\dot{D}) related to each component presented are mathematically described as follows:

- For compressor:

$$\dot{W}_{comp} = \dot{m}_{comp} \cdot (h_{comp,out} - h_{comp,in}) \quad (3-18)$$

$$\dot{D}_{comp} = \dot{m}_{comp} \cdot (e_{comp,in} - e_{comp,out}) + \dot{W}_{comp} \quad (3-19)$$

- For evaporator:

$$\dot{Q}_{evap} = \dot{m}_{CO_2} \cdot (h_{evap,out} - h_{evap,in}) \quad (3-20)$$

$$\dot{D}_{evap} = \dot{m}_{evap} \cdot (e_{evap,out} - e_{evap,in}) + \dot{m}_{evap} \cdot e_{evap,incr} \quad (3-21)$$

- For gas cooler:

$$\dot{Q}_{GC} = \dot{m}_{CO_2} \cdot (h_{GC,in} - h_{GC,out}) \quad (3-22)$$

$$\dot{D}_{GC} = \dot{m}_{GC} \cdot (e_{GC,in} - e_{GC,out}) + \dot{m}_{GC} \cdot e_{GC,incr} \quad (3-23)$$

- For expansion valve:

$$\dot{m}_{in} \cdot h_{in} = \dot{m}_{out} \cdot h_{out} \quad (3-24)$$

$$\dot{D}_{ex,v} = \dot{m}_{ex,v} \cdot (e_{in} - e_{out}) \quad (3-25)$$

- For ejector:

$$\dot{D}_{ej} = \dot{m}_{MN} \cdot e_{MN} + \dot{m}_{SN} \cdot e_{SN} - (\dot{m}_{MN} + \dot{m}_{SN}) \cdot e_{ej,out} \quad (3-26)$$

The total destruction of the cooling system is a sum of the exergy destruction of each component. However, the set of the exergy and energy balance equations will facilitate the identification of irreversibilities concerning each component and illustrate the ejector's contribution to the system improvement.

4 EXPERIMENTAL METHOD

This section will report on the test facility installed at the Norwegian University of Science and Technology/SINTEF laboratory in Trondheim-Norway, where the experimental work took place. The description of the system setting and the components were mention in detail. The chapter also includes the monitoring acquisition system and the instrumentations used together with the uncertainty analysis.

4.1 Test facility Set-Up

The experimental work was performed on the R744 transcritical cooling system, which was installed at the NTNU/SINTEF energy research laboratory in Trondheim-Norway and modified for the experiment of the vapor ejectors. The test rig was manufactured by Enex Company in collaboration with Danfoss Company and SINTEF Energy Research. The experiment was implemented on the commercial ejector cartridge type ELP60 by Danfoss denoted by (VEJ_1), as shown on the test rig represented in Figure 4.1. This ejector characterizes the smallest profile produced by the manufacture, which has not been studied before. The facility consisted of a refrigerant circuit using R744 as the refrigerant and a glycol cycle which was integrated to serve as a gas cooler heat sink and the evaporator heat source.

The process and installation diagram of the system can be seen in Appendix A, including the electrical and controlling circuits. However, the simplified R744 vapor compression unit pipeline and instrumentation diagram (P&ID) is illustrated in Figure 4.3. Additionally, the auxiliary cooling water network was utilized to provide the cooling media for the second-stage gas cooler. The refrigerant loop of the multi-ejector test rig contains MT based-load compressor and two other parallel compressors. The unit has six different heat exchangers for heat rejection and absorption, including internal heat exchanges. The system is supplied with appropriate oil management, which consists of an oil separator and an oil reservoir with several solenoid valves connecting the oil separators to the reservoir and feed the returning oil to the compressors.

The system contains three electronic expansion valves manufactured by Danfoss. There is a high-pressure valve (HPV) that reduces the pressure at the outlet of the gas cooler to an intermediate pressure level of the liquid separator, whereas the other two work as metering valves at evaporators. There are 50-L pressure tanks liquid receiver and separator, which are

provided with liquid level indicators. The facility data acquisition system is supplied with temperature sensors, pressure transmitters, and calibrated mass flow meters for refrigerant and glycol circuits. HPV was running in parallel with the ejector to secure having an accurate high-pressure level during the system operation. The ejector and HPV help to control the suction accumulator tank pressure level by changing the HPV opening degree and determining the multi-ejector block capacity. The ejector inlet port for the motive flow stream is connected to the gas cooler outlet through the mass flow meter. Both ejector vapor and liquid suction are provided with a separate mass flow meter aiding to monitor the flow into the ejector from the liquid receiver located upstream. The ejector discharges the outlet mixed flow into the liquid separator, where the vapor is separated and compressed by the parallel compressors. The liquid portion is fed back the evaporators through the expansion valves and then the refrigerant is recirculated to the suction accumulator tank.

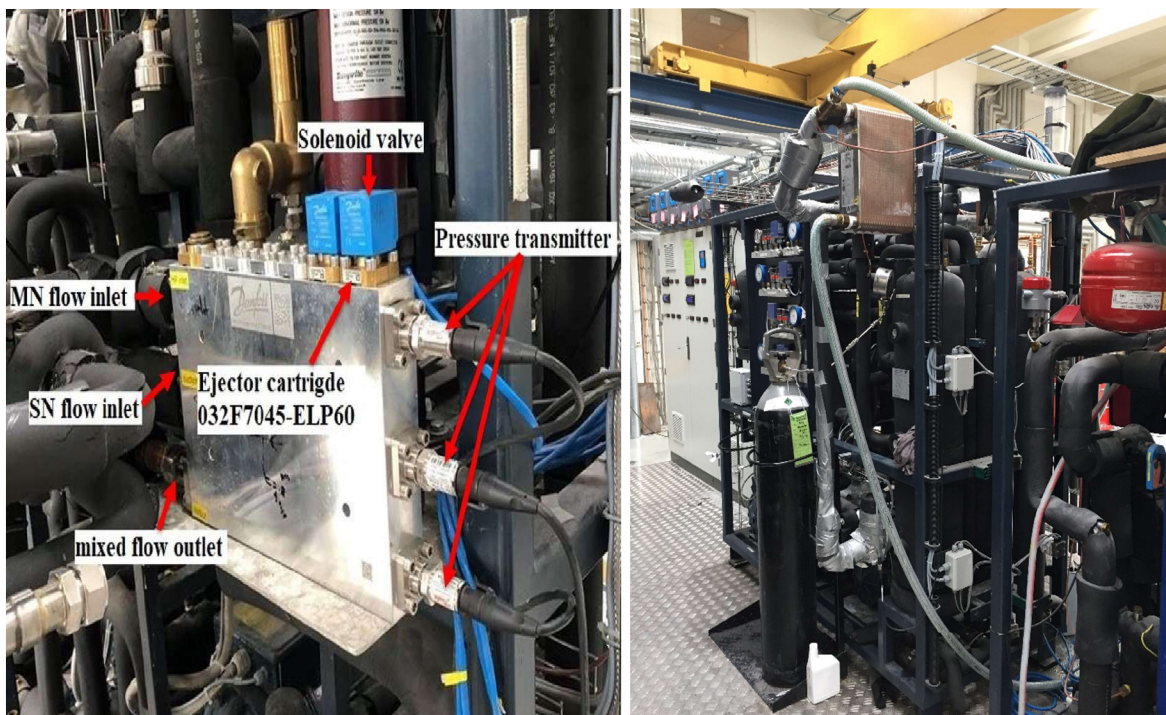


Figure 4.1 The test rig equipped with a multi-ejector pack.

The system consists of different pressure levels described in different colors. The CO₂ loop consists of a high-pressure level (red lines), which varies from 110 bar to 50 bar from the compressor discharge to the HPV and ejector motive nozzle. Afterward, the refrigerant will be throttled to the intermediate pressure level from 50 bar to 30 bar (green lines) and passed to the liquid separator. The liquid part in the receiver is supplied to the evaporators with the required

refrigerant through the connected thermal expansion valves while the receiver vapor part is connected with the parallel compressors suction line. The throttled refrigerant from the evaporators flows to the suction accumulator tank, which is represented as the low-pressure level (MT pressure) at 25 bar to 30 bar (blue lines), where the liquid separation takes place, and fluid recirculated to the ejector suction manifold and base-load compressor.

The ejector performance is controlled by the liquid separator pressure level, which represents the ejector discharge mixed-flow pressure together with the inlet pressure and temperature of the motive and suction nozzle flow streams. The system was designed to control and maintain all the required boundary conditions flexibly by following different procedures. For example, it adjusts the inlet coolant water mass flow rate in the gas cooler to control the motive nozzle flow temperature. Similarly, it controls the receiver pressure by regulating the opening degree of the flash gas valve, etc.

4.2 System components description

4.2.1 The compressors rack

The system contains three semi-hermetic reciprocating compressors, which were manufactured by Dorin company and are illustrated in Figure 4.2. The compressors could vary the capacity based on the requested load and suction line parameters by changing the frequency. The compressor models are (Dorin CD1400H) as the based-load compressor and (Dorin CD1000H and Dorin CD380H) representing the parallel compressors containing inverters for continuous work regulation.

The compressors manufacturer provides polynomial functions for each compressor, as shown in equation (4-1). The functions are used to determine the electric power supply in W and the mass flow rate of the refrigerants in kg/s at a nominal frequency of 50 HZ.

$$y = C_1 + C_2 \cdot T_{evap} + C_3 \cdot P_d + C_4 \cdot T_{evap}^2 + C_5 \cdot T_{evap} \cdot P_d + C_6 \cdot P_d^2 + C_7 \cdot T_{evap}^3 + C_8 \cdot P_d \cdot T_{evap}^2 + C_9 \cdot T_{evap} \cdot P_d^2 + C_{10} \cdot P_d^3 \quad (4-1)$$

where y represented the compressor power and discharged R744 mass flow rate, P_d is the discharged compressor pressure in bar and T_{evap} is the evaporation temperature in °C. The constants value for Dorin CD1400H and CD380H are mentioned in Table 4.1, since they will be used in the modeling.



Figure 4.2 R744 piston-type compressors pack. Base-load compressor (Dorin CD1400H) at the left and parallel compressors (Dorin CD1000H and Dorin CD380H) at the right.

Table 4.1 Dorin compressors polynomial coefficients [113].

Coefficients	Dorin CD 1400H		Dorin CD 830H	
	mass flow kg/s	power W	mass flow kg/s	power W
C ₁	2.43638E-01	-11206.18000	8.43560E-02	-3929.07860
C ₂	6.69282E-03	-414.00102	2.38595E-03	-156.06729
C ₃	-9.26341E-04	454.41647	-3.94810E-04	162.77111
C ₄	6.26562E-05	-4.56956	2.26064E-05	-1.98566
C ₅	-5.22192E-06	6.01739	-3.17360E-06	2.39803
C ₆	2.73504E-06	-3.03982	1.03439E-06	-1.10325
C ₇	0	-0.01238	0	-0.00823
C ₈	0	0.01547	0	0.00926
C ₉	0	-0.01583	0	-0.00630
C ₁₀	0	0.00858	0	0.00291

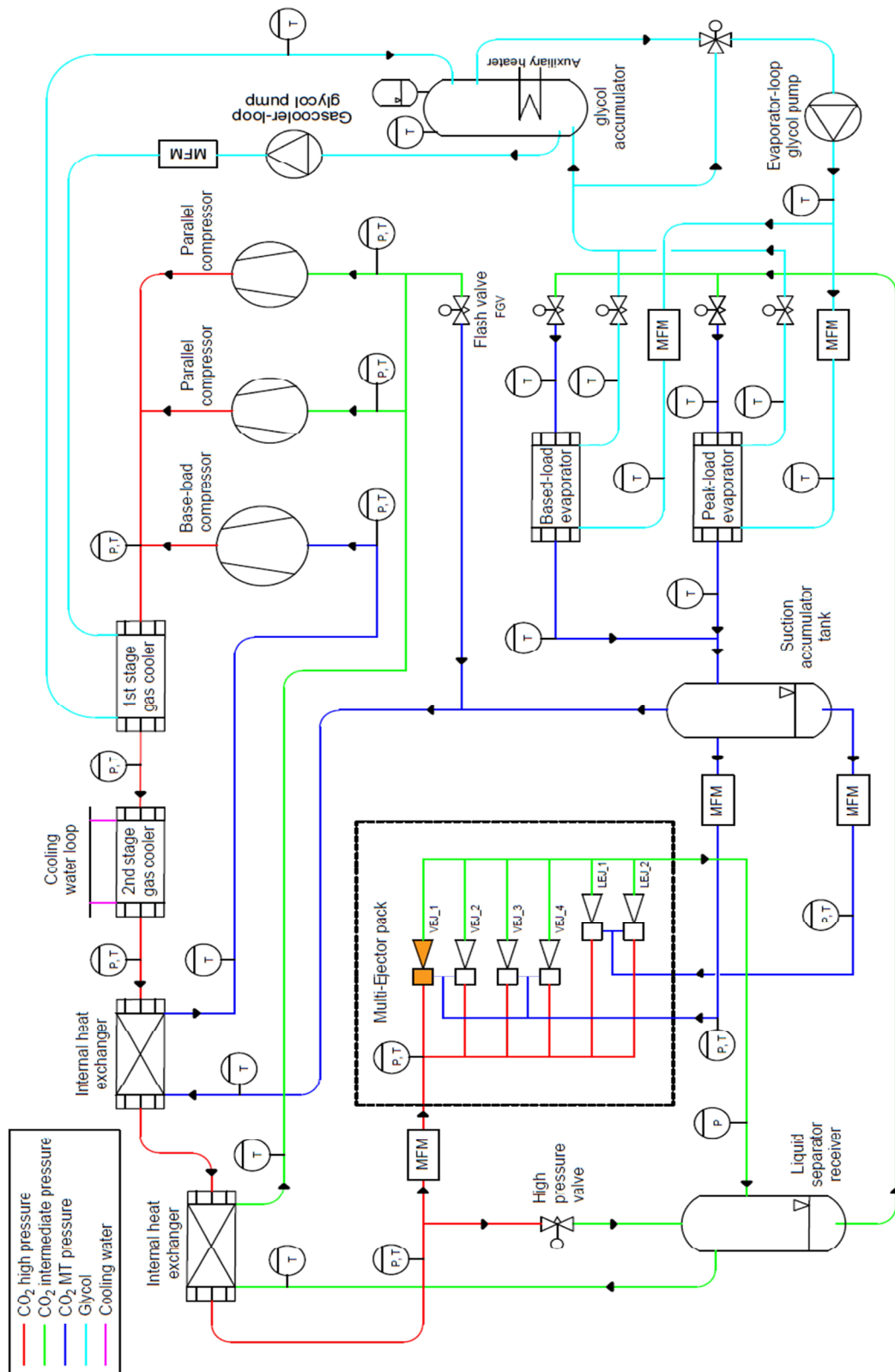


Figure 4.3 The Simplified process and instrumentation diagram of the experimental test facility, including the R744 refrigerant and the glycol loop.

4.2.2 The ejector profile

The test rig was equipped with a multi-ejector pack type (CTM-6 LP 935) manufactured by Danfoss and containing a series of parallel ejector cartridges. There are shut-off valves (solenoid valves) installed on every cartridge that allow control of the motive nozzle individually to supply the high-pressure flow. There exist four vapor ejectors and two liquid ejectors connected with two different liquid separator suction ports to feed the ejector with vapor and liquid, as well as to control the suction flow steam quality by mixing. However, this experimental work was performed using the ejector cartridge type (032F7045 CTM ELP 60), as illustrated in Figure 4.4. The main cartridge geometries are shown in Table 4.2.

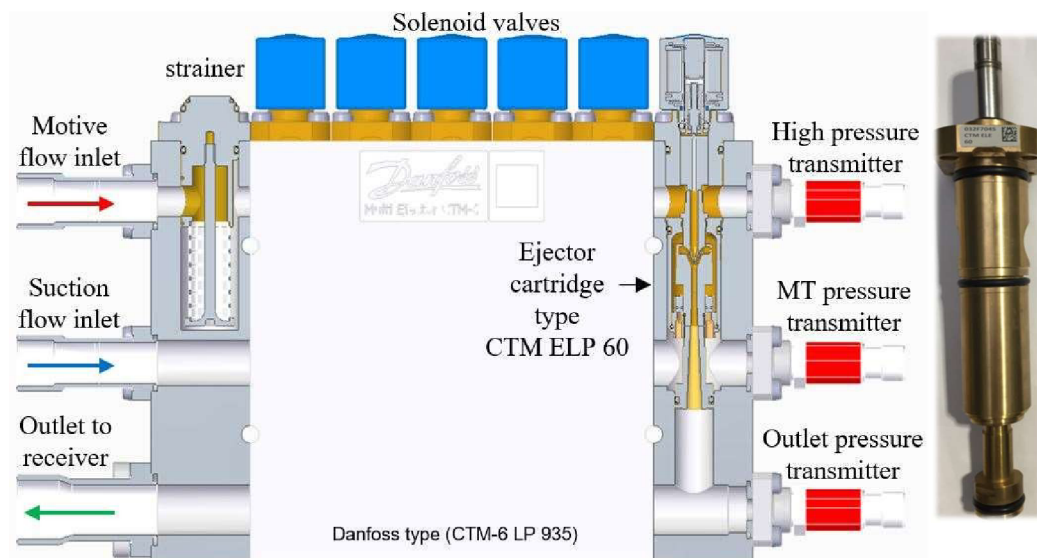


Figure 4.4 Sketch of the multi-ejector block and the used cartridge from Danfoss (for internal use only) [100].

Table 4.2 Ejector cartridge CTM ELP 60 main geometry parameters.

Parameter name	Unit	Value
Motive nozzle inlet diameter	mm	3.8
Motive nozzle throat diameter	mm	0.71
Motive nozzle outlet diameter	mm	0.78
Motive nozzle converging angle	degree	30
Motive nozzle diverging angle	degree	2
Diffuser diameter	mm	7.3
Diffuser angle	degree	5

4.2.3 Heat exchangers

The system utilized six different heat exchangers as following:

- Type (SWEP B18Hx100) brazed plate heat exchanger with 30 plates serves as the first stage gas cooler.
- Two brazed plate heat exchangers with 20 plates type (Kaori K095C-30C- NP8M), one serves as the second stage gas cooler and the other as a peak-load evaporator.
- Type (SWEP B16DWHx100) brazed plate heat exchanger with 30 plates serves as the base-load evaporator.
- Two internal heat exchangers are connected to the house glycol/water supply system.

The gas coolers control the outlet temperature of the refrigerant by absorbing heat using the glycol loop. In contrast, the internal heat exchangers are utilized to set the subcooling degree as protecting the compressors from having any liquid droplets at the suction line.

All the result was collected at the steady-state conditions, assuming that the heat absorbed by the evaporator equals the load rejected by the glycol loop. The ethylene glycol used in the system consists of 70% water and 30% glycol in volume concentration. However, for the glycol brine loop, the specific heat capacity used to calculate the total heat load rejected can be expressed as follows [114]:

$$C_p(T_{gly}) = 0.0028 \cdot T_{gly} + 3.5896 \quad (4-2)$$

Where $C_p(T_{gly})$ represents the specific heat capacity in kJ/ kg.K and T_{gly} is the glycol temperature in °C.

4.2.4 Valves and tanks

The system includes a different set of electronic expansion valves manufactured by Danfoss and applicable for R744. The valves regulate the pressure reduction based on the system controller signal by changing the opening degree. They can be stated as follow:

- The high pressure valve and the flash gas removal valve are type CCMT8, manufactured by Danfoss and operated with a maximum pressure of 140 bar.
- Two Danfoss metering valves type CCM20 are for the evaporators with a maximum working pressure of 90 bar.

The system is also secured with safety and shut-off valves in addition to the electronic expansion valves. The test rig is equipped with the next tank receivers:

- 200-liters IMA thermal storage tank for the glycol.
- 21-liters Frigomec pressure vessel for oil accumulator.
- Two 50-liters Frigomec pressure vessels for suction accumulator tank (known as liquid receiver) and liquid separator supplied with AKS 4100 Danfoss level sensors.

4.2.5 Data acquisition and monitoring system

The facility is supplied with a data acquisition system containing temperature and pressure sensors to control, safeguard and monitor the test rig. Additionally, the system is provided with inverters and mass flow meters to set the operating conditions, as shown in Figure 4.3. The sensors can be described as follows:

- Pressure gauges are piezoelectric transmitters type AKS 2050 manufactured by Danfoss. The sensors vary from 0 bar to 150 bar depending on location in the system and alter the measured absolute pressure as voltage output signals synchronized to the system.
- Mass flow meters are type Coriolis RHEONIK RHM06 for refrigerant circuit and RHEONIK RHM15 for glycol circuit. The flow meters working principle is based on the vibration of the curved tube as a function of the phase shift angle between the inlet and the outlet flow. During the experiment, six different sizes of the Coriolis Effect mass flow meters were used, as illustrated in the P&ID diagram.
- Temperature sensors type AKS 21 A PT1000 were manufactured by Danfoss. The resistance thermometer working range is from -70 °C to 180 °C. The sensor working principle is based on the proportional relation between the electrical resistance of the platinum coil build inside the sensor and the measured temperature magnitude.
- Frequency inverter IP55/Type 12 measures the electric power consumption and adapt the frequency from 30Hz to 60Hz manufactured by Danfoss.

The instrumentation accuracy and their data range used to monitor and control the test rig are listed in Table 4.3.

All the output signals from each sensor are transmitted and processed by the control unit to the Minilog system, which is set to record them in the computer every five seconds and to treat any specific parameter during the experiment. The system is very flexible in operation. It is working in automatic mode and can shift some equipment to manual operation for some testing. The time step for the averaging collected data was assumed to be six minutes to minimize the fluctuation and the oscillation of the result and to ensure the stabilization of the

parameter. The recorded data was converted to .csv files, then sorted and converted to an ME post-processing spreadsheet for further analysis. More details regarding the test facility operating and setting can be found in the operators manual provided by NTNU, Department of Energy and Process Engineering [115].

Table 4.3 The set of the instrumentations used for experimental investigation

Measured quantity	Instrument	Data range	Accuracy
Temperature	Resistance thermometer PT1000	-70°C÷180°C	$\pm(0.3 + 0.005 t)$, T in °C
Mass flow rate	Coriolis-type RHM06	0÷20 kg min ⁻¹	$\pm 0.2\%$ of reading
	Coriolis-type RHM15	0÷200 kg min ⁻¹	$\pm 0.2\%$ of reading
Pressure	Piezoelectric transmitter	0÷150 bar	$\pm 0.3\%$ of reading
Electric power consumption	Inverter IP55 Type 12	0÷20 kW	± 0.05 kW

4.3 Uncertainty analysis

Error in uncertainty analyses is a difference between the true value and measured value. In other words, the results obtained experimentally by measuring represent the approximations of actual value of specific quantity. The uncertainty analysis accompanied the measurements to justify the quality and reliability of the experimental results and the derived quantities. The uncertainty used to reflect the error distribution of these indirectly measured variables were calculated based on Guide to the Expression of Uncertainty in Measurement [116].

The experimental measurements include two types of errors, random and systematic errors. The random error (error of the precision index of a measurement) indicates the unexpected error that affects the measurement precision and implies fluctuations in measurement device readings either below or above the true value, usually expressed as error bars. Random error can be decreased by averaging repeated measurements for the same collected data conditions. The systematic error (accuracy of indicator) is considered to be a fixed error at which repeating the measurement will lead to new results differing from the other values. It can be caused by the limitation of the measuring method, imperfect calibration of the devices, and the impact of the environment on the measurement process. This means that repeating the same set of the collected data will not improve the accuracy and may be corrected by refining the measurement method or calibrating the instruments.

The standard uncertainty can be attained from the arithmetic means of the measured values distribution. The standard uncertainty can be divided into two types; based on the series of measurements (type A) and other elements, including data from calibration, manufacture specifications, and previously measured data (type B). Type A usually provides the best estimation through the arithmetic mean value expressed in the experimental standard deviation. On the other hand, type B depends on the considered correlations for different sensors in the unit. However, the law of propagation of uncertainty has been applied for the experimental measurements since the measurands were calculated from other variables defined by a room-sum-square method:

$$u_{(y)} = \sqrt{\sum_{i=1}^n \left(\frac{\partial f}{\partial x}\right)^2 u_{(x)}^2} \quad (4-3)$$

where y represents the measurand, $u_{(x)}^2$ is the total standard uncertainty, the partial derivative $\frac{\partial f}{\partial x}$ is the sensitivity coefficient (SC) describes how the output measurand varies with changes in the values of the input arithmetic mean. The uncertainty values for the main collected data and derived functions were registered in Table 4.4.

Table 4.4 The uncertainty values for the main collected data and derived functions.

Quantity	unit	uncertainties values
Pressure	bar	±0.3
Temperature	K	±0.18
COP	-	±0.27
Mass flow rate	kg/s	±7.5E-5
Entrainment ratio	-	±3.1E-3
Ejector efficiency	-	±6.9E-3
Work recovery rate	kW	±3.1E-5
Overall available work	kW	±8.2E-4
Compressor power consumption	kW	±0.05

5 RESULTS AND DISCUSSION

This chapter aimed to provide two main things; first, it will present an extensive result on the ejector performance map and clarify the influence of different operation conditions on the behavior of the ejector performance through a sensitive analysis of different variables. The ejector performance was measured in terms of entrainment ratio, pressure lift, ejector efficiency, and work rate recovery, including the exergy distribution investigation based on the collected experimental data. The second part will illustrate the impact of this ejector profile on the system performance and its contribution to energy savings.

The system is a comprehensive test rig with many experimental possibilities involving testing an extensive range of system conditions and configurations. The experimental work was carried out to evaluate the two-phase flow ejector performance under various operating conditions. Figure 5.1 represents the experimental operation points selected. The motive nozzle MN flow conditions for the working ejector are illustrated in Figure 5.1(a). The ejector motive nozzle flow pressure was tested at 60, 70, 80, 90, and 100 bar, whereas the outlet temperatures of the gas cooler were varied for 20, 25, 30, and 35 °C to evaluate the ejector at transcritical and subcritical regions. The evaporation temperatures were selected in terms of refrigeration application usage at -6 °C and -3 °C with ejector suction nozzle SN flow pressure between 29.5 and 32 bar, as shown in Figure 5.1(b). The ejector outlet conditions were determined by the liquid separator pressure and the vapor quality defined based on the energy balance for the motive and suction nozzle flow to the ejector outlet, as represented in Figure 5.1(c). Overall, around 236 experimental tests were conducted to form a qualitative test campaign related to the different tendencies of separator pressure and entrainment ratio. During the operation, if the liquid mass of the ejector outlet two-phase flow at the liquid separator is in balance, then the system is running at a steady-state condition. In that case, the measurement data can be collected and analyzed. For that reason, the coefficient of liquid mass balance in the liquid separator (β) was determined using equation (5-1), which indicates the ejector expansion system steady-state operation and shows how the load at the heat exchangers is stable [117]. This coefficient depends on the ejector mass entrainment ratio and the liquid fraction of the ejector outlet flow. If the coefficient value is situated close to zero, then the system is running at its ideal state, and thus, the steady-state condition has been reached.

$$\beta = x_{rec} + \frac{x_{rec}}{ER} - 1 \tag{5-1}$$

The result in Figure 5.1(d) indicates that the ejector was running under steady-state conditions and the coefficient of liquid mass balance rises with higher liquid separator pressure because of the mass entrainment ratio decreases, which results in less liquid mass flow from the separator compared to the liquid mass flow from the ejector exit. This result might be similar when comparing the coefficient of liquid mass balance at higher pressure of the motive nozzle flow. The specific enthalpy of the motive flow CO₂ will decrease and the mass fraction at the ejector exit will be increased to obtain a similar trend.

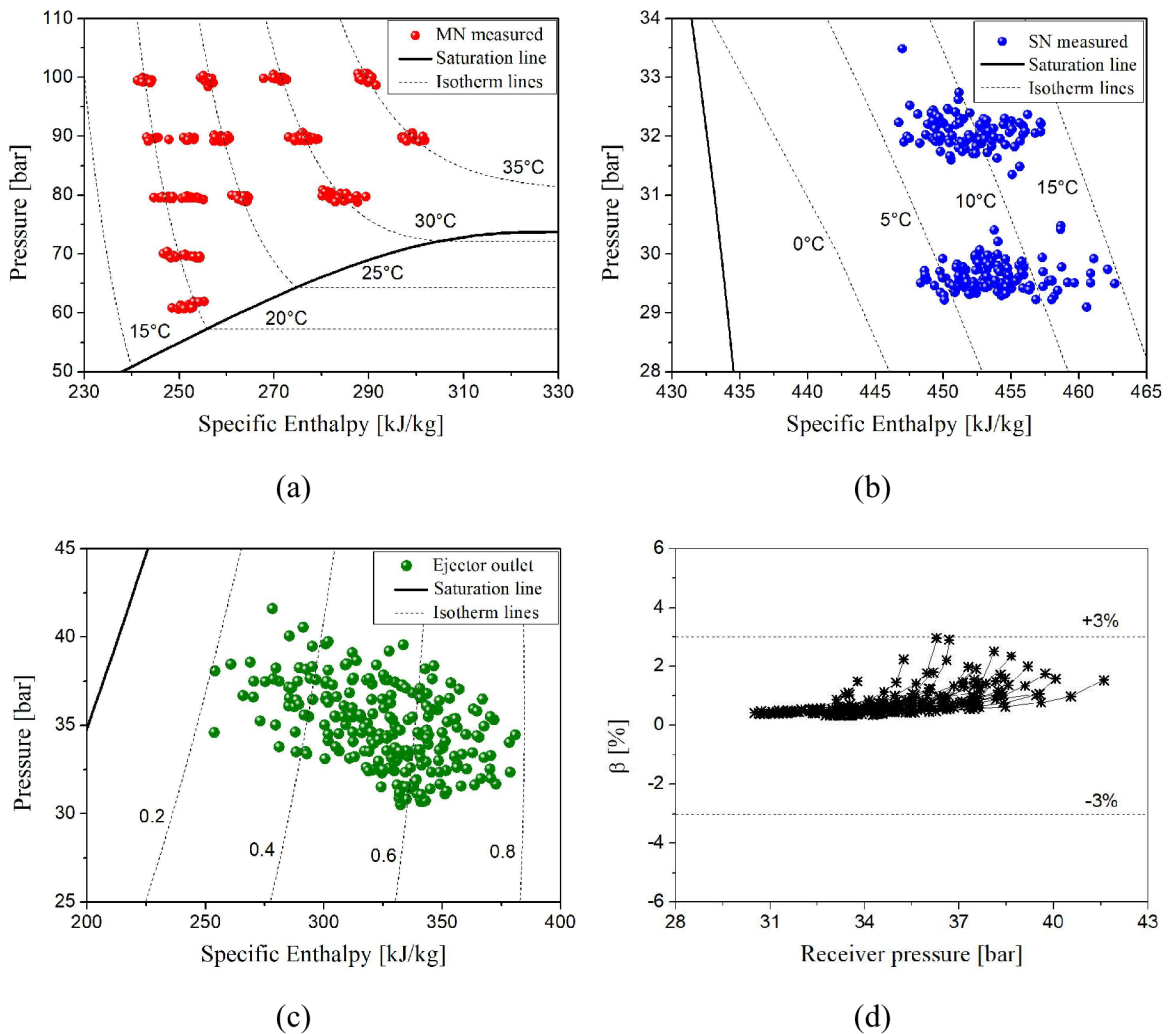


Figure 5.1 R744 ejector overall conducted experiments, (a) p-h diagram representing MN flow inlet conditions, (b) p-h diagram representing SN flow inlet conditions, (c) p-h diagram representing the outlet mixed flow to the liquid separator, (d) the calculated coefficient of liquid mass balance for different liquid separator pressure.

5.1 Effect of the operation conditions

In this section, the ejector operating parameters such as pressure lift, mass entrainment ratio, ejector efficiency, and work rate recovery will be discussed at different boundary conditions. In Figure 5.2, a comparison between the maximum ejector pressure lift with different inlet motive nozzle flow conditions is illustrated for all the collected data. The results reveal the expected outcome based on the ejector theory. At higher motive pressure, the ejector performed higher pressure lift according to the high expansion work potential in the motive nozzle. Measuring different ranges of the motive nozzle flow temperature (the gas cooler outlet temperature) at low motive pressure was not possible due to the system functional limitation. However, it can be noted that the lowest measured value for the pressure lift was 0.81 bar and the highest was 9.51 bar. Besides, the maximum pressure lift gained at $P_{MN} = 60, 70, 80, 90,$ and 100 bar were 4.91, 5.57, 7.19, 8.98, and 9.51 bar, respectively.

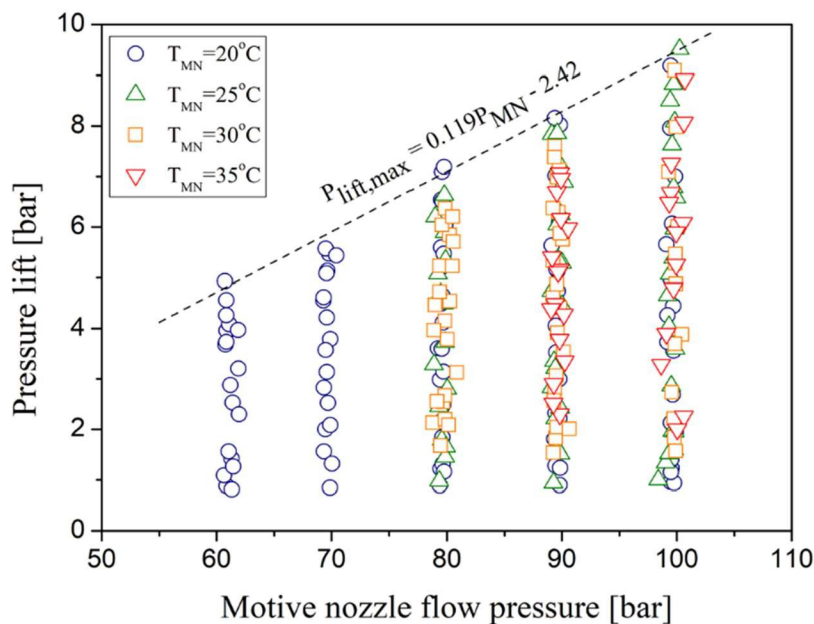


Figure 5.2 Pressure lift as a function of motive nozzle inlet pressure.

Based on the experimental result, the ejector maximum pressure lift could be predicted in terms of the gas cooler pressure with linear relation, as presented in Figure 5.2. The correlation could help the controller system define the highest possible ejector pressure lift, which indeed reduces the parallel compressor pressure ratio and plays a role in saving energy consumed and contribute to improving the system performance.

The ejector efficiency proved an effective compression over the most working range conditions. Giving the result presented in Figure 5.3, the ejector recorded the highest efficiency of 0.369 at $P_{MN} = 90$ bar and $T_{MN} = 25$ °C. The graph represents the best working region of the ejector efficiency at which the pressure lift of the ejector can be selected. It can be noted that the points characterized by efficiency greater than 0.30 are recorded at a substantial P_{lift} from 2.4 to 8.2 bar.

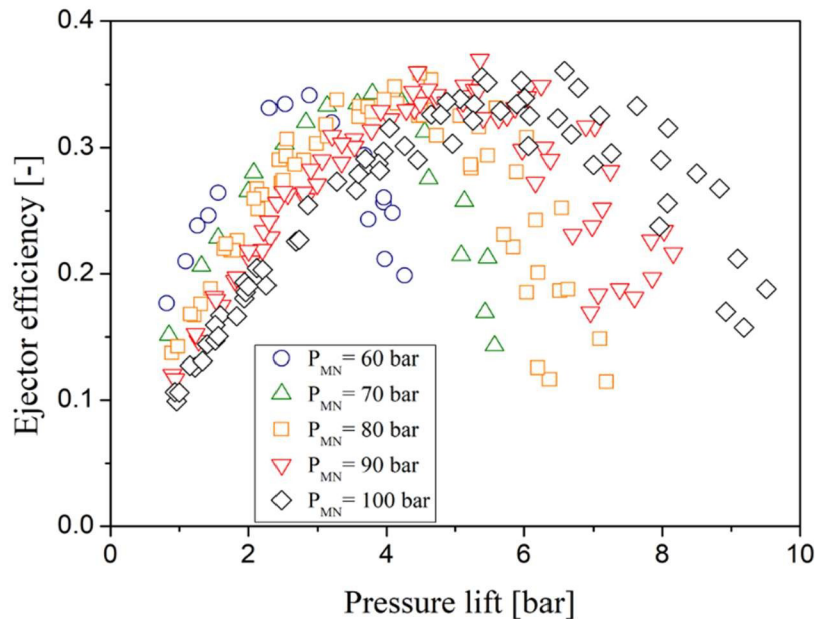


Figure 5.3 Variation of ejector efficiency with pressure lift at different motive nozzle pressure.

Moreover, increasing the motive nozzle flow pressure or temperatures will shift the working ejector efficiency peak to be at a higher pressure lift and extend the high efficiency region where the ejector can operate. For example, at $P_{MN} = 70$ bar, the ejector could work with reasonable efficiency higher than 0.1 with pressure lift from 0.8 to 5.6 bar, whereas at $P_{MN} = 100$ bar the range is extended to $P_{lift} = 9.5$ bar. Compared to the previous study in this field, the result concluded by Banasiak et al. [105] experimentally demonstrated that the ejector efficiency of 0.3 could be achieved for an individual ejector hosted in a multi-ejector pack concerning the pressure lift and other inlet flow conditions. The current ejector cartridge efficiency was reasonably consistent with the results reported by Banasiak et al. [43], who registered a similar efficiency range when testing four different ejector cartridges with larger geometries. Furthermore, Fredslund et al. [118] obtained field data from installations placed in various places. The results observed vapor ejector efficiencies above 0.25 measured in the laboratory at typical operating conditions ($P_{lift} = 6$ bar).

Boccardi et al. [70, 71] evaluated a multi-ejector expansion pack having four different ejector geometries with motive nozzle throat diameters from 0.7 mm (similar to the current work) to 2.0 mm. The result revealed a maximum ejector efficiency, calculated by equation (3-3), of 0.18 due to the module's design for high pressure lift and low ER. Lucas et al. [66] recorded a maximum ejector efficiency of 0.22 in the experimental investigation using 0.62 mm throat diameter of driving nozzle at various operation conditions. The authors stated that the pressure losses within the mixing chamber most significantly affect the ejector efficiency. Despite all attempts to control the ejector discharged pressure to recover the expansion work effectively by regulating the motive nozzle geometries, controlling the mixer/diffuser geometries would be a challenging research to reach higher efficiency in the future. Moreover, Haida et al. [92] and Banasiak et al. [69] managed to reach high efficiency up to 0.33 based on their different geometries and operating conditions for R744 systems even though higher ejector efficiency were published for other systems using different working fluids than CO₂ [119]. Thus, to equip the ejector in an ideal way, the ejector pressure lift should be better adjusted according to the gas cooler heat sink conditions. Hence, the overall system performance will be maximized.

In such an analysis, it is not easy to represent the performance map of the ejector because the suction nozzle mass flow rate is a function of many derivative parameters such as entrainment ratio, work recovery rate, and ejector efficiency. However, Figure 5.4 introduces the mass entrainment ratio characteristics at different liquid separator pressure. The analysis was performed at different motive nozzle flow pressure and temperature concerning two different evaporation temperatures, mainly -6 °C and -3 °C (approximately $P_{SN} = 29.5$ and 32 bar). The results expose the expected outcome based on the ejector theory principles. It is observed that the pressure lift is inversely proportional to mass entrainment ratio of the ejector, at which increasing the liquid separator pressure for higher P_{lift} causes the mass entrainment ratio to drop sharply. This can be clarified by the working region mode of the ejector. For instance, when the liquid separator pressure is increasing, the shock waves will move closer to the region where the mixing process occurs and disturb the mixing. As a result, the suction nozzle flow stream will no longer be choked in the mixing chamber. Thus, less amount of suction nozzle fluid is drawn, and the mass entrainment ratio decreases further [120].

Figure 5.4(a) illustrates the effect of different motive nozzle flow pressure on the ejector as the required amount of energy needed to accelerate and suck the suction flow by transforming the pressure energy of the motive flow into kinetic energy while mixing. Therefore, the mass entrainment ratio was predicted over several liquid separator pressure range. At double choking mode, when the motive nozzle flow pressure is increasing at constant motive flow temperature ($T_{MN} = 20 \text{ }^\circ\text{C}$), the ejector will work at lower mass entrainment ration and operate at higher critical pressure (the exit pressure where the double choking mode ends). The reason is associated with the increase of motive nozzle mass flow rate and with enlargement of the expansion angle at the motive nozzle exit flow jet, causing a reduction of the ejector annular effective area (area formed by the primary jet core and the mixing chamber wall where the suction fluid flow is choked) and increasing the resulting momentum of the mixed stream due to the higher velocity of the entrained stream attained. Therefore, the shock waves will move downstream with a high compression ratio and pressure lift.

On the other hand, if both motive and suction nozzle flow pressure and temperature will remain constant with increasing the liquid separator pressure, then the mass entrainment ratio will remain constant as represented in Figure 5.4(a) at the critical mode only for the case at $P_{MN} = 100 \text{ bar}$ and P_{rec} from the range of 30.5 bar to 31.18 bar within $ER = 0.7$. Conversely, when the ejector operates at a single choking mode, increasing the motive nozzle flow pressure at fixed motive flow temperature will decrease the entrainment ratio at a higher liquid separator pressure range. This reduction will be characterized by a steeper slope at lower motive nozzle flow pressure. According to the author's knowledge, most of the vapor compression CO_2 ejectors work in subcritical mode. The figure also illustrates the possible liquid separator working range at each motive nozzle pressure. For example, at $T_{evap} = -6 \text{ }^\circ\text{C}$ the ejector could work till $P_{rec} = 34.6, 35.2, 36.6, 38,$ and 38.5 bar at $P_{MN} = 60, 70, 80, 90$ and 100 bar respectively. Besides, at $T_{evap} = -3 \text{ }^\circ\text{C}$, as shown in Figure 5.4(b), the liquid separator working range will shift to start at $P_{rec} = 33 \text{ bar}$.

When the system is working at a relatively higher evaporation temperature, then the suction nozzle flow pressure will increase, and at fixed motive flow conditions, the ejector will produce a higher entrainment ratio. This comes at a sacrifice of ejector pressure lift, as can be seen in Figure 5.4(b), where the highest possible $P_{lift} = 6.51$ at and $T_{evap} = -3 \text{ }^\circ\text{C}$ comparing with 9.18 bar at $T_{evap} = -6 \text{ }^\circ\text{C}$. For example, at $P_{MN} = 60 \text{ bar}$ and $P_{rec} = 33.5 \text{ bar}$, the mass entrainment

ratio increased from 0.248 to 0.809 while P_{lift} dropped from 3.96 to 0.891 bar within increasing T_{evap} from -6 to -3 °C. Likewise, at $P_{MN} = 80$ bar and $P_{rec} = 32.9$ bar, ER increased by 39% with 2.72 bar declined. Overall, higher evaporation temperature served for a higher ejector mass entrainment ratio, while lower evaporation temperature for freezing and cooling applications will provide a high ejector pressure lift and compression ratio.

To find out the optimum motive nozzle flow condition, one can compare with the highest entrained suction nozzle flow at the widening range of liquid separator pressure, high ejector efficiency, and great pressure lift could be gained. Among the different inlet motive nozzle flow pressures, 90 bar provided the maximum ejector performance based on the high efficiency and pressure lift comparatively.

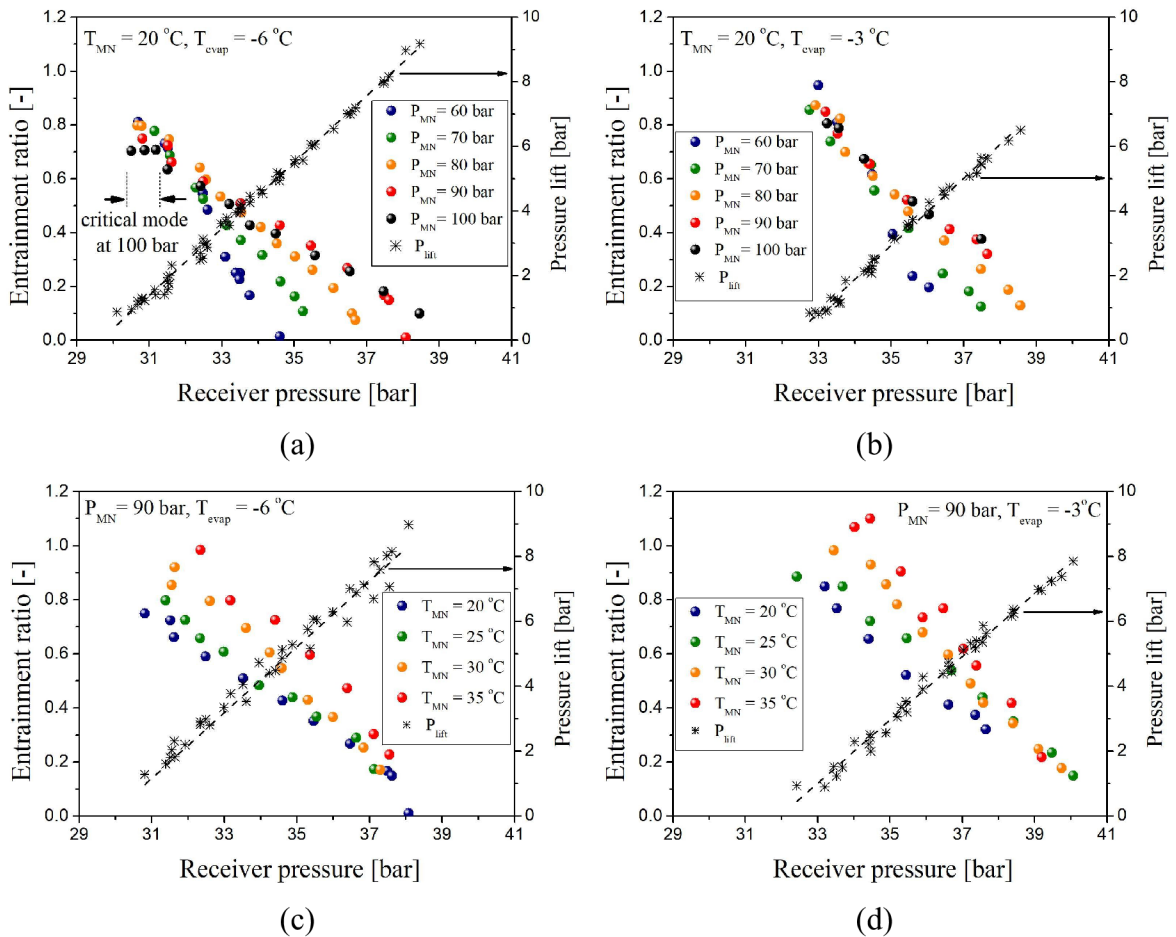


Figure 5.4 Variation of ejector mass entrainment ratio with liquid separator pressure (receiver pressure) and pressure lift as a function of motive flow conditions.

It is worth mentioning that CO₂ has a rather small working range when changing P_{rec} (determined as the ejector back pressure). As observed in the figures, downward trends are

steeper due to the low compression ratio of the R744 compared to other refrigerants [89]. In the same context, Figure 5.4(c and d) show the effect of the motive nozzle flow temperature on the ejector performance, considering a fixed P_{MN} at 90 bar as an optimal motive pressure as well as to express the transcritical and subcritical test regions. The result revealed that the mass entrainment ratio is decreasing with decreasing motive nozzle flow temperatures. Despite having a higher pressure lift, the separator pressure working range becomes much smaller for a higher motive nozzle flow temperature and then the mass entrainment ratio drops steeply. However, at the higher region of P_{rec} , the mass entrainment ratio behaved the same, and motive nozzle flow temperature does not play a crucial role in controlling the mass entrainment ratio. In contrast, at low liquid separator pressure, the attitudes are contradictory. For example, roughly at P_{rec} equal to 37.5 bar, $ER = 0.227$ and 0.167 for $35\text{ }^{\circ}\text{C}$ and $20\text{ }^{\circ}\text{C}$ motive nozzle flow temperature respectively, when reducing the pressure to 5 bar, then the mass entrainment ratio will increase to 0.590 and 0.984 accordingly. In the standard booster systems with target size from 40 to 150 kW cooling capacity, this result from low-pressure type ejectors is required to guarantee high suction mass flow, for instance, high mass entrainment ratio with reasonable pressure lift. This is suitable for applications in northern Europe, where the climate is rather moderate, and little flash gas is formed depending on the ambient conditions. Linking with higher evaporative temperature, as demonstrated in Figure 5.4(d), the ejector shifts to work under higher separator pressure with a further steeper mass entrainment ratio. For instance, the ejector is working under the liquid separator pressure from 32.4 to 40 bar reaching a maximum mass entrainment ratio of 1.10. It should be emphasized that the mass entrainment ratio in the traditional ejector cooling system is relatively low compared with the two-phase CO_2 ejector.

5.2 Ejector efficiency investigations

In the transcritical R744 refrigeration systems, one of the improvement areas is the use of ejector-based expansion work recovery. The aforementioned results illustrated the effect of different boundary conditions on the ejector performance system. However, to achieve optimum energy efficiency, it is essential to control the exit gas cooler pressure precisely to maintain an efficient expansion work recovery with respect to the liquid separator pressure. The work recovery rate can be interpreted as the power used to compress the suction nozzle flow from the suction nozzle inlet to the ejector outlet isentropically.

Figure 5.5 presents the ejector work recovery rate via liquid separator receiver pressure at $T_{MN} = 20\text{ }^{\circ}\text{C}$ and $T_{\text{evap}} = -6\text{ }^{\circ}\text{C}$. The highest ejector work recovery rate value was recorded as 0.096 kW at $P_{MN} = 100$ bar. It was recognized how the work recovery rate is increased when the motive nozzle flow pressure is raised at fixed suction nozzle flow conditions. For example, at the $P_{\text{rec}} \approx 31.5$ bar, the work recovery rate was doubled from 0.034 kW at $P_{MN} = 60$ bar to 0.068 kW at $P_{MN} = 90$ bar. The reason behind this rise relies on the higher amount of energy from the motive flow nozzle (higher momentum due to higher mass flow rate) which drives the entrained flow stream and accelerates it. The result also implies that at constant motive nozzle flow pressure, the work recovery rate increases with increasing the liquid separator pressure to the maximum, at which further increase in liquid separator pressure causes the work recovery rate to decline. Based on the previous result from Figure 5.4, a similar trend of work recovery rate is predicted in the case of running the ejector at higher evaporation temperature or suction nozzle flow pressure with shifting the outlet pressure to higher liquid separator pressure.

Based on equation (3-3), the experimental result was used to compare the ejector work rate recovery potential with the actual work rate recovery, as represented in Figure 5.6. The lines of constant ejector efficiency for these measurement data are represented as well. The value demonstrated that the ejector achieved an efficiency of 1.8% to 35%. The data markers on the figure were taken at different outlet gas cooler pressure. Overall, increasing the motive nozzle flow pressure positively affects the ejector performance, indicating higher work rate recovery. It can be observed that higher motive nozzle flow pressure results in a high motive mass flow rate and generate more considerable pressure difference in the system, which contributes to improving the overall available work recovery potential. In addition, increasing the motive nozzle flow pressure at constant inlet temperature leads to higher specific enthalpies at which greater kinetic energies could be extracted in the ejector.

However, when the motive nozzle flow pressure exceeds 90 bar, the maximum work recovery rate will continue to some extent increase with a slight decrease in the maximum ejector efficiency, which proves the capability of the ejector to provide adequate performance over some range of operating conditions. Compared with the commonly observed HFCs and HFOs refrigerants, CO_2 excess work recovery efficiency is 30% because it can overcome the significant pressure loss in the ejector due to higher vapor density [121].

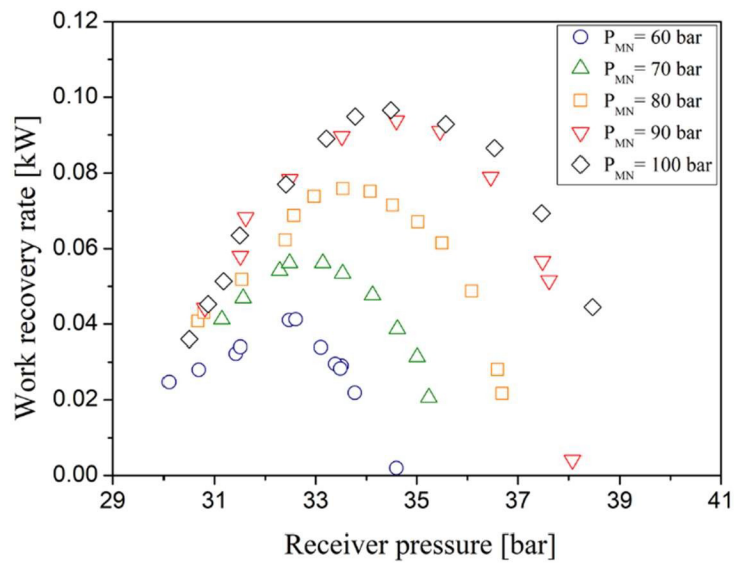


Figure 5.5 Potential work recovery rate vs. liquid separator pressure at $T_{MN} = 20\text{ }^{\circ}\text{C}$, $T_{\text{evap}} = -6\text{ }^{\circ}\text{C}$.

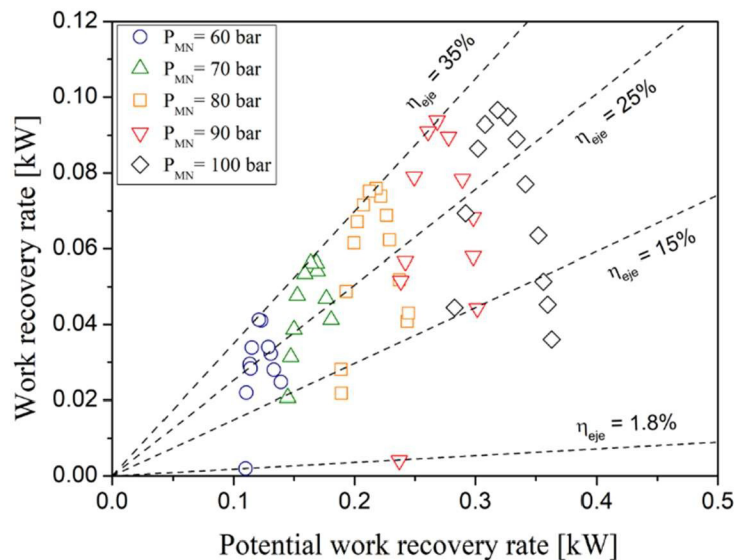


Figure 5.6 Ejector efficiency for different motive nozzle pressure at $T_{MN} = 20\text{ }^{\circ}\text{C}$ and $T_{\text{evap}} = -6\text{ }^{\circ}\text{C}$.

Under different liquid separator and motive nozzle flow pressures, the ejector performance of the efficiency, work rate recovery, mass entrainment ratio, pressure lift, and the cooling system COP are analyzed and discussed. In Figure 5.7, the analysis was performed at $P_{\text{rec}} = 34.6\text{ bar}$, $T_{MN} = 20\text{ }^{\circ}\text{C}$, and $T_{\text{evap}} = -6\text{ }^{\circ}\text{C}$ via different motive nozzle flow pressure. The result indicates that the ejector efficiency was rising with increasing the motive nozzle flow pressure up to 90 bar, where the ejector efficiency $\eta_{\text{eje}} = 35\%$, then started to decrease. As expected, having very high pressure will require more compressor power and lead to an increase in potential work recovery, and then the ejector work recovery starts to drop. This explains the

reason for the COP reduction since the data represented is at constant evaporation temperature. At the fixed receiver pressure, the pressure lift continued to remain at the range of 5 bar for these cases. The mass entrainment ratio was reported to continuously increase from 0.014 to 0.428 until the motive nozzle flow pressure reaches 90 bar, influenced by the rapid increase of the entrained mass flow compared to the motive mass flow, then dropping down.

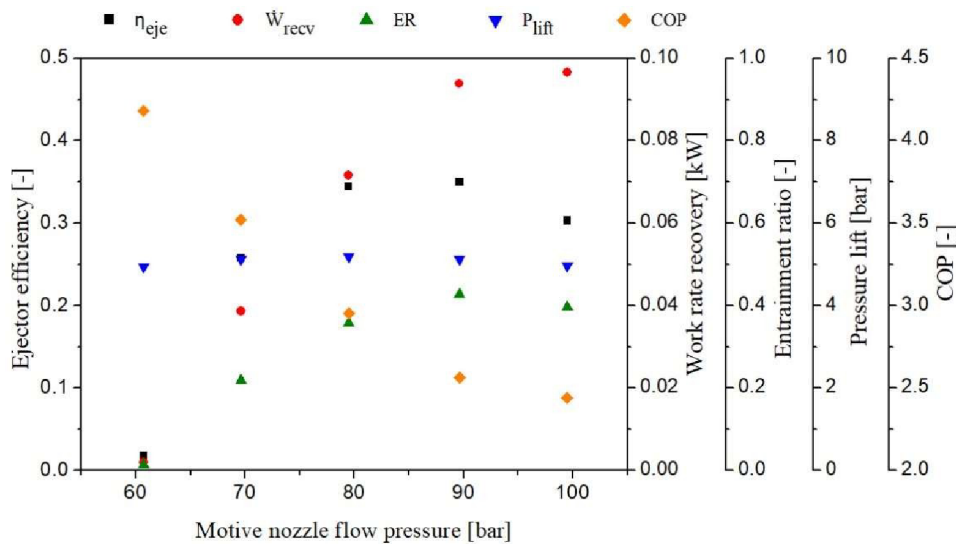


Figure 5.7 Cooling COP, η_{eje} , P_{lift} , \dot{W}_{recv} , and ER vs. different P_{MN} at $P_{rec} = 34.6$ bar, $T_{MN} = 20$ °C and $T_{evap} = -6$ °C.

Figure 5.8 shows the ejector performance data plotted at different receiver pressure. The experimental result was obtained at a motive nozzle flow pressure of 90 bar as an optimal motive working pressure. The motive nozzle flow temperature was set at 20 °C, and the evaporation temperature was equal to -6 °C. Again, the pressure lift in the ejector cooling system is the desired benefit. With increasing the receiver pressure as the ejector mixed-flow outlet, the pressure lift will keep increasing linearly to the maximum of 8.99 bar at which $P_{rec} = 38.1$ bar. In contrast, the mass entrainment ratio decreases with increasing liquid separator pressure from 0.75 to 0.01. A further increase in the liquid separator pressure will come as a sacrifice of the mass entrainment ratio and cause an ejector malfunction where it works as an expansion valve for higher pressure lift. Therefore, the ejector suction port is occupied with the check valve to prevent backflow. In other words, the small mass entrainment ratio results in a significant pressure lift at constant motive nozzle flow pressure. Based on this reverse proportionality between the pressure lift and the mass entrainment ratio, one should control the operation condition of the ejector for optimum performance. This should be evaluated at the

highest work recovery rate and ejector efficiency of 34.95%. Therefore, the liquid separator pressure was selected to be 34.6 bar. The cooling COP of the system remains almost unchanged at 2.59 because the compressor power was fixed for constant gas cooler pressure and the cooling load.

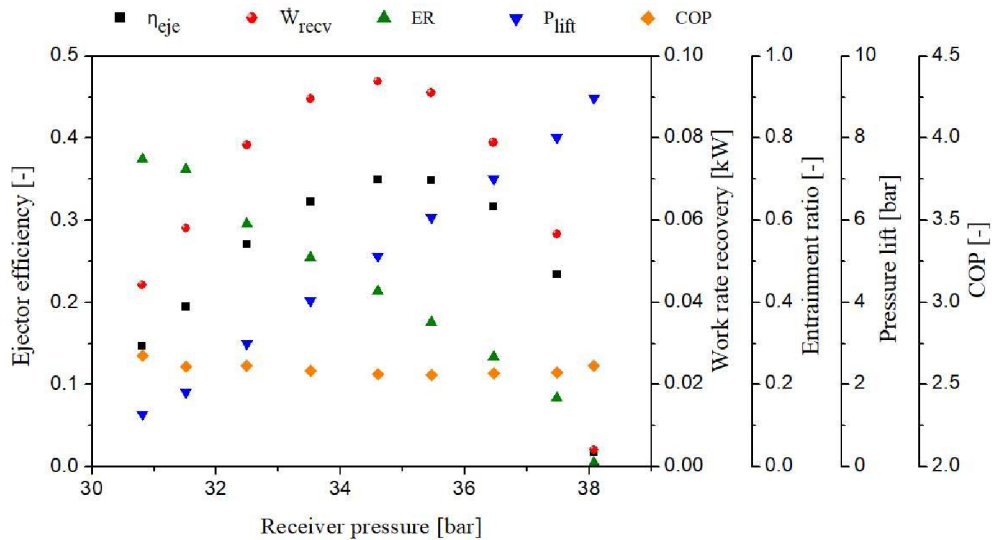


Figure 5.8 Cooling COP, η_{eje} , P_{lift} , \dot{W}_{recv} , and ER vs. different P_{rec} at $P_{MN} = 90$ bar, $T_{MN} = 20$ °C and $T_{evap} = -6$ °C.

5.3 Ejector exergy analysis

The exergetic efficiency and irreversibility in the ejector are determined based on the analysis of exergy transit for different operation conditions. The comparison analysis of exergy produced, exergy consumed, and exergy destructed was evaluated in terms of different motive flow and separator pressure based on the experimental results. Figure 5.9(a) shows the variation of the ejector exergy efficiencies and the exergy destruction at $T_{MN} = 20$ °C and $T_{evap} = -6$ °C for different motive nozzle flow pressure represented via different liquid separator pressure. When the separator pressure increased, the ejector exergy efficiency rose to a certain level where it reached the maximum, then witnessed a decrease with any further receiver pressure rise. There existed a maximum exergy efficiency of 17.9% at corresponding $P_{MN} = 90$ bar, which grows as the optimum exergy efficiency from 14.9% at $P_{MN} = 60$ bar then declines to 15.6% with increasing the motive nozzle flow pressure to 100 bar. Nonetheless, the exergy destruction was increasing with higher motive nozzle flow pressure. The maximum loss was 0.98 kW at $P_{MN} = 100$ bar, while the minimum took place at $P_{MN} = 60$ bar with 0.4 kW inside this two-phase ejector. It may be observed that the total exergy destruction increased by about

17% when increasing the motive nozzle flow pressure from 90 to 100 bar. Based on that, the result nominated $P_{MN} = 90$ bar as the optimal gas cooler pressure, which agrees with the previous section analysis. Therefore, a comparison of different evaporation temperatures as well as outlet gas coolers was investigated under 90 bar of motive nozzle flow pressure.

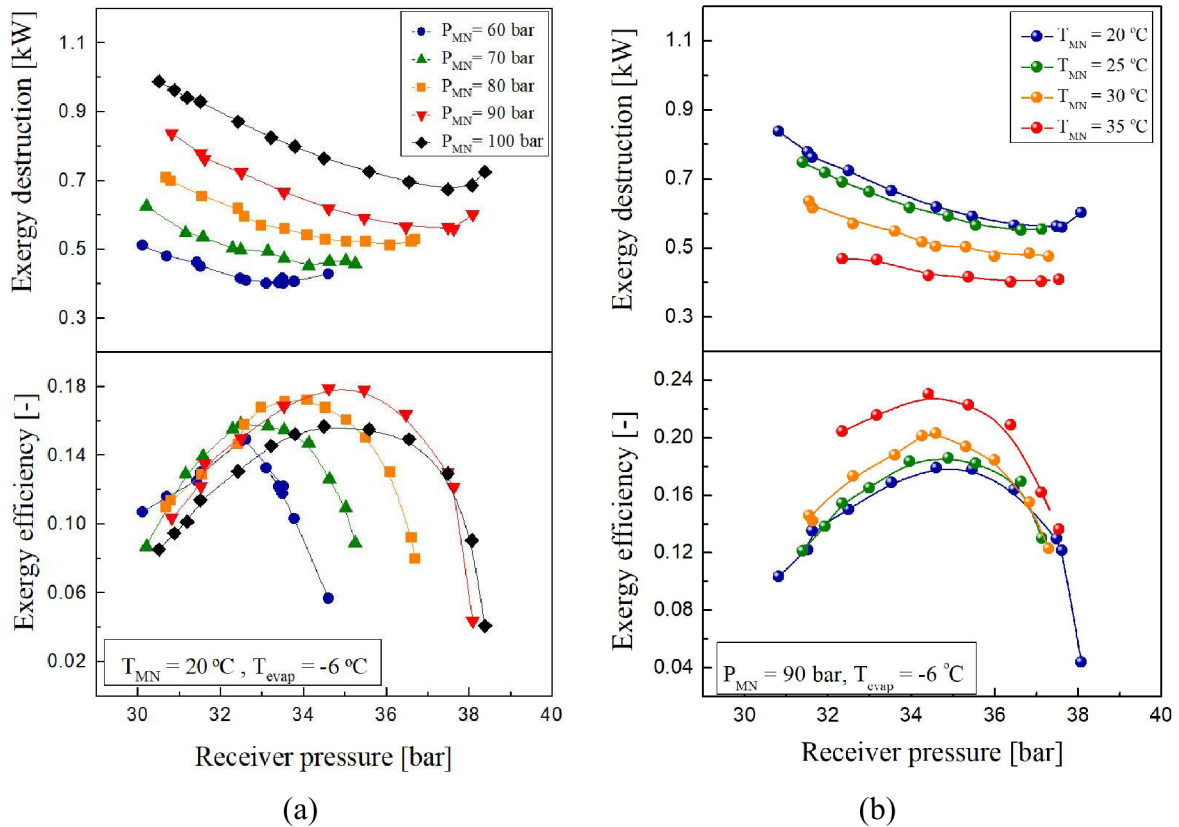


Figure 5.9 Ejector exergy efficiency and exergy destruction vs. liquid separator pressure P_{rec} , (a) at different motive pressure, (b) at different motive temperatures.

Figure 5.9(b) represents the influence of different motive nozzle flow temperatures on the ejector exergy efficiency and destruction at $P_{MN} = 90$ bar and $T_{\text{evap}} = -6\text{ }^{\circ}\text{C}$. It can be noted that regardless of the separator pressure, working at higher exit gas cooler temperatures will increase the exergy efficiency and decrease the loss of the exergy significantly. The reason lies in the lower exergy consumed associated with low inlet mass flow rate through the ejector. For instance, at $T_{MN} = 20\text{ }^{\circ}\text{C}$ and receiver pressure around 34.5 bar, the maximum exergy efficiency recorded was 17.9%, with 0.619 kW exergy destruction. This loss will shrink by 32% in the case of working under a motive nozzle flow temperature of $35\text{ }^{\circ}\text{C}$ and raise the exergy efficiency to 23%. Moreover, the experimental data did not illustrate much performance improvement when increasing the motive nozzle flow temperature from $20\text{ }^{\circ}\text{C}$ to $25\text{ }^{\circ}\text{C}$ and showed somewhat

similar exergy destruction. As a result, working at a supercritical motive flow region will allow the ejector to avoid the massive amount of exergy destruction and expressively increase the exergy efficiency.

For the sake of introducing the optimum motive flow working condition, the exergy analyses should be represented. Figure 5.10 showed the characteristic of the ejector under different motive nozzle flow temperature and pressure. Figure 5.10(a) analysed the data at $P_{rec} \approx 35.4$, $T_{evap} = -6$ °C and $P_{MN} = 34.5$ bar while Figure 5.10(b) assessed the result at $P_{rec} \approx 34.6$ bar, $T_{evap} = -6$ °C and $T_{MN} = 20$ °C. It could be noted that the ejector performed higher exergy efficiency in the case of running at $T_{MN} = 35$ °C by 22.3% and lower the exergy consumed and destroyed gradually, while the total exergy production remained level at approximately 0.124 kW through the motive temperature increase.

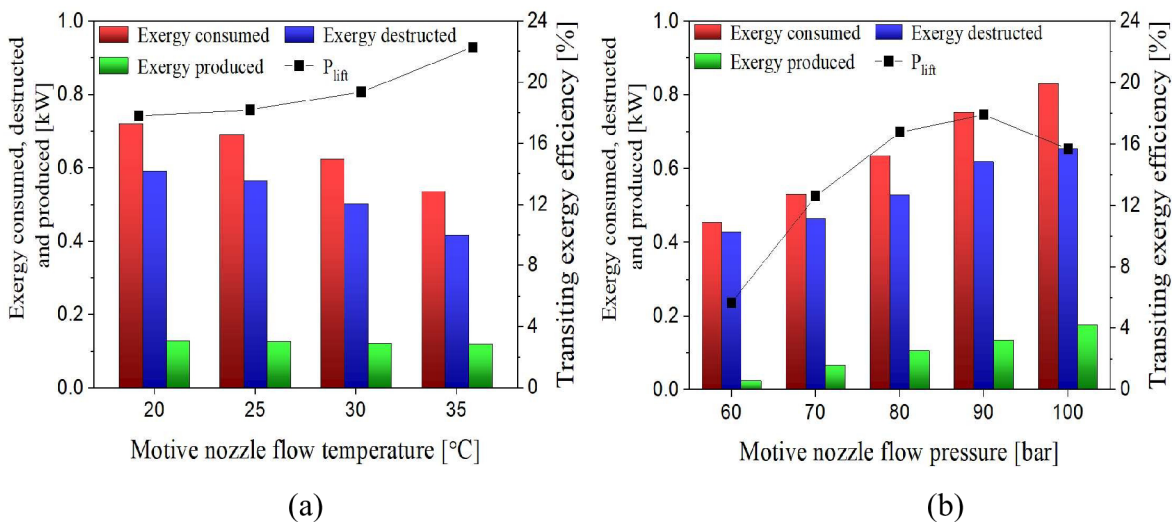


Figure 5.10 Ejector exergy metrics at different motive nozzle flow temperatures and pressure at $T_{evap} = -6$ °C, (a) $P_{rec} \approx 35.4$ bar and $P_{MN} = 34.5$ bar, (b) $P_{rec} \approx 34.6$ bar and $T_{MN} = 20$ °C.

The exergy efficiency slowly grew when T_{MN} raised from 20 °C to 25 °C as discussed previously, then strikingly increased. In Figure 5.10(b), the highest exergy efficiency recorded was at $P_{MN} = 90$ bar. It dramatically increased from 5.67% at $P_{MN} = 60$ bar to 17.92%, then declined noticeably. In contrast, the exergy consumed and destroyed increased progressively with higher motive nozzle flow pressure while the exergy produced grew from 0.026 kW at $P_{MN} = 60$ bar to 0.142 kW at $P_{MN} = 90$ bar then remained level with further pressure increase.

All behavior of the thermodynamic metrics, including exergy consumed as the feeding exergy, exergy produced as the useful exergy product, the exergy destruction, transiting inlet

and outlet exergy are represented in Table 5.1 at $P_{MN} = 90$ bar and $T_{MN} = 35$ °C over various separator pressure. These conditions were specified based on the optimal motive nozzle flow pressure and temperature represented in the previous part discussion. The analysis evaluated the ejector at different evaporation pressure to study the effect of the suction nozzle flow parameters.

Table 5.1 Exergy metrics of the experiment for different evaporation temperatures and liquid separator pressure.

T_{evap} [°C]	P_{rec} [bar]	Exergy consumed [kW]	Exergy produced [kW]	Exergy destruction [kW]	Transiting exergy [kW]	Exergy efficiency %	Inlet exergy [kW]	Outlet exergy [kW]
-6	32.34	0.590	0.121	0.470	7.765	20.44	8.355	7.886
-6	33.17	0.595	0.128	0.466	7.354	21.58	7.949	7.482
-6	34.40	0.547	0.126	0.421	6.889	23.06	7.436	7.015
-6	35.37	0.535	0.119	0.416	6.554	22.30	7.090	6.674
-6	36.38	0.509	0.106	0.402	5.985	20.89	6.494	6.092
-6	37.11	0.482	0.078	0.404	5.254	16.19	5.735	5.332
-6	37.55	0.473	0.064	0.409	4.958	13.62	5.431	5.023
-3	34.45	0.544	0.090	0.453	8.380	16.60	8.923	8.470
-3	35.31	0.544	0.102	0.441	7.956	18.85	8.500	8.059
-3	35.91	0.530	0.108	0.423	7.307	20.32	7.837	7.414
-3	36.47	0.486	0.107	0.379	7.048	22.04	7.533	7.155
-3	37.39	0.470	0.099	0.370	6.323	21.12	6.792	6.422
-3	38.36	0.442	0.085	0.357	5.640	19.27	6.083	5.726
-3	39.19	0.427	0.058	0.369	4.904	13.64	5.331	4.962

In general, working under low evaporation temperature is required to discharge more heat load from the system at the gas cooler and directly impact the compressor capacity. Also, the ejector suction pressure is decreased at lower evaporation temperature and the suction mass flow rate is reduced too. Therefore, at the same motive flow condition, the total exergy consumed will be higher. It can be noted that the exergy consumed and destructed, as well as the transiting exergy, are decreasing with increasing the receiver pressure. The maximum exergy consumed at $T_{\text{evap}} = -6$ °C equals 0.595 kW, which is 8.6% higher than the maximum exergy consumed in the case of running at $T_{\text{evap}} = -3$ °C.

The result indicated excessive exergy destruction compare to the useful one. According to the data characterized in the table, the exergy produced represents 13.6% to 23% of the total exergy consumed. Most exergy losses took place at higher separator pressure equipped with

low ejector exergy efficiency. In that respect, working at $T_{\text{evap}} = -3^{\circ}\text{C}$ could minimize the exergy destruction due to lower total exergy consumed but account for a slightly lower efficiency working region. One can observe the slow increase of the transiting exergy efficiency by 3% at $T_{\text{evap}} = -6^{\circ}\text{C}$ and 5% at $T_{\text{evap}} = -3^{\circ}\text{C}$ with higher receiver pressure to 23% and 22% respectively, then decreased for both of them to 14%. However, both inlet and outlet exergy represent an increase with increasing the evaporator temperature and decline with increasing the liquid separator pressure based on the presence of transiting exergy.

5.4 System performance calculations

This research aims to indicate the potential effect of integrating a small-scale ejector into a CO_2 transcritical system and assign the contribution of the ejector to the total energy consumption. The basic R744 booster refrigeration system exemplifies in the conventional parallel system and the ejector-supported layout are represented in Figure 5.11. Basically, the gas cooler flow exit will expand at the HPV. When the ejector solenoid valve is active, some refrigerants expand isentropically throughout the ejector to a pressure level lower than the evaporator pressure, creating a local pressure drop and entrain the suction flow to the ejector mixing chamber. The amount of the motive mass flow depends on the exit gas cooler flow properties and the ejector motive nozzle size. The flow is then compressed to the liquid separator through the ejector diffuser by converting the kinetic energy into pressure energy. Afterward, the liquid portion from the separator will feed the evaporator, and the vapor fraction will be slightly superheated when it passes through an internal heat exchanger and then compressed back by the parallel compressor. This operation of R744 refrigeration systems is classified as transcritical booster system configuration with or without parallel compression. The R744 system was tested at -6°C evaporation temperature with reference evaporator outlet superheated temperature of 10K. The cooling capacity was set to 15 kW for the investigated boundary conditions.

The system components were analyzed based on the first and second law of thermodynamic, considering the mass conservation for each control volume. The calculation assumes the following constraints:

- The pressure drop in the gas cooler, evaporator, and piping system is neglected.
- The environmental dead states temperature used for the exergy calculation is 20°C at one atmospheric pressure.

- The analysis was conducted at steady-state conditions.
- Potential and kinetic energies were not considered.
- Heat losses and heat gains in the whole system were negligible.

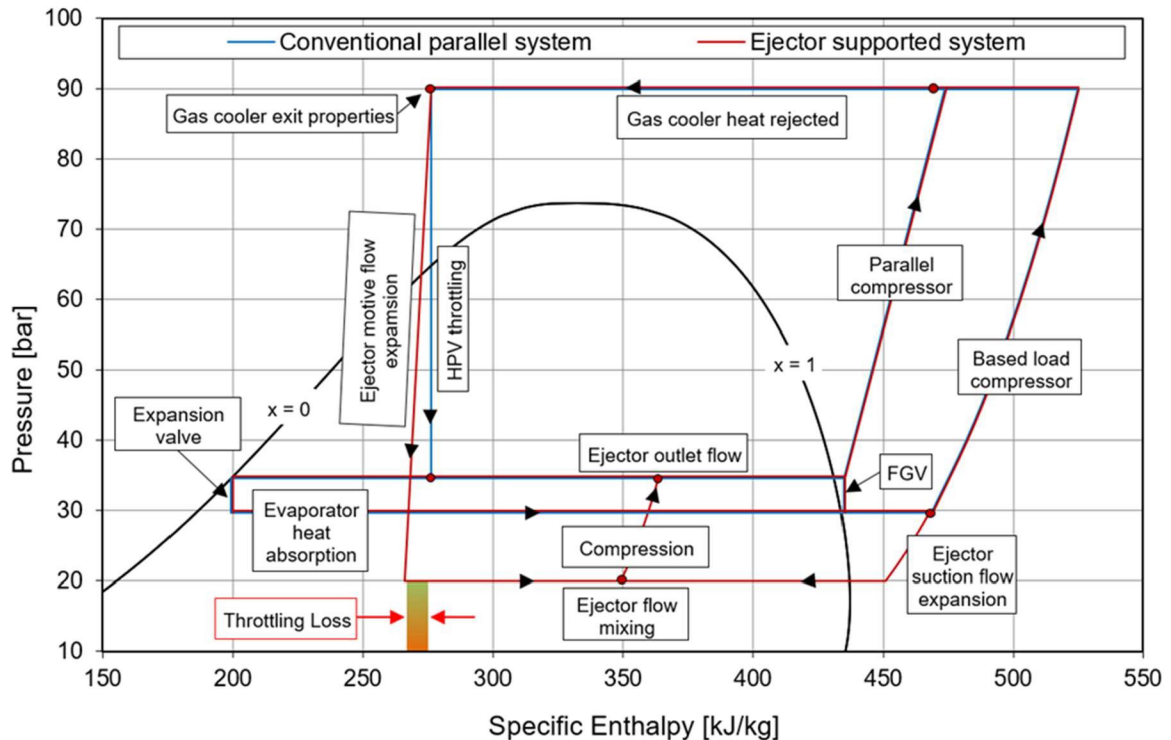


Figure 5.11 P-h diagram of the conventional parallel R744 transcritical refrigeration cycles and the ejector support cycle.

The investigation consists of (i) the ejector performance based on validating the extensive experimental result used to calculate the ejector inlet mass flow rates. The proposed functions define the ejector efficiency metric and the entrainment ratio. (ii) the contribution of the ejector to the work recovery potential and the influence on the R744 transcritical refrigeration system. (iii) the impact of the ejector on the system performance improvement and the power consumption at different exit gas cooler temperatures. (iv) the exergy analysis based on the second law of thermodynamic for each component for the parallel and ejector-supported refrigeration system configurations.

5.4.1 Ejector characteristic functions

The particular main characteristic of the current ejector profile is its remarkable high ejector efficiency over the most range of working conditions, which was able to recover up to 36.9% of the throttling losses experimentally and deliver maximum exergy efficiency of 23%

compared to the previous studies. In this section, the ejector will be tested at motive flow pressure varied from 60 to 100 bar, whereas the motive temperature will be varied from 20 to 35 °C. These selections were to ensure that both the subcritical and transcritical regions were considered. The ejector outlet conditions were controlled by setting different liquid separator pressure to set the required pressure lift. However, the previous research showed that the inlet flow properties (density and pressure) influenced the ejector profiles. Because of the supersonic flow at the ejector motive nozzle exit, the motive nozzle mass flow rate is not influence by pressure lift or the amount of the suction pressure. In the numerical approach, the mass flow rate at the motive nozzle was predicted to be choked at the throat achieving maximum mass flux. The calculations involved some polytropic efficiency coefficients and relied on different relations to calculate the speed of sound based on the homogeneous two-phase model where the assumption of instantaneous phase change is less reliable [122]. In this regard, the discrepancy with the experimental result is notable [88]. It should be noted that the error in the ejector inlet mass flow rate values is a function of the condition of the operating regime and how close it is to the critical point [123]. The small size of the ejector could be one of the reasons behind the divergence in the result, especially the operation under very high driving pressure, which requires further research into turbulence, multiphase effects, and shock structures, including the estimation of the presence of lubricants mixed with R744 to meet satisfactory accuracy. Therefore, the correlation of the motive mass flow rate for the ejector profile (VEJ_1) is expressed in equation (5-2). The proposed function was constructed in Matlab/Simulink. The results produced were able to verify the whole range of the experimental data with reasonable accuracy of relative error lies between -3.05% and 2.69%, as demonstrated in Figure 5.12.

$$\dot{m}_{MN} = A_{\text{throat}} \left[a \cdot \rho_{MN}^2 + b \cdot \rho_{MN} + c \cdot \left(\frac{P_{MN}}{P_{cr}} \right)^2 + d \cdot \left(\frac{P_{MN}}{P_{cr}} \right) + e \cdot \left(\frac{\rho_{MN} \cdot P_{MN}}{P_{cr}} \right) + f \right] \quad (5-2)$$

where A_{throat} is the motive nozzle throat area, ρ_{MN} and P_{MN} are the motive nozzle inlet density and pressure, P_{cr} is the critical pressure of CO₂ equal to 73.8 bar. The coefficient values are as follows; $a = 9.11178 \cdot 10^{-2} \text{ m}^4/\text{kg} \cdot \text{s}$, $b = 1.48812 \cdot 10^2 \text{ m/s}$, $c = -2.33483 \cdot 10^4 \text{ kg/m}^2 \cdot \text{s}$, $d = 1.79150 \cdot 10^5 \text{ kg/m}^2 \cdot \text{s}$, $e = -9.38807 \cdot 10^1 \text{ m/s}$, $f = -1.90182 \cdot 10^5 \text{ kg/m}^2 \cdot \text{s}$. The registered error was almost 50% lower than the correlation provided by Banasiak et al. [43] for different ejector profile geometry. The reason could be the mathematical model operational envelop used by the

authors or the absence of the term value with coefficient e . However, the derived approximation function will be strictly limited to the investigated working range of the performed experimental work.

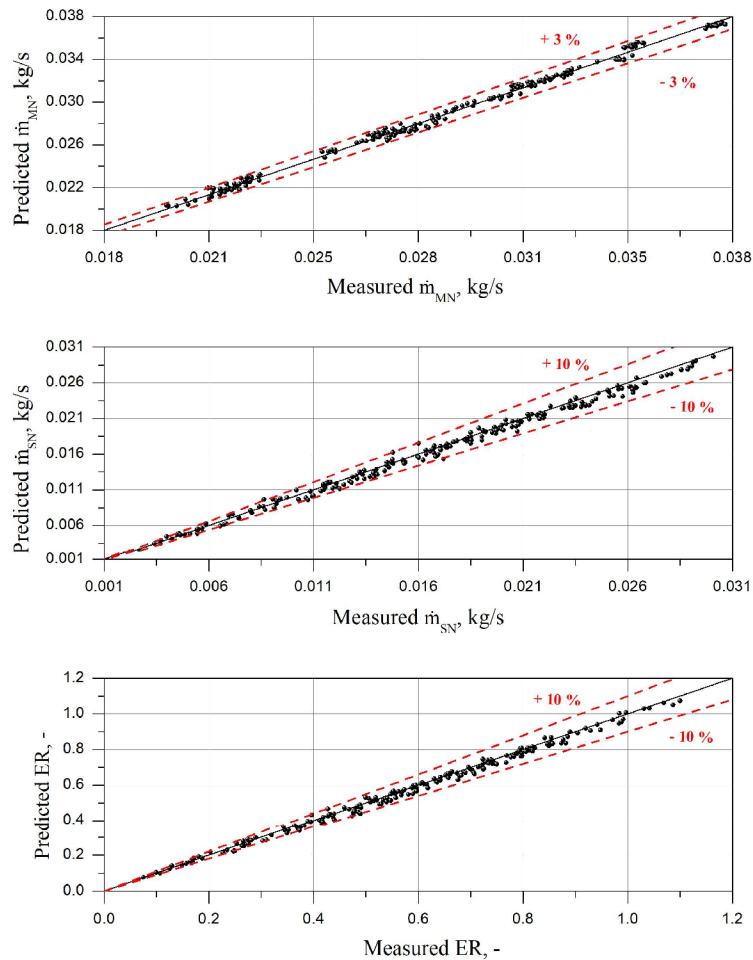


Figure 5.12 The relative error between measured (horizontal axis) and the predicted result (vertical axis) for motive nozzle mass flow rate (top), suction nozzle mass flow rate (middle), and mass entrainment ratio (bottom).

The ejector suction nozzle mass flow rate is a function of different independent parameters such as the ejector outlet pressure, the ejector inlet pressure, and density. Therefore, the correlation of VEJ_1 suction nozzle mass flow rate is expressed in equation (5-3) following the work of Banasiak et al. [43] for evaluating the performance of one individual ejector cartridge. The result obtained by the correlation showed a suction nozzle mass flow rate relative error between -10.8% and 11.7%. The mass entrainment ratio was significantly varied from 1.10 to 0.074; therefore, the relative error registered for ER was laid between -10.9% and 9.4%, as shown in Figure 5.12. The error increased when the mass entrained ratio was decreased, and if

the value of ER was close to zero, then the relative error could approach infinity. Therefore, the absolute error for the registered ER was lower than ± 0.03 , excepting 36 points of the overall measurements data with an absolute error of less than ± 0.048 .

$$\frac{\dot{m}_{SN}}{\dot{m}_{MN}} = \left[S_1 \left(\frac{P_{rec}}{P_{SN}} \right)^2 + S_2 \frac{P_{rec}}{P_{SN}} + S_3 \right] \quad (5-3)$$

The parameters S_1 , S_2 , S_3 were defined in equation (5-4), and all the values of the coefficients in the equation are listed with their units in Table 5.2.

$$S_i = \left[s_{i,1} \rho_{MN}^2 + s_{i,2} \left(\frac{P_{MN}}{P_{cr}} \right)^2 + s_{i,3} \left(\frac{P_{SN}}{P_{cr}} \right)^2 + s_{i,4} \rho_{MN} + s_{i,5} \frac{P_{MN}}{P_{cr}} + s_{i,6} \frac{P_{SN}}{P_{cr}} + s_{i,7} \rho_{MN} \frac{P_{MN} P_{SN}}{P_{cr}^2} + s_{i,8} \right] \quad (5-4)$$

Table 5.2 Coefficient values in equation (5-4) for the ejector profile.

Coefficient S_i	$i = 1$	$i = 2$	$i = 3$
$s_{i,1}$ [m^6/kg^2]	-2.1840×10^{-4}	4.2594×10^{-4}	-2.0290×10^{-4}
$s_{i,2}$ [-]	1.2579×10^1	-3.4491×10^1	2.1721×10^1
$s_{i,3}$ [-]	-5.3677×10^3	1.1301×10^4	-5.9051×10^3
$s_{i,4}$ [m^3/kg]	5.1324×10^{-1}	-1.0100	4.8396×10^{-1}
$s_{i,5}$ [-]	5.8573×10^1	-9.1183×10^1	3.0943×10^1
$s_{i,6}$ [-]	4.8672×10^3	-1.0262×10^4	5.3689×10^3
$s_{i,7}$ [m^3/kg]	-2.8180×10^{-1}	5.7258×10^{-1}	-2.8530×10^{-1}
$s_{i,8}$ [-]	-1.3400×10^3	2.7706×10^3	-1.4164×10^3

It can be seen from the derived equations that the ratio between the ejector outlet pressure and the suction nozzle pressure portrays a role in obtaining the optimum ejector working condition. Therefore, based on these correlations, the ejector cartridge performance could be mapped and examine applying any defined boundary conditions.

5.4.2 Test of the ejector performance

The ejector was theoretically investigated using the outlet gas cooler pressure at 90 bar as it revealed a better overall performance. The motive nozzle flow inlet temperatures were set at 20, 25, 30, and 35 °C. The dynamic changes of derived parameters such as ejector efficiency, the mass entrainment ratio, and expansion work rate recovery were represented via different pressure lifts (characterized for increasing the liquid separator pressure), as shown in Figure 5.13.

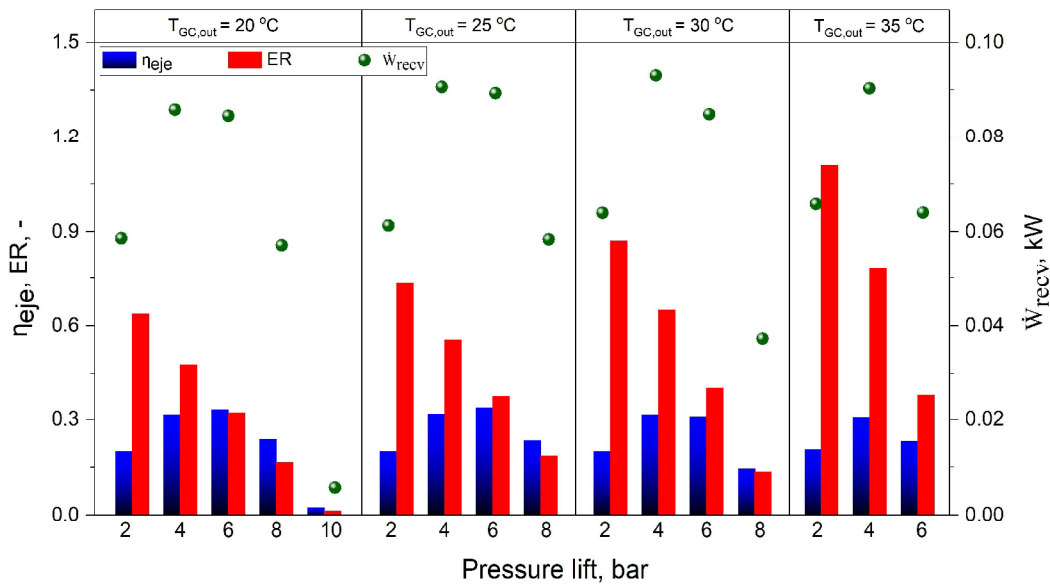


Figure 5.13 Calculation of the ejector profile characteristics depending on the pressure left and the inlet motive nozzle temperature.

The result satisfies the ejector principle at which increasing the pressure lift at each fixed motive temperature will affect the axial velocity of the flow at the mixed chamber inside the ejector and force the oblique shock waves to move upstream to the motive nozzle exit. This movement will disturb the motive flow stream jet core. Therefore, the entrainment ratio will dramatically decrease to the high pressure lift limit that prevents the suction flow stream from being drawn in and thus, transforms the ejector into an expansion valve task. Moreover, the ejector entrainment ratio and pressure lift were clearly dependent on the motive flow temperature, i.e., increasing the exit gas cooler temperature as the motive nozzle flow temperature will decrease the ejector pressure lift range and allow to entrain additional suction stream. The relation is manifested by a sharp decrease of CO₂ density with high temperature, causing a reduction in the motive nozzle mass flow rate. Thus, the entrainment ratio will rise to achieve the peak of ER 1.10 at $P_{lift} = 2$ bar.

The ejector profile registered relatively high efficiency at $T_{MN} = 25\text{ °C}$ of 34.3% from the calculations. The result matches the experimental work outcome as this ejector working region holds the optimum operation condition to recover the available potential work. However, increasing the motive flow temperature to the transcritical state indicated slightly lower ejector efficiency. Hence, the range of the liquid separator pressure at the intermediate pressure level should be carefully selected to match the high ejector efficiency and pressure lift with the large entrained suction flow, and at the same time, achieve a high-performance ejector.

The amount of the expansion work rate (\dot{W}_{recv}) recovered by this small-scale ejector is illustrated in Figure 5.13 along the right y-axis. The distinctive attribute of this metric calculation is the requirement of the inlet ejector parameters obtained from the design condition, unlike some other correlations which for example, involve the effect of the thermal non-equilibrium exist [124]. The work recovery rate had a similar efficiency pattern with an optimal value of 0.094 kW out of the maximum potential work of 0.284 kW at a pressure lift of about 4 bar and $T_{\text{MN}} = 30^\circ\text{C}$. By evaluating the cycle thermodynamically as representing in Figure 5.11 and depending on the run of the basic transcritical parallel system configuration without the ejector, the total throttling loss in the process could reach 0.965 kW, which could be partially compensated using the ejector under the same operation conditions.

In general, when the system run at lower liquid separator pressure and high outlet gas cooler temperature, there are bound to be significant throttling losses. Hence the maximum work recovery potential would be very high, and the ejector efficiency low. However, changing the inlet motive flow temperature does not significantly affect the expansion work recovery rate; the reason lies in the enthalpy difference between the suction nozzle inlet and the ejector outlet pressure which is compressed isentropically from the evaporator.

5.4.3 Ejector system performance improvement

The comparison between the calculated and the experimental result achieved reasonably good accuracy which varied with $\pm 3.97\%$. However, Figure 5.14 represents the calculation results of the system performance characterized by the cooling COP in the parallel system configuration and with the VEJ_1 ejector system at different exit gas cooler temperatures via pressure lift in the range of 1 bar to 11 bar. However, the calculations indicated a moderate increase of the COP upon increasing the pressure lift at a fixed exit gas cooler temperature in the parallel system. In contrast, the COP in the ejector system raised to the maximum at the ultimate ejector efficiency then drop to the parallel system COP value. In addition, increasing the exit gas cooler temperature allowed to lower the COP as a consequence of the higher flash gas removed from the liquid separator downstream the high-pressure valve.

The result indicated a significant improvement in the system COP obtained by running the ejector. The highest recorded system COP was 3.12 at $T_{\text{GC, out}} = 20^\circ\text{C}$ and $P_{\text{lift}} = 11$. When running with VEJ_1 ejector cartridge at 6 bar and $T_{\text{GC, out}}$ of 20°C , the system exhibited a higher

COP of 2.05% than the parallel configuration. The optimum COP improvement then declined to 1.91%, 1.53%, and 0.88% when the exit gas cooler temperature raised to 25, 30, and 35°C, respectively.

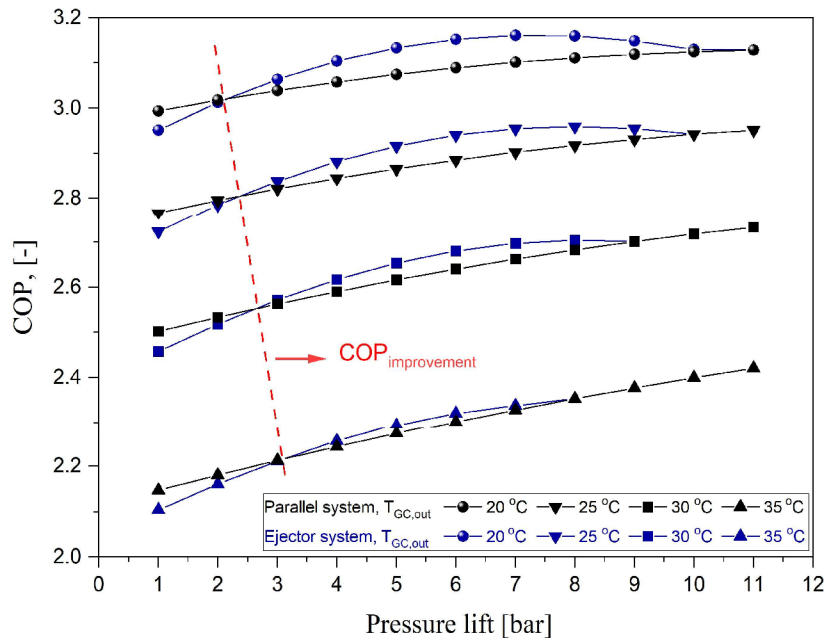


Figure 5.14 System COP characteristics vs. pressure lift for the parallel system layout and ejector supported system at different gas cooler outlet temperatures.

It can be observed that the ejector system exhibited poorer performance when operated at low pressure lift compared to the parallel system baseline. The highest COP degradation was obtained for $T_{GC, out} = 35\text{ }^{\circ}\text{C}$ and $P_{lift} = 1\text{ bar}$ up to -2%. This can be explained by the higher portion of the vapor in the liquid separator along with the low ejector mass entrainment ratio. Also, the reason can be associated with the high throttling loss and the gliding heat rejection temperature, making the COP of the CO₂ transcritical refrigeration system susceptible to the gas cooler exit temperature [5]. The region at which the performance starts to improve upon increasing the pressure level in the liquid separator using the ejector at different exit gas cooler temperatures is identified by a red dashed line in the figure. The COP range enlarges when increasing the pressure lift from 3.1 bar at $T_{GC, out} = 35\text{ }^{\circ}\text{C}$ linearly to and 2.1 bar at $T_{GC, out} = 20\text{ }^{\circ}\text{C}$ by running the ejector limited by the ejector mass entrainment ratio. For example, the ejector improves the system performance till the pressure lift of 11 bar at $T_{GC, out} = 20\text{ }^{\circ}\text{C}$. In comparison, this improvement was restricted to the liquid separator pressure range that provided the COP improvement only to $P_{lift} = 8\text{ bar}$ at $T_{GC, out} = 35\text{ }^{\circ}\text{C}$ linked to the ejector working range.

It is noteworthy that this type of analysis will be difficult to perform experimentally in total with and without the ejector because of the small geometry of the ejector profile and the opening characteristics of the high-pressure valve when running with a multi-ejector block, which invoked a fluctuation of the control discrepancy [43].

The impact of different compressor discharge pressures from 60 to 100 bar on the system performance is illustrated in Figure 5.15. The results were selected at $P_{\text{lift}} = 5$ bar since it characterized the region where the ejector provided the highest efficiency. The COP was analyzed at exit gas cooler temperature varied from 20 to 35 °C to account for the subcritical and transcritical mode of operation. The advantage of this type of comparison at constant evaporation and exit gas cooler temperature is that the heat exchangers' heat transfer characteristics do not influence the result [66]. The COP improvement by running the ejector was indicated in red color at the right y-axis. The result shows an increase in system COP when the gas cooler pressure dropped because of the reduction in the compressors input power at fixed evaporation pressure. It can be seen that the system performed well when it operated subcritical. The highest system COP recorded was 4.94 at a gas cooler pressure of 60 bar and $T_{\text{GC, out}} = 20$ °C.

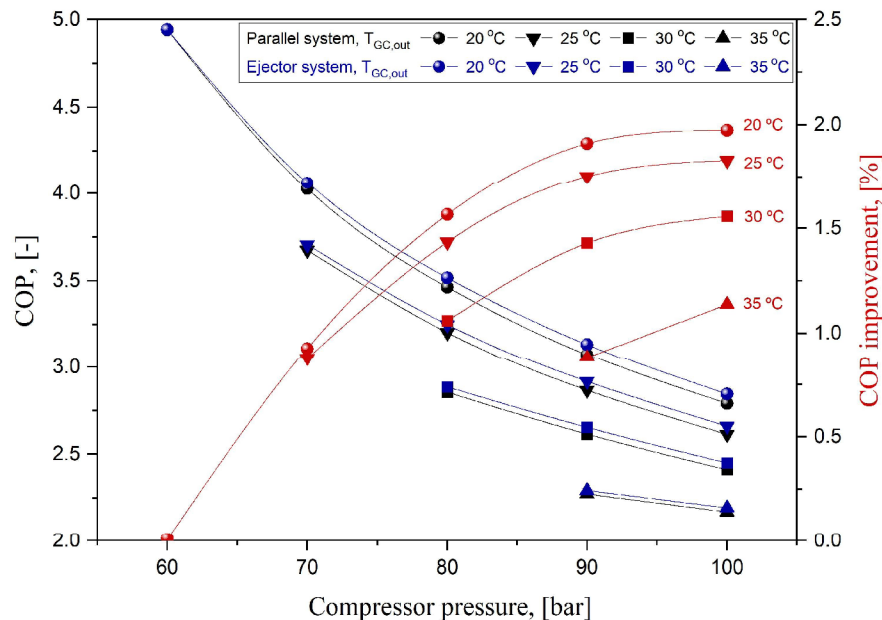


Figure 5.15 System COP characteristics vs. pressure lift for the parallel system layout and ejector supported system at different gas cooler pressure levels.

On the other hand, running the ejector aids in raising the system COP significantly with respect to the compressor discharge pressure for all exit gas cooler temperatures compared to

the parallel system as the baseline. For instance, the ejector profile improves the system COP by 1.97% at P_{GC} of 100 bar and $T_{GC, out} = 20^\circ\text{C}$, while it provides 1.14% higher COP by increasing the exit gas cooler temperature to 35°C . Basically, when the ejector was running at a high exit gas cooler temperature, it exhibited lower energy recovery potential, which decreased the COP. Similar results of the COP improvement were obtained experimentally by Nakagawa et al. [125] and Elbel et al. [32] concerning the trends. Theoretically, the optimum compressor discharge pressure for each exit gas cooler temperature was provided with a curve fitting function generated by many researchers, i.e., Chen and Gu [126] and Sawalha [127]. However, the region where the current analysis was performed was partially covered at the high exit gas cooler temperature.

Despite the COP assessment, no information was given about the ultimate system performance and the massive losses in each component. The exergy balance can describe the actual cooling efficiency of the cooling system. Therefore, the exergy analysis has been performed for the refrigeration system with and without the ejector.

Figure 5.16 illustrates the performance of the system characterized by the exergy efficiency η_{ex} under different gas cooler exit temperatures and pressure lift in the range of 1 bar to 11 bar at both parallel and ejector supported systems. When the system examined an increase in the pressure lift, the exergy efficiency of the system was heightened. The parallel system exhibited a higher exergy efficiency of 24.18% at an exit gas cooler of 20°C and the highest possible pressure lift of 11 bar based on the second law analysis. The result indicated a most remarkable improvement when activating the ejectors by 1.92 % at $T_{GC, out} = 20^\circ\text{C}$, and $P_{lift} = 6$ bar comparing when running in the absence of ejectors. However, the peak of the exergy efficiency improvement in the ejector system continues to shrink to less than 1% when increasing the exit gas cooler temperature to 35°C . The exergy efficiency improvement took place at the region of high pressure lift which varies from 3.14 bar at $T_{GC, out} = 35^\circ\text{C}$, and 2.1 bar at $T_{GC, out} = 20^\circ\text{C}$ as it is indicated by the red dashed line in the figure. It can be observed that running the ejector beyond these parameters, a small value of the liquid separator pressure for low pressure lift, caused a worse performance than operating in parallel system layout as a result of the high compressor load.

The degradation of the efficiency according the second law efficiency reached a maximum of 2% lower value than the parallel system for a gas cooler outlet temperature of 35°C

°C at $P_{\text{lift}} = 1$ bar. In other words, the cooling system rejects the heat from the CO₂ cycle in the subcritical mode for the surrounding temperature below the critical temperature, which minimizes the degradation of the system performance. For example, at exit gas cooler temperature of 20 °C, the parallel system had an exergy efficiency of 1.43% higher than running with the ejectors at $P_{\text{lift}} = 1$ bar then switched to introduce the ejector system solution to improve the system performance at $P_{\text{lift}} > 2.1$ bar. Nevertheless, suppose that different ejector cartridges are added to this small-scale ejector in the multi-ejector block, then the exergy efficiency will witness an increase characterized by a steeper slope depending on the pressure lift. The current profile could also increase the total system exergy efficiency and the COP to 12% if the total cooling capacity of the system is analyzed for 3 kW.

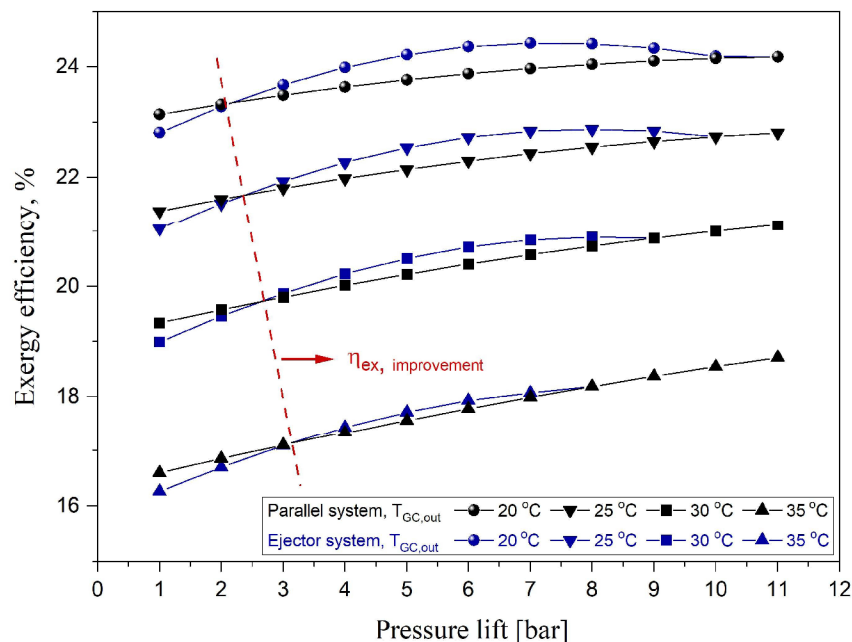


Figure 5.16 System exergy efficiency characteristics vs. pressure lift for the parallel system and (VEJ_1) ejector system layout at different gas cooler outlet temperatures.

It was approved in many research investigations that applying the ejector in the R744 refrigeration system is a competitive solution to decrease the overall system power consumption. The influence of the small size ejector profile VEJ_1 on the compressor power saving for different pressure lifts is represented in Figure 5.17 at different gas cooler exit temperatures and compressor discharge pressure of 90 bar. The result demonstrates that utilizing the small size ejector contributes to significant energy saving and optimizes the system performance by reducing the compressor power. Running the system in the transcritical mode

had the minimum effect on power reduction compare to lowering the gas cooler temperature to work subcritical. For example, VEJ_1 allowed reducing the compressor power to 2.67% at $P_{\text{lift}} = 4$ bar and $T_{\text{GC, out}} = 35$ °C, while at 20 °C, the power consumption drops by 3.46% compared to the parallel system. The maximum saving with this small-scale ejector profile was 3.6% at $P_{\text{lift}} = 5$ bar and $T_{\text{GC, out}}$ of 20°C.

The result of the compressor energy saving was susceptible to the liquid separator pressure lift. For instance, the amount of the power reduction started to reduce the power from more than 1% when the pressure lift is 1 bar and increased to the optimum based on the ejector efficiency then dropped to become dysfunctional. It is also noteworthy that the calculated data of the total compressor power-saving did not improve substantially when decreasing the exit gas cooler temperature from 25 °C to 20 °C, which for instance slowly grew by 0.06% compared with 0.64% and 1.43% differences in case of the decrease in the exit gas cooler temperature from 30 °C to 25 °C, or from 35 °C to 30 °C respectively, all at the $P_{\text{lift}} = 7$ bar. The staging result is associated with the R744 properties distribution with respect to the fluid mass fraction. However, this type of analysis is essential to evaluate the impact of any individual multi-ejector cartridges, especially on the systems rated for higher cooling capacity.

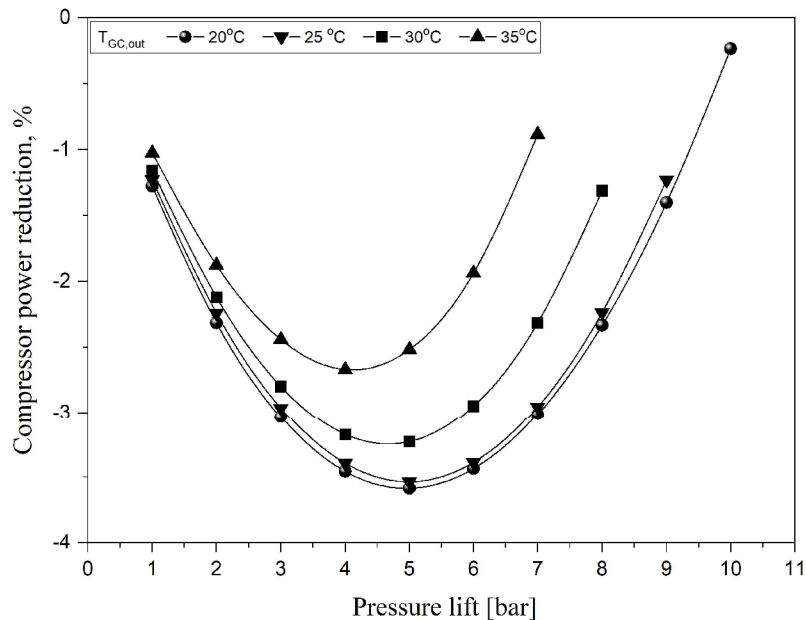


Figure 5.17 The impact of the ejector profile on the compressor power-saving as a function of the different pressure lift and exit gas cooler temperatures.

Figure 5.18 illustrates the system overall power consumption labeled with the different gas cooler outlet temperatures and pressures selected at pressure lift of 4 bar. Generally, the

power consumption was increased as the compressor discharge pressure increased to produce a higher compression ratio. As depicted in the figure, working subcritical at $T_{GC, out}$ of 20 °C, showed the least energy consumption. When the system operated at a gas cooler pressure of 60 bar, the compressors consumed in total 3.07 kW while running the ejector helped recover 1.32% of this energy.

The energy saved then increased to 5.4% by using the ejector when the system operated at a gas cooler pressure of 100 bar. The result also revealed an increase in the overall compressor energy consumption by increasing the exit gas cooler temperature due to the higher amount of flash gas removed from the liquid separator by the parallel compressor. For example, the power needed at 90 bar discharge compressor pressure was increased by 7.5% when the exit gas cooler temperature increased from 20 to 25°C and propagated to 36.3% higher if the temperature was increased to 35°C. Therefore, implementing the ejector leads to a reduction in power consumption compared to operation without the ejector. In the studied 90 bar gas cooler pressure, the ejector could save 2.67-3.46% of the total compressor power when the system is running at exit gas cooler temperature of 20°C to 35°C.

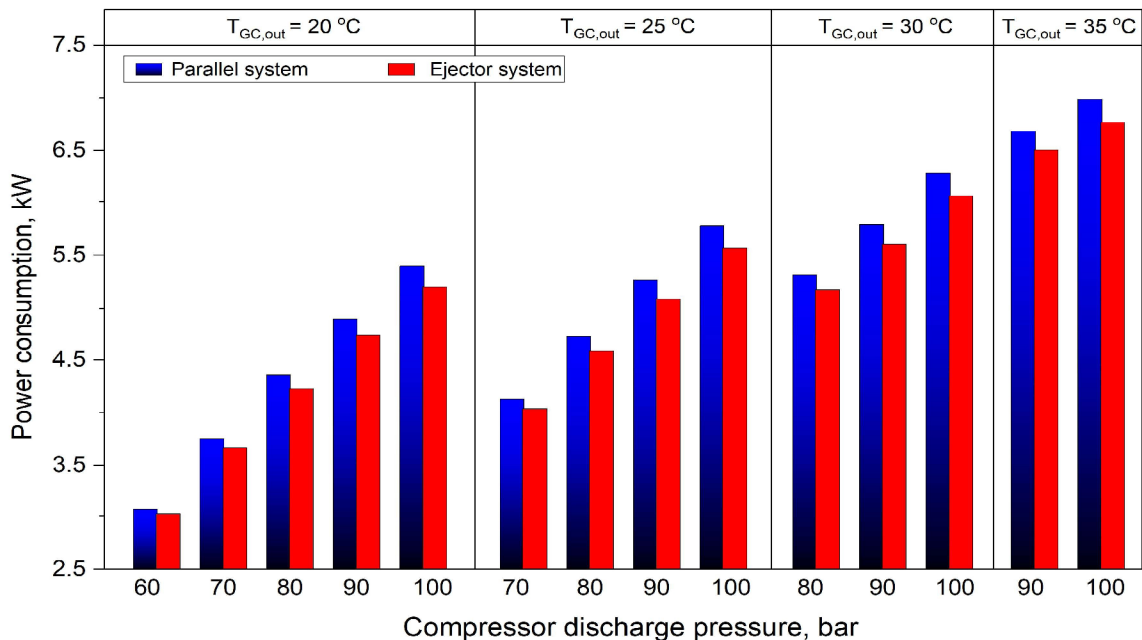


Figure 5.18 Total power consumption of the compressors as a function of the different exit gas cooler pressure and temperature with and without ejector supported system.

In the previous analysis, the ejector profile was evaluated at the cooling capacity of 15 kW. The impact of this small size ejector profile on the overall system COP improvement and

the reduction of the power consumption (Δ_{comp}) for different system cooling capacities are represented in Figure 5.19. The analysis was performed under compressor discharge pressure of 90 bar and $P_{\text{lift}} = 5$ bar via different exit gas cooler temperatures.

The result provided a significant COP improvement when running the ejector at low system cooling capacity. The great COP improvement recorded was 11.22% than operating in parallel configuration baseline at $T_{\text{GC, out}} = 20$ °C while the compressor power was reduced by 4.92% under the same cooling load of 3 kW at $T_{\text{GC, out}} = 35$ °C. As long as the system cooling capacity increased, the positive effect of the ejector diminished. For example, COP improvement sharply dropped to less than half when the cooling load was doubled to 6 kW, then witnessed a moderate decrease with the system cooling capacity growth. Furthermore, implementing the ejector to the system helped to save some of the energy needed for the compressors. Based on the calculation, up to 18% of the supplied power could be saved at the lower cooling load of 3 kW depending on the exit gas cooler temperature. In contrast, running the system with a higher cooling capacity increased overall power consumption and reduced system performance. The savings were significantly reduced when the system worked transcritically for a higher cooling load. It was observed that operating at exit gas cooler temperature of 35 °C reduced savings to 70% and operation at 30°C reduced overall savings to 78% compared to the operation at 20 °C.

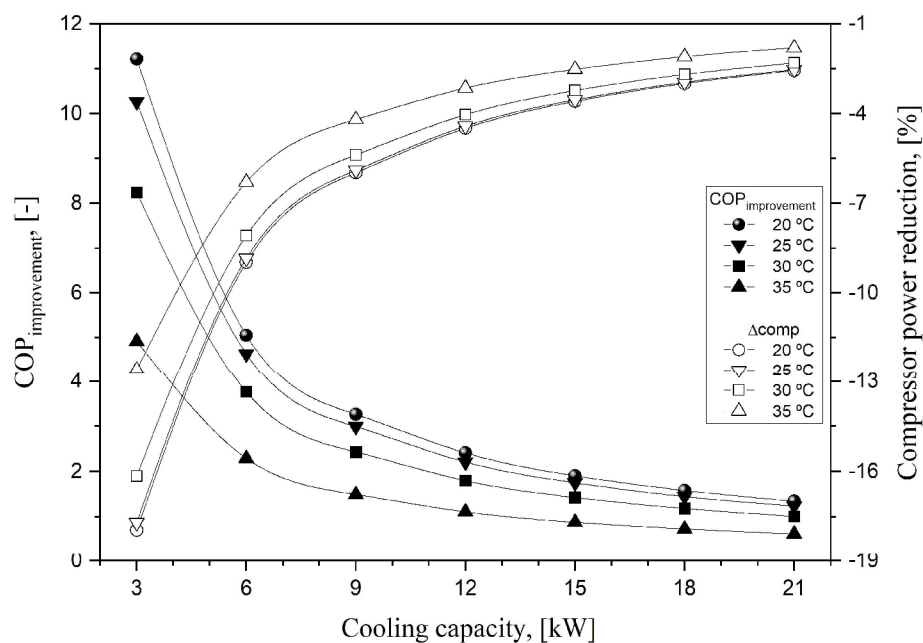


Figure 5.19 Contribution of the ejector on the system COP improvement and compressor power reduction versus different system cooling capacities.

5.4.4 System exergy analysis

The maximum amount of the useful work at any specific thermodynamic state in the system is determined by the exergy analysis at which the system reaches the equilibrium state with the surroundings. Decreasing the exergy destruction encourages an increase in the useful exergy product out of the feeding exergy. R744 transcritical cycles exemplify significant exergy destruction due to the throttling losses in the expansion process. Therefore, the HPV could be replaced (or supported in parallel for safety reasons) by an ejector to recover this work and improve the performance. Figure 5.20 shows the exergy destruction rates of the main system components in case of operating with ejector or in the parallel system baseline at two different exit gas cooler temperatures and pressure lift of 5 bar. The analysis was performed at compressor discharge pressure of 90 bar and 15 kW system cooling capacity. The result revealed a significant decrease in total system exergy destruction by employing the ejector profile in the system. At exit gas cooler temperature of 20 °C, the ejector saved up to 24.7% of the base-load compressor exergy destruction by compression the sucked flow in the ejector suction nozzle to the intermediate pressure level.

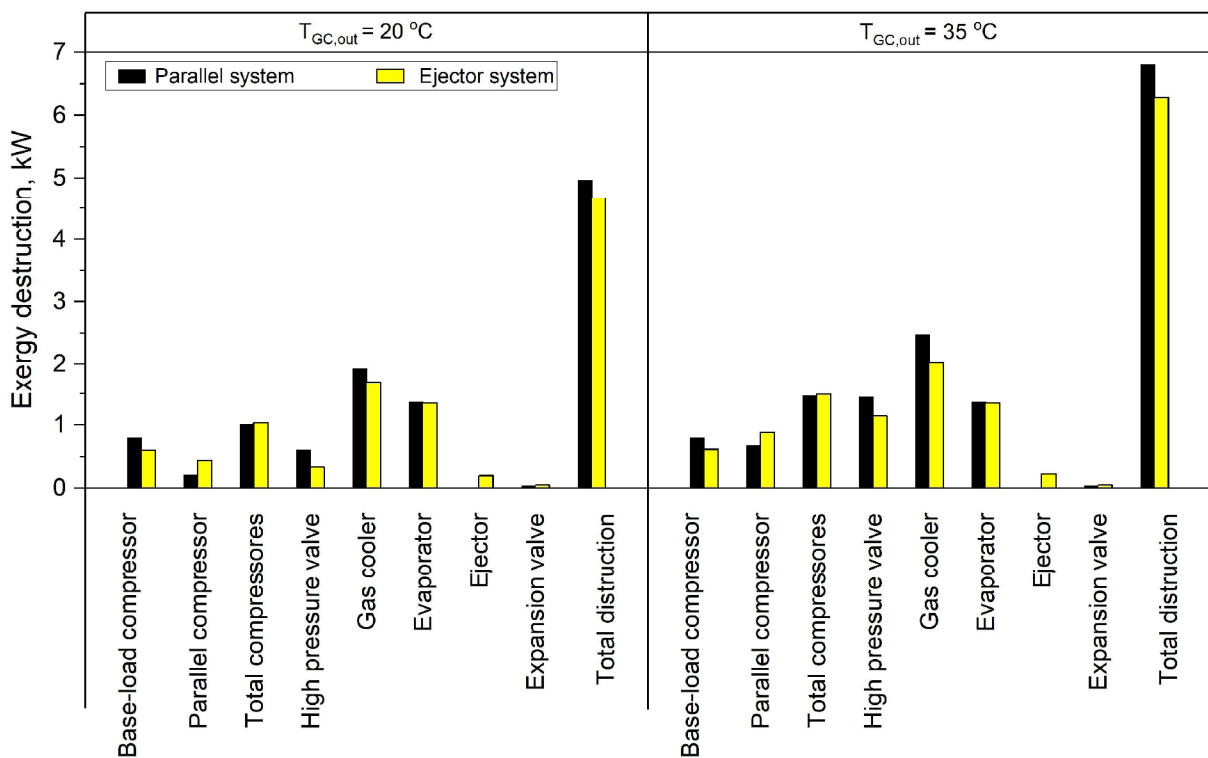


Figure 5.20 Exergy destruction of the total system and each component for both parallel and ejector supported systems at different exit gas cooler temperatures and pressure lift of 5 bar.

In contrast, the exergy loss at the parallel compressors doubled by implementing the ejector, especially at the condition of higher mass entrainment ratio and low pressure lift. Therefore, the total compressor exergy destruction was a bit higher when using the ejector. When the exit gas cooler outlet temperature increased to 35 °C, the exergy destruction in the parallel compressor increased three times compared with the 20 °C exit gas cooler operating condition. However, running the ejector under the same conditions increased the parallel compressor exergy destruction to 31%. This growth was associated with the rise in the vapor portion needed to be compressed by the parallel compressor in the liquid separator downstream the high pressure valve and the high vapor content flow from the ejector exit.

It is assumptive from the R744 transcritical refrigeration system that HPV is responsible for considerable amount of irreversibility in the cycle. The result indicated a significant exergy destruction rate of 0.61 kW through the HPV at $T_{GC, out} = 20$ °C, and an enormous drop to 46% of the exergy losses when the ejector was invested together with the HPV to recover the expansion work compared to 21% when running transcritical at 35 °C. Among all the system components, the gas cooler faced particular challenges, which exhibited the most considerable exergy destruction rate of 1.93 kW at $T_{GC, out} = 20$ °C.

The result aligned with the conventional exergy outcome analyzed by Gullo et al. [128], where the gas cooler accounted for the highest irreversibilities in the investigation. On the other hand, the higher the designed exit gas cooler temperature, the more detrimental the exergy destruction would be. For example, at $T_{GC, out} = 35$ °C, the exergy losses increased to 2.47 kW. Therefore, reducing the gas cooler irreversibilities will allow achieving higher system performance. Lowering the gas cooler approach temperature could be one solution. This improvement could be attained by using a more efficient compressor, increasing the evaporation temperature, or adopting a more sophisticated system layout, such as employing the ejector. The proposed ejector solution contributed to recover 11.4% to 18% of the gas cooler exergy destruction at $T_{GC, out}$ of 20 °C and 35 °C, respectively.

The analysis introduced the evaporator as the second highest exergy destruction component at $T_{GC, out} = 20$ °C by 1.37 kW, while increasing the exit gas cooler temperature does not have a prominent influence because of the fixed cooling capacity. In addition, the ejector provided a minor improvement of 1.6% lower exergy destruction compared to the parallel system baseline. The ejector profile shared little amount of the exergy losses of 0.2 kW at the

subcritical mode, then increased to 0.22 kW when the motive nozzle inlet temperature increased to 35 °C. The analysis was conducted for the metering expansion valve used to control the pressure level in the evaporator. The result revealed a minimal exergy destruction rate of less than 0.05 kW throughout the valve and is not affected by the temperature since a similar mass flow rate for the fixed cooling capacity is delivered. As a result, the ejector supported concept of the CO₂ system could save from 6.2% to 7.8% total exergy destruction rate compared to the parallel system layout (Thanks to the presence of ejector). This value varied based on the pressure lift provided by the liquid separator working setpoint and the system cooling load, as will be emphasized later.

The breakdown of the contribution of each system component in the exergy losses was represented in Figure 5.21 at gas cooler pressure of 90 bar, $T_{GC, out} = 20$ °C, and pressure lift of 5 bar with and without the ejector. The outcome brought to the light that the ejector has a significant impact on the exergy destruction rate of the HPV and the base-load compressor. The HPV losses dramatically dropped from 12.3% and it was responsible for 7.1% of the exergy destruction.

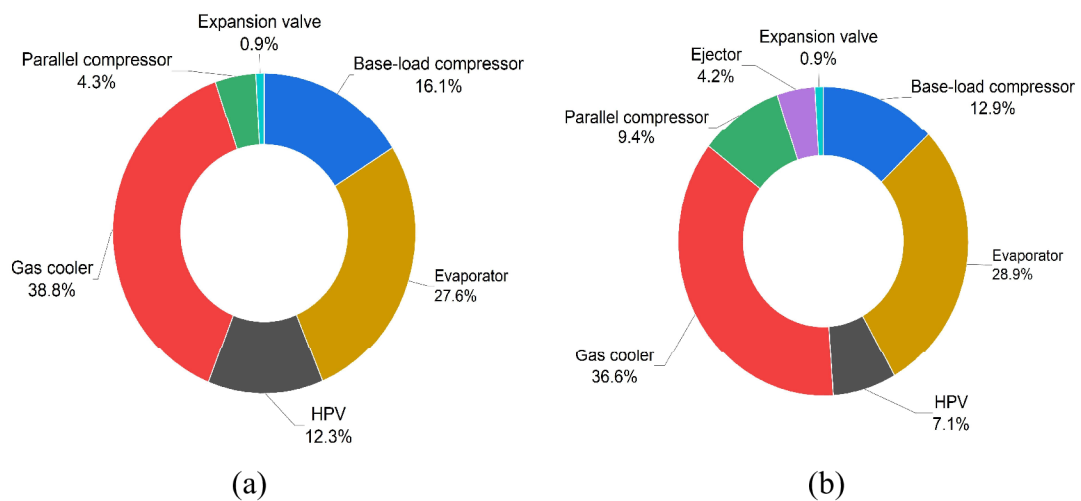


Figure 5.21 Breakdown of the exergy destruction rate of each system component contribution at $T_{GC, out} = 20$ °C, $P_{lift} = 5$ bar and 90 bar gas cooler pressure (a) without ejector. (b) with ejector.

Moreover, despite the low value of the losses in the HPV, a noteworthy difference could be achieved by operating at a very low pressure lift and high exit gas cooler temperature. In comparison, 3.2% of the total losses were saved through the based-load compressor by running the ejector. However, the gas cooler and the evaporator are main components responsible together for more than 65% of the total exergy losses. A more in-depth study could be

performed to classify the part of the irreversibilities that can be avoided and the technological limitation based on the advanced exergy analysis but exceeding the scope of this thesis.

Figure 5.22 represents the total system exergy destruction rate due to the varying cooling loads at pressure lift of 5 bar and two different exit gas cooler temperatures; this highlights the amount of the total losses that the ejector profile could recover. It could be noticed that operating at low exit gas cooler temperatures provided lower total exergy losses for the system. At $T_{GC, out} = 35\text{ }^{\circ}\text{C}$, the total exergy destruction rose by 37.6% compared with running at $20\text{ }^{\circ}\text{C}$. However, the ejector offers a solution to significantly reduce overall losses.

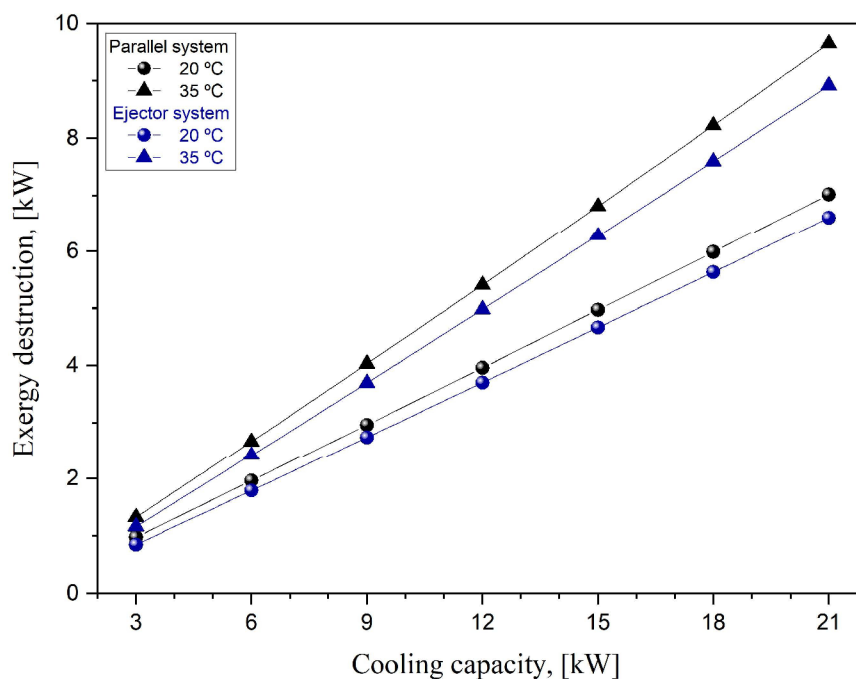


Figure 5.22 Total exergy destruction rate of the baseline parallel system and ejector supported system via different cooling capacities at two different exit gas cooler temperatures.

The potential improvement of the entire system exergy destruction due to the ejector was indicated from 7.66% to 12.35% for system cooling capacity varied from 21 kW to 3 kW, at an exit gas cooler temperature of $35\text{ }^{\circ}\text{C}$. On the other hand, the adoption of this small-size ejector profile allowed the reduction of 5.82% of the total system exergy losses at the higher cooling load of 21 kW, while the maximum of 13.2% from the total exergy destruction could be saved when the cooling capacity reduced to the minimum at $T_{GC, out} = 20\text{ }^{\circ}\text{C}$.

The two-phase ejectors conquered the CO_2 refrigeration and heat pump sector as due to the fact that they have proven to be a reliable solution for reducing system exergy losses and

optimizing energy consumption, and have led to a very efficient system. The performance of the system proved to be influenced by the ejector efficiency, which led the system to operate at the optimal working condition. However, further analysis on the use of the different ejector cartridge combinations and geometries (for example, when using a multi-ejector module) would be desired to maximize the COP of the CO₂ refrigeration system.

6 CONCLUSIONS AND FUTURE WORK

6.1 Conclusions

The thesis investigated a detailed experimental work and exergy analysis of the R744 transcritical ejector cooling system. The influence of different motive nozzle flow pressure and temperature, evaporation temperature, and ejector outlet flow pressure in the liquid separator on the ejector performance were evaluated. In order to ensure a stable load at the heat exchangers, the coefficient of liquid mass balance was calculated to guarantee that all the experimental data was collected at the steady-state conditions. Finding the optimum working range of the ejector is necessary for an efficient R744 system. Therefore, the ejector operating parameters such as pressure lift, mass entrainment ratio, work rate recovery, and efficiency were evaluated. Moreover, the potential impact of the tested ejector profile on the R744 transcritical refrigeration system was investigated based on the first and the second law of thermodynamic analysis for different operating conditions. The concept of ejector performance was shown on examples of approximation functions considered in the study and validated by the experiment with reasonable accuracy. The implementation of the ejector profile in the cooling cycle was compared with the conventional parallel system layout as a baseline. The most relevant findings can be drawn and summarized as follows:

1. The tested ejector could provide a maximum pressure lift of 9.51 bar, which was defined in a linear relation with the motive nozzle flow pressure. The concluded correlation helps control the parallel compressor pressure ratio and contributes to improving the system performance.
2. The results indicated that increasing the evaporation temperature influence the ejector pressure lift by decreasing and holding up the inverse proportional with the mass entrainment ratio. Additionally, with higher evaporative temperature, the ejector is shifting to work under higher separator pressure with further steeper mass entrainment ratio while increasing the motive nozzle flow pressure allows stretching the ejector separator pressure working range.
3. Among different exit gas cooler conditions, the ejector was able to recover up to 36.9% of the throttling losses according to the efficiency metric definition.

4. With respect to the motive nozzle flow pressure, the ejector profile evaluation results revealed a better overall performance when the ejector operated at supercritical conditions close to 90 bar. It was found that the ejector was working at subcritical mode (single choking) in most of the cases and the separator pressure range was very short (less than 10 bar) comparing to other refrigerants.
5. Based on the exergy distribution findings, the ejector holds high exergy efficiency when working at higher exit gas cooler temperatures, along with providing lower exergy destruction. The amount of the exergy consumed and destructed proved to be increasing progressively with higher motive nozzle flow pressure while, in contrast, decreasing with higher motive nozzle flow temperature.
6. The ejector profile managed to improve the COP of the system by 2.05% for the working temperature lower than the critical point. In comparison, the maximum improvement of 11.22% could be reached when the system cooling capacity decreased to 3 kW. Furthermore, the peak of 1% to 1.92% of the system exergy efficiency improvement was recorded and was characterized by the highest ejector efficiency and exit gas cooler temperature. In general, the ejector gradually degraded the system performance for the lower limit of the pressure lift.
7. The calculation results define how to exploit the ejector to reduce the total compressor power consumption. The current ejector profile saved up to 3.46% of the compressor input energy when working at subcritical conditions. It saved up to 2.67% when operating transcritical at the maximum compressor discharge pressure of 90 bar. On the other hand, utilizing this ejector for lower system cooling capacity is capable of reducing the supplied power by up to 18%.
8. The exergy analysis revealed a prominent reduction of total system exergy destruction by employing the ejector in parallel with the high pressure valve. The ejector recovered 21% of the expansion work and saved 46% of the HPV exergy losses. In general, the exergy destruction rate increased when the exit gas cooler temperature was higher than the critical point. However, the gas cooler and the evaporator are the most important system components in terms of losses. Additionally, the result exhibited a maximum system exergy loss of 7.8% that could be saved at the set conditions and a maximum of 13.2% total system exergy destruction rate recovered by the ejector occupied at a lower cooling load.

6.2 Assessment of objectives

The assessment of the thesis objectives listed in the introduction chapter at the beginning of the thesis are presented below:

- A comprehensive literature review has been presented for state of the art on CO₂ refrigeration system technologies supported with a two-phase ejector. The ejector control strategy and the properties of this natural refrigerant were also included in detail.
- An extensive experimental test campaign has been performed to set the ejector performance map and the effect of different operation conditions on the ejector profile with comparative analysis.
- The ejector exergy distributions and exergy destruction for each component and the whole system were represented and discussed.
- The positive impact of the ejector profile on the R744 transcritical refrigeration system was clarified, and the system operational characteristics improvements were declared in all aspects.

6.3 Future works

- Based on the challenges we face during experiments and data processing, as well as the results of other researchers in this field, the author would like to suggest future work: Because of high ejector exergy destruction, numerical modeling with the help of computational fluid dynamics could be performed on this ejector to predict the main location of the exergy loss and probe the physical insight of this two-phase flow ejector. However, CFD-based approaches could be accomplished using a homogeneous relaxation model and validate the result with the data from the performed experiment.
- The CO₂ compressor discharge temperature is very high, especially at the high gas cooler pressure. Therefore, the author suggests using this rejected heat as a low-grade heat source for conventional ejector refrigeration systems (ERS). This novel proposal can be applied in a compact brazed heat exchanger between the CO₂ in the gas cooler on one side and HFOs refrigerants on the other side in the generator.

- To increase the ejector efficiency over a broad operation range, the ejector geometries should be simultaneously controlled. This can be performed using multi-objective evolutionary algorithm optimization (MOEA), which has not yet been done for the two-phase flow ejector, especially when coupled with computational fluid dynamics analyses.
- For the overall system improvements, 4E (energy, exergy, economic and environmental) analysis could be studied. This evaluation will help the designers and researchers set the economic and ecological problems and introduce efficient thermo-economic solutions to the globe.

BIBLIOGRAPHY

- [1] Shestopalov KO, Huang BJ, Petrenko VO, Volovyk OS. Investigation of an experimental ejector refrigeration machine operating with refrigerant R245fa at design and off-design working conditions. Part 2. Theoretical and experimental results. *Int J Refrig* 2015;55:201–11. <https://doi.org/10.1016/j.ijrefrig.2015.01.016>.
- [2] Gullo P, Hafner A, Banasiak K, Minetto S, Kriezi EE. Multi-ejector concept: A comprehensive review on its latest technological developments. *Energies* 2019;12. <https://doi.org/10.3390/en12030406>.
- [3] J.S.H. Carbon dioxide as a refrigerant. *J Franklin Inst* 1923;196:713. [https://doi.org/10.1016/s0016-0032\(23\)90612-5](https://doi.org/10.1016/s0016-0032(23)90612-5).
- [4] Haida M, Smolka J, Palacz M, Bodys J, Nowak AJ, Bulinski Z, et al. Numerical investigation of an r744 liquid ejector for supermarket refrigeration systems. *Therm Sci* 2016;20:1259–69.
- [5] Kim MH, Pettersen J, Bullard CW. Fundamental process and system design issues in CO₂ vapor compression systems. vol. 30. 2004. <https://doi.org/10.1016/j.pecs.2003.09.002>.
- [6] Edition I. 2009 ASHRAE Handbook - Fundamentals (SI Edition). Am Soc Heating, Refrig Air-Conditioning Eng Inc 2009.
- [7] Chasserot M, Masson N, Jia H, Burkel S, Maratou A, Skačanová K. Guide 2014: Natural refrigerants - continued growth and innovation in Europe. Report 2014:1–195.
- [8] Neksa P, Walnum HT, Hafner A. Keynote: CO₂ - a refrigerant from the past with prospects of being one of the main refrigerants in the future. 9th IIR-Gustav Lorentzen Conference on Natural Working Fluids. 9th IIR Gustav Lorentzen Conf 2010.
- [9] International Energy Agency. Air conditioning use emerges as one of the key drivers of global electricity-demand growth 2018. <https://www.iea.org/newsroom/news/2018/may/air-conditioning-use-emerges-as-one-of-the-key-drivers-of-global-electricity-dema.html>.
- [10] Elbel S. Historical and present developments of ejector refrigeration systems with emphasis on transcritical carbon dioxide air-conditioning. *Int J Refrig* 2011;34:1545–61.
- [11] Chunnanond K, Aphornratana S. Ejectors: Applications in refrigeration technology. *Renew Sustain Energy Rev* 2004;8:129–55. <https://doi.org/10.1016/j.rser.2003.10.001>.
- [12] Gay NH. Refrigerating System. U.S. 1,836,318. 1931.
- [13] Beithou N, Aybar HS. A mathematical model for steam-driven jet pump. *Int J Multiph Flow* 2000;26:1609–19. [https://doi.org/10.1016/S0301-9322\(99\)00116-0](https://doi.org/10.1016/S0301-9322(99)00116-0).
- [14] Power RB. Steam Jet Ejectors for the Process Industries. 2021.
- [15] Bartosiewicz Y, Aidoun Z, Desevaux P, Mercadier Y. Numerical and experimental investigations on supersonic ejectors. *Int J Heat Fluid Flow* 2005;26:56–70.
- [16] Alperin M, Wu JJ. Thrust augmenting ejectors, part I. *AIAA J* 1983;21:1428–36. <https://doi.org/10.2514/3.60148>.
- [17] L Addy A, C Dutton J, C Mikkelsen C. Supersonic Ejector-Diffuser Theory and Experiments 1982:106.
- [18] Hafner A, Banasiak K. R744 ejector technology future perspectives. *J Phys Conf Ser* 2016;745. <https://doi.org/10.1088/1742-6596/745/3/032157>.
- [19] Elbel S, Hrnjak P. Flash gas bypass for improving the performance of transcritical R744 systems that use microchannel evaporators. *Int J Refrig* 2004;27:724–35.

- [20] Sawalha S, Piscopiello S, Karampour M, Manickam L, Rogstam J. Field measurements of supermarket refrigeration systems . Part II: Analysis of HFC refrigeration systems and comparison to CO₂. *Appl Therm Eng* 2022;111:170–82. <https://doi.org/10.1016/j.applthermaleng.2016.09.073>.
- [21] Andri I, Pina A, Ferrão P, Fournier J, Lacarrière B, Corre O Le. ScienceDirect ScienceDirect State-of-the-art technologies for transcritical refrigeration systems – a theoretical assessment of energy advantages for Assessing the feasibility of using the heat demand-outdoor European food retail industry temperature func. *Energy Procedia* 2017;123:46–53. <https://doi.org/10.1016/j.egypro.2017.07.283>.
- [22] Gullo P, Elmegaard B, Cortella G. Energy and environmental performance assessment of R744 booster supermarket refrigeration systems operating in warm Évaluation de la performance énergétique et environnementale de systèmes frigorifiques de supermarché au R744 de type « booster » fonctionn. *Int J Refrig* 2016;64:61–79. <https://doi.org/10.1016/j.ijrefrig.2015.12.016>.
- [23] Sarkar J, Agrawal N. International Journal of Thermal Sciences Performance optimization of transcritical CO₂ cycle with parallel compression economization. *Int J Therm Sci* 2010;49:838–43. <https://doi.org/10.1016/j.ijthermalsci.2009.12.001>.
- [24] Bajja SH. Experimental analysis of R744 multi-ejector modules 2019.
- [25] Chesi A, Esposito F, Ferrara G, Ferrari L. Experimental analysis of R744 parallel compression cycle. *Appl Energy* 2014;135:274–85. <https://doi.org/10.1016/j.apenergy.2014.08.087>.
- [26] Version D. Energetic , Exergetic and Exergoeconomic Analysis of CO₂ Refrigeration Systems Operating in Hot Climates 2015.
- [27] Karampour M, Sawalha S. State-of-the-art integrated CO₂ refrigeration system for supermarkets : A comparative analysis État de l ' art des systèmes frigorifiques au CO₂ intégrés pour les supermarchés : analyse comparative. *Int J Refrig* 2018;86:239–57. <https://doi.org/10.1016/j.ijrefrig.2017.11.006>.
- [28] Fazelpour F, Morosuk T. Exergoeconomic analysis of carbon dioxide transcritical refrigeration machines. *Int J Refrig* 2014;38:128–39. <https://doi.org/10.1016/j.ijrefrig.2013.09.016>.
- [29] Zhang Z, Ma Y, Li M, Zhao L. Recent advances of energy recovery expanders in the transcritical CO₂ refrigeration cycle. *HVAC R Res* 2013;19:376–84. <https://doi.org/10.1080/10789669.2013.784644>.
- [30] Kakuda M, Nagata H, Ishizono F. Development of a scroll expander for the CO₂ Refrigeration Cycle. *HVAC R Res* 2009;15:771–83. <https://doi.org/10.1080/10789669.2009.10390863>.
- [31] Elbarghthi AFA, Mohamed S, Nguyen VV, Dvorak V. CFD based design for ejector cooling system using HFOS (1234ze(E) and 1234yf). *Energies* 2020;13. <https://doi.org/10.3390/en13061408>.
- [32] Elbel S, Hrnjak P. Experimental validation of a prototype ejector designed to reduce throttling losses encountered in transcritical R744 system operation. *Int J Refrig* 2008;31:411–22. <https://doi.org/10.1016/j.ijrefrig.2007.07.013>.
- [33] Lee JS, Kim MS, Kim MS. Experimental study on the improvement of CO₂ air conditioning system performance using an ejector. *Int J Refrig* 2011;34:1614–25.
- [34] Nakagawa M, Marasigan AR, Matsukawa T. Experimental analysis on the effect of internal heat exchanger in transcritical CO₂ refrigeration cycle with two-phase ejector. *Int J Refrig* 2011;34:1577–86. <https://doi.org/10.1016/j.ijrefrig.2010.03.007>.
- [35] Lawrence N, Elbel S. Analysis of two-phase ejector performance metrics and comparison of

- R134a and CO₂ ejector performance. Sci Technol Built Environ* 2015;21:515–25.
- [36] Schönerberger J, Hafner A, Banasiak K, Giroto S. Experience with ejectors implemented in a R744 booster system operating in a supermarket. *11th IIR Gustav Lorentzen Conf Nat Refrig Nat Refrig Environ Prot GL* 2014 2014:755–65.
- [37] Hafner A, Försterling S, Banasiak K. Multi-ejector concept for R-744 supermarket refrigeration. *Int J Refrig* 2014;43:1–13. <https://doi.org/10.1016/j.ijrefrig.2013.10.015>.
- [38] Gullo P, Hafner A, Banasiak K. Transcritical R744 refrigeration systems for supermarket applications: Current status and future perspectives. *Int J Refrig* 2018;93:269–310. <https://doi.org/10.1016/j.ijrefrig.2018.07.001>.
- [39] Liu F, Li Y, Groll EA. Performance enhancement of CO₂ air conditioner with a controllable ejector. *Int J Refrig* 2012;35:1604–16. <https://doi.org/10.1016/j.ijrefrig.2012.05.005>.
- [40] Carel. *Electronic Modulating Ejector* 2017:4.
- [41] Nekså P, Hafner A, Bredesen A, Eikevik TM. CO₂ as working fluid—Technological development on the road to sustainable refrigeration. *Proc. 12th IIR Gustav Lorentzen Nat. Work. Fluids Conf. Edinburgh, UK, 2016*, p. 21–4.
- [42] Giroto S. Improved transcritical CO₂ refrigeration systems for warm climates. *Proc. 7th IIR Ammon. CO₂ Refrig. Technol. Conf. Ohrid, Maced., 2017*, p. 11–3.
- [43] Banasiak K, Hafner A, Kriezi EE, Madsen KB, Birkelund M, Fredslund K, et al. Développement et cartographie de performance du pack de récupération du travail de détente à multi éjecteur pour des unités de compression de vapeur de R744. *Int J Refrig* 2015;57:265–76. <https://doi.org/10.1016/j.ijrefrig.2015.05.016>.
- [44] Smolka J, Bulinski Z, Fic A, Nowak AJ, Banasiak K, Hafner A. A computational model of a transcritical R744 ejector based on a homogeneous real fluid approach. *Appl Math Model* 2013;37:1208–24. <https://doi.org/10.1016/j.apm.2012.03.044>.
- [45] Palacz M, Smolka J, Fic A, Bulinski Z, Nowak AJ, Banasiak K, et al. Application range of the HEM approach for CO₂ expansion inside two-phase ejectors for supermarket refrigeration systems. *Int J Refrig* 2015;59:251–8. <https://doi.org/10.1016/j.ijrefrig.2015.07.006>.
- [46] Palacz M, Smolka J, Kus W, Fic A, Bulinski Z, Nowak AJ, et al. CFD-based shape optimisation of a CO₂ two-phase ejector mixing section. *Appl Therm Eng* 2016;95:62–9. <https://doi.org/10.1016/j.applthermaleng.2015.11.012>.
- [47] Palacz M, Haida M, Smolka J, Nowak AJ, Banasiak K, Hafner A. HEM and HRM accuracy comparison for the simulation of CO₂ expansion in two-phase ejectors for supermarket refrigeration systems. *Appl Therm Eng* 2017;115:160–9. <https://doi.org/10.1016/j.applthermaleng.2016.12.122>.
- [48] Palacz M, Smolka J, Nowak AJ, Banasiak K, Hafner A. Shape optimisation of a two-phase ejector for CO₂ refrigeration systems. *Int J Refrig* 2017;74:210–21. <https://doi.org/10.1016/j.ijrefrig.2016.10.013>.
- [49] Haida M, Smolka J, Hafner A, Ostrowski Z, Palacz M, Madsen KB, et al. Performance mapping of the R744 ejectors for refrigeration and air conditioning supermarket application: A hybrid reduced-order model. *Energy* 2018;153:933–48.
- [50] Bodys J, Palacz M, Haida M, Smolka J, Nowak AJ, Banasiak K, et al. Full-scale multi-ejector module for a carbon dioxide supermarket refrigeration system: Numerical study of performance evaluation. *Energy Convers Manag* 2017. <https://doi.org/10.1016/j.enconman.2017.02.007>.
- [51] Bodys J, Smolka J, Palacz M, Haida M, Banasiak K, Nowak AJ, et al. Performance of fixed geometry ejectors with a swirl motion installed in a multi-ejector module of a CO₂ refrigeration

- system. *Energy* 2016;117:620–31.
- [52] Danfoss AS. *Multi Ejector Solution TM for R744 (CO 2) Product type - CTM 6 Low Pressure (LP)* 2018;744:1–8.
- [53] ASHRAE. *2018 ASHRAE Handbook-Refrigeration*. 2018.
- [54] United Nations Development Programme. *Montreal Protocol on Substances that Deplete the Ozone Layer. 20 years of success*. *Development* 2007:50.
- [55] Witkowski A, Majkut M, Rulik S. *Analysis of pipeline transportation systems for carbon dioxide sequestration*. *Arch Thermodyn* 2014;35:117–40. <https://doi.org/10.2478/aoter-2014-0008>.
- [56] Rony RU, Yang H, Krishnan S, Song J. *Recent advances in transcritical CO 2 (R744) heat pump system: A review*. vol. 12. 2019. <https://doi.org/10.3390/en12030457>.
- [57] Nawaz K, Shen B, Elatar A, Baxter V, Abdelaziz O. *Le R1234yf et le R1234ze(E) comme frigorigènes à faible GWP pour des chauffe-eau domestiques à pompe à chaleur*. *Int J Refrig* 2017;82:348–65. <https://doi.org/10.1016/j.ijrefrig.2017.06.031>.
- [58] Lemmon EW, Bell IH, Huber ML, McLinden MO. *NIST Standard Reference Database 23: Reference Fluid Thermodynamic and Transport Properties-REFPROP, Version 9.0*, National Institute of Standards and Technology 2018:135.
- [59] Jiang PX, Xu RN. *Heat transfer and pressure drop characteristics of mini-fin structures*. *Int J Heat Fluid Flow* 2007;28:1167–77. <https://doi.org/10.1016/j.ijheatfluidflow.2006.11.008>.
- [60] Cavallini A, Zilio C. *Carbon dioxide as a natural refrigerant*. *Int J Low Carbon Technol* 2007;2:225–49. <https://doi.org/10.1093/ijlct/2.3.225>.
- [61] The European Parliament and the Council of the European Union. *REGULATION (EU) No 517/2014*. *Off J Eur Union* 2014;57:195–230.
- [62] Lorentzen G. *Revival of carbon dioxide as a refrigerant*. *H V Eng* 1994;66:9–14.
- [63] Ringstad KE, Allouche Y, Gullo P, Ervik Å, Banasiak K, Hafner A. *A detailed review on CO₂ two-phase ejector flow modeling*. *Therm Sci Eng Prog* 2020;20. <https://doi.org/10.1016/j.tsep.2020.100647>.
- [64] Elbarghthi AFA, Hafner A, Banasiak K, Dvorak V. *An experimental study of an ejector-boosted transcritical R744 refrigeration system including an exergy analysis*. *Energy Convers Manag* 2021;238:114102. <https://doi.org/10.1016/j.enconman.2021.114102>.
- [65] Elbel S, Lawrence N. *Review of recent developments in advanced ejector technology*. *Int J Refrig* 2016;62:1–18. <https://doi.org/10.1016/j.ijrefrig.2015.10.031>.
- [66] Lucas C, Koehler J. *Experimental investigation of the COP improvement of a refrigeration cycle by use of an ejector*. *Int J Refrig* 2012;35:1595–603. <https://doi.org/10.1016/j.ijrefrig.2012.05.010>.
- [67] Lucas C, Koehler J, Schroeder A, Tischendorf C. *Experimentally validated CO₂ ejector operation characteristic used in a numerical investigation of ejector cycle*. *Int J Refrig* 2013;36:881–91. <https://doi.org/10.1016/j.ijrefrig.2012.10.035>.
- [68] Sarkar J. *Optimization of ejector-expansion transcritical CO₂ heat pump cycle*. *Energy* 2008;33:1399–406. <https://doi.org/10.1016/j.energy.2008.04.007>.
- [69] Banasiak K, Hafner A, Andresen T. *Experimental and numerical investigation of the influence of the two-phase ejector geometry on the performance of the R744 heat pump*. *Int J Refrig* 2012;35:1617–25. <https://doi.org/10.1016/j.ijrefrig.2012.04.012>.
- [70] Boccardi G, Botticella F, Lillo G, Mastrullo R, Mauro AW, Trinchieri R. *Thermodynamic Analysis of a Multi-Ejector, CO₂, Air-To-Water Heat Pump System*. *Energy Procedia* 2016;101:846–53. <https://doi.org/10.1016/j.egypro.2016.11.107>.

- [71] Boccardi G, Botticella F, Lillo G, Mastrullo R, Mauro AW, Trinchieri R. Experimental investigation on the performance of a transcritical CO₂ heat pump with multi-ejector expansion system. *Int J Refrig* 2017;82:389–400. <https://doi.org/10.1016/j.ijrefrig.2017.06.013>.
- [72] He Y, Deng J, Zheng L, Zhang Z. Performance optimization of a transcritical CO₂ refrigeration system using a controlled ejector. *Int J Refrig* 2017;75:250–61. <https://doi.org/10.1016/j.ijrefrig.2016.12.015>.
- [73] He Y, Deng J, Yang F, Zhang Z. An optimal multivariable controller for transcritical CO₂ refrigeration cycle with an adjustable ejector. *Energy Convers Manag* 2017;142:466–76. <https://doi.org/10.1016/j.enconman.2017.03.070>.
- [74] Chen Z, Guo N, Qiu RC. Demonstration of real-time spectrum sensing for cognitive radio. *Proc - IEEE Mil Commun Conf MILCOM 2010*;14:323–8. <https://doi.org/10.1109/MILCOM.2010.5680333>.
- [75] Xu XX, Chen GM, Tang LM, Zhu ZJ. Experimental investigation on performance of transcritical CO₂ heat pump system with ejector under optimum high-side pressure. *Energy* 2012;44:870–7. <https://doi.org/10.1016/j.energy.2012.04.062>.
- [76] Smolka J, Palacz M, Bodys J, Banasiak K, Fic A, Bulinski Z, et al. Performance comparison of fixed- and controllable-geometry ejectors in a CO₂ refrigeration system. *Int J Refrig* 2016;65:172–82. <https://doi.org/10.1016/j.ijrefrig.2016.01.025>.
- [77] Palacz M, Smolka J, Nowak AJ, Banasiak K, Hafner A. Optimisation de forme d'un éjecteur diphasique pour les systèmes frigorifiques au CO₂. *Int J Refrig* 2017;74:210–21. <https://doi.org/10.1016/j.ijrefrig.2016.10.013>.
- [78] Liu F, Groll EA, Li D. Modeling study of an ejector expansion residential CO₂ air conditioning system. *Energy Build* 2012;53:127–36. <https://doi.org/10.1016/j.enbuild.2012.07.008>.
- [79] Liu F, Groll EA, Li D. Investigation on performance of variable geometry ejectors for CO₂ refrigeration cycles. *Energy* 2012;45:829–39. <https://doi.org/10.1016/j.energy.2012.07.008>.
- [80] Nakagawa M, Marasigan AR, Matsukawa T, Kurashina A. Experimental investigation on the effect of mixing length on the performance of two-phase ejector for CO₂ refrigeration cycle with and without heat exchanger. *Int J Refrig* 2011;34:1604–13. <https://doi.org/10.1016/j.ijrefrig.2010.07.021>.
- [81] Taleghani ST, Sorin M, Poncet S. Analysis and Optimization of Exergy Flows inside a Transcritical CO₂ Ejector for Refrigeration, Air Conditioning and Heat Pump Cycles. *Energies* 2019;12. <https://doi.org/10.3390/en12091686>.
- [82] Ersoy HK, Bilir N. Performance characteristics of ejector expander transcritical CO₂ refrigeration cycle. *Proc Inst Mech Eng Part A J Power Energy* 2012;226:623–35.
- [83] Kornhauser AA. The use of an ejector in a geothermal flash system. *Proc Intersoc Energy Convers Eng Conf* 1990;5:79–84. <https://doi.org/10.1109/iecec.1990.747930>.
- [84] Richter CC. Proposal of New Object-Oriented Equation-Based Model Libraries for Thermodynamic Systems. PhD Thesis. PhD Thesis 2008:1–157.
- [85] Elbel S, Hrnjak P. Effect of Internal Heat Exchanger on performance of transcritical CO₂ systems with ejector. *Int Refrig Air Cond Conf Purdue* 2004;R166:1–8.
- [86] Li D, Groll EA. Transcritical CO₂ refrigeration cycle with ejector-expansion device. *Int J Refrig* 2005;28:766–73. <https://doi.org/10.1016/j.ijrefrig.2004.10.008>.
- [87] Zhang Z, Tian L. Effect of suction nozzle pressure drop on the performance of an ejector-expansion transcritical CO₂ refrigeration cycle. *Entropy* 2014;16:4309–21. <https://doi.org/10.3390/e16084309>.

- [88] Ameer K, Aidoun Z, Ouzzane M. Modeling and numerical approach for the design and operation of two-phase ejectors. *Appl Therm Eng* 2016;109:809–18. <https://doi.org/10.1016/j.applthermaleng.2014.11.022>.
- [89] Taslimi Taleghani S, Sorin M, Poncet S. Modeling of two-phase transcritical CO₂ ejectors for on-design and off-design conditions. *Int J Refrig* 2018;87:91–105. <https://doi.org/10.1016/j.ijrefrig.2017.10.025>.
- [90] Ameer K, Aidoun Z. Two-phase ejector enhanced carbon dioxide transcritical heat pump for cold climate. *Energy Convers Manag* 2021;243:114421. <https://doi.org/10.1016/j.enconman.2021.114421>.
- [91] Açıkkalp E, Aras H, Hepbasli A. Advanced exergy analysis of a trigeneration system with a diesel-gas engine operating in a refrigerator plant building. *Energy Build* 2014;80:268–75. <https://doi.org/10.1016/j.enbuild.2014.05.029>.
- [92] Haida M, Banasiak K, Smolka J, Hafner A, Eikevik TM. Experimental analysis of the R744 vapour compression rack equipped with the multi-ejector expansion work recovery module. *Int J Refrig* 2016;64:93–107. <https://doi.org/10.1016/j.ijrefrig.2016.01.017>.
- [93] Gullo P, Tsamos KM, Hafner A, Banasiak K, Ge YT, Tassou SA. Crossing CO₂ equator with the aid of multi-ejector concept: A comprehensive energy and environmental comparative study. *Energy* 2018;164:236–63. <https://doi.org/10.1016/j.energy.2018.08.205>.
- [94] Cecchinato L, Corradi M, Minetto S. Energy performance of supermarket refrigeration and air conditioning integrated systems working with natural refrigerants. *Appl Therm Eng* 2012;48:378–91. <https://doi.org/10.1016/j.applthermaleng.2012.04.049>.
- [95] Pardiñas Á, Hafner A, Banasiak K. Novel integrated CO₂ vapour compression racks for supermarkets. Thermodynamic analysis of possible system configurations and influence of operational conditions. *Appl Therm Eng* 2018;131:1008–25. <https://doi.org/10.1016/j.applthermaleng.2017.12.015>.
- [96] Bai T, Yu J, Yan G. Advanced exergy analyses of an ejector expansion transcritical CO₂ refrigeration system. *Energy Convers Manag* 2016;126:850–61. <https://doi.org/10.1016/j.enconman.2016.08.057>.
- [97] Taslimitaleghani S, Sorin M, Poncet S. Energy and exergy efficiencies of different configurations of the ejector-based CO₂ refrigeration systems. *Int J Energy Prod Manag* 2018;3:22–33. <https://doi.org/10.2495/EQ-V3-N1-22-33>.
- [98] Fangtian S, Yitai M. Thermodynamic analysis of transcritical CO₂ refrigeration cycle with an ejector. *Appl Therm Eng* 2011;31:1184–9.
- [99] Gullo P, Hafner A, Banasiak K. Thermodynamic performance investigation of commercial R744 booster refrigeration plants based on advanced exergy analysis. *Energies* 2019;12:1–24. <https://doi.org/10.3390/en12030354>.
- [100] Danfoss. How to design a transcritical CO₂ system Type CTM 6 High Pressure (HP) and Low Pressure (LP) 2018.
- [101] Kracik J, Dvorak V, Nguyen Van V, Smierciew K. Experimental and Numerical Study on Supersonic Ejectors Working with R-1234ze(E). *EPJ Web Conf* 2018;180:02047. <https://doi.org/10.1051/epjconf/201818002047>.
- [102] Zhang T, Mohamed S. Conceptual Design and Analysis of Hydrocarbon-Based Solar Thermal Power and Ejector Cooling Systems in Hot Climates. *J Sol Energy Eng* 2014;137:021001. <https://doi.org/10.1115/1.4028365>.
- [103] Butrymowicz D, Śmierciew K, Karwacki J, Gagan J. Experimental investigations of low-

- temperature driven ejection refrigeration cycle operating with isobutane. *Int J Refrig* 2014;39:196–209. <https://doi.org/10.1016/j.ijrefrig.2013.10.008>.
- [104] Eames IW, Ablwaiifa AE, Petrenko V. Results of an experimental study of an advanced jet-pump refrigerator operating with R245fa. *Appl Therm Eng* 2007;27:2833–40.
- [105] Banasiak K, Hafner A, Haddal O, Eikevik T. Test facility for a multiejector R744 refrigeration system. *11th IIR Gustav Lorentzen Conf. Nat. Refrig. Nat. Refrig. Environ. Prot. GL* 2014, vol. 31, 2014, p. 783–90.
- [106] Köhler J, Richter C, Tegethoff W, Tischendorf C. *Experimental and Theoretical Study of a CO₂ Ejector Refrigeration Cycle* 2007:15.
- [107] Zheng L, Deng J. Research on CO₂ ejector component efficiencies by experiment measurement and distributed-parameter modeling. *Energy Convers Manag* 2017;142:244–56. <https://doi.org/10.1016/j.enconman.2017.03.017>.
- [108] Dvorak V, Vit T. *Experimental And Numerical Study Of Constant Area Mixing*. *16th Int Symp Transp Phenom* 2005:1–7. <https://doi.org/10.1016/j.mechmat.2008.10.015>.
- [109] Liu F. *Review on Ejector Efficiencies in Various Ejector Systems*. *15th Int Refrig Air Cond Conf* 2014:1–10.
- [110] Brodyanski VM, Sorin M V, Le Goff P. *The Efficiency of Industrial Processes: Exergy Analysis and Optimization*. Netherlands: Elsevier Science B. V; 1994.
- [111] Rosen MA, Dincer I. Effect of varying dead-state properties on energy and exergy analyses of thermal systems. *Int J Therm Sci* 2004;43:121–33. <https://doi.org/10.1016/j.ijthermalsci.2003.05.004>.
- [112] Fang G, Xing L, Yang F, Li H. Exergy analysis of a dual-mode refrigeration system for ice storage air conditioning. *Int J Archit Sci* 2005;6:6.
- [113] Dorin Software Version: 20.12, Available online from: <<http://www.dorin.com/en/Software/>> (Accessed 31 August 2021) 2020.
- [114] Jakobsen A, Rasmussen BD, Andersen SE. CoolPack—Simulation tools for refrigeration systems. *Scan Ref* 1999;28:7–10.
- [115] Munk S. MULTIEJECTOR STAND R744 (GALLERIET) OPERATORS MANUAL 2017;744.
- [116] J.C.F.G.I.M. Jcgm, (JCGM/WG. Evaluation of measurement data — Guide to the expression of uncertainty in measurement. *Int Organ Stand Geneva ISBN* 2008;50:134.
- [117] Zhu Y, Li C, Zhang F, Jiang PX. Comprehensive experimental study on a transcritical CO₂ ejector-expansion refrigeration system. *Energy Convers Manag* 2017;151:98–106.
- [118] Fredslund K, Kriezi EE, Madsen KB, Birkelund M, Olsson R. CO₂ installations with a multi ejector for supermarkets, case studies from various locations. *Proc. 12th IIR Gustav Lorentzen Nat. Work. Fluids Conf. Edinburgh, UK, 2016, p. 21–4*.
- [119] Bilir Sag N, Ersoy HK, Hepbasli A, Halkaci HS. Energetic and exergetic comparison of basic and ejector expander refrigeration systems operating under the same external conditions and cooling capacities. *Energy Convers Manag* 2015;90:184–94. <https://doi.org/10.1016/j.enconman.2014.11.023>.
- [120] Ruangtrakoon N, Thongtip T, Aphornratana S, Sriveerakul T. CFD simulation on the effect of primary nozzle geometries for a steam ejector in refrigeration cycle. *Int J Therm Sci* 2013;63:133–45. <https://doi.org/10.1016/j.ijthermalsci.2012.07.009>.
- [121] Lawrence N, Elbel S. Experimental investigation of a two-phase ejector cycle suitable for use with low-pressure refrigerants R134a and R1234yf. *Int J Refrig* 2014;38:310–22. <https://doi.org/10.1016/j.ijrefrig.2013.08.009>.

- [122] Giacomelli F, Mazzelli F, Banasiak K, Hafner A, Milazzo A. *Experimental and computational analysis of a R744 flashing ejector*. *Int J Refrig* 2019;107:326–43. <https://doi.org/10.1016/j.ijrefrig.2019.08.007>.
- [123] Knut RINGSTAD, Yosr ALLOUCHE, Paride GULLO, Krzysztof BANASIAK, Armin HAFNER. *CO₂ ejector modelling using CFD: current status*. *ICR2019 – 25th IIR Int Congr Refrig* 2019. <https://doi.org/10.18462/iir.icr.2019.1870>.
- [124] Henry RE, Fauske HK. *The two-phase critical flow of one-component mixtures in nozzles, orifices, and short tubes*. *J Heat Transfer* 1971;93:179–87. <https://doi.org/10.1115/1.3449782>.
- [125] NAKAGAWA M, MARASIGAN AR, MATSUKAWA T. *Experimental Analysis of Two-Phase Ejector System With Varying Mixing Cross-Sectional Area Using Natural Refrigerant Co 2*. *Int J Air-Conditioning Refrig* 2010;18:297–307. <https://doi.org/10.1142/s2010132510000320>.
- [126] Chen Y, Gu J. *The optimum high pressure for CO₂ transcritical refrigeration systems with internal heat exchangers*. *Int J Refrig* 2005;28:1238–49. <https://doi.org/10.1016/j.ijrefrig.2005.08.009>.
- [127] Sawalha S. *Theoretical evaluation of trans-critical CO₂ systems in supermarket refrigeration. Part I: Modeling, simulation and optimization of two system solutions*. *Int J Refrig* 2008;31:516–24. <https://doi.org/10.1016/j.ijrefrig.2007.05.017>.
- [128] Gullo P, Elmegaard B, Cortella G. *Advanced exergy analysis of a R744 booster refrigeration system with parallel compression*. *Energy* 2016;107:562–71. <https://doi.org/10.1016/j.energy.2016.04.043>.

COURSEWORK AND EXAMINATIONS

Subjects name	Guarantor / Teacher	Exam Date	Result
1.Heat and Mass Transfer	Prof. Ing. Tomáš Vít, Ph.D.	27/03/2018	Excellent
2.Thermodynamics	Prof. Ing. Pavel Šafařík, CSc.	15/05/2018	Excellent
3.Experimental Fluid Mechanics	Doc. Ing. Zdeněk Trávníček, CSc	02/07/2018	Excellent
4.Applied Fluid Mechanics	Prof. Ing. Václav Dvořák, Ph.D.	31/08/2018	Excellent
5.Applied mathematics	Doc. RNDr. Miroslav Brzezina, CSc	08/03/2019	Excellent

LIST OF PUBLICATIONS

Research papers

- ✓ **Anas F. A. Elbarghthi**, A. Hafner, K. Banasiak, V. Dvorak, An experimental study of an ejector-boosted transcritical R744 refrigeration system including an exergy analysis, Energy Conversion and Management 238 (2021) 114102. <https://doi.org/10.1016/j.enconman.2021.114102>. I.F.(9.709).
- ✓ **Anas F. A. Elbarghthi**, V. Dvorak, A. Hafner, K. Banasiak, The Potential Impact of the Small-scale Ejector on the R744 Transcritical Refrigeration, Energy Conversion and Management 249 (2021) 114860. <https://doi.org/10.1016/j.enconman.2021.114860>. I.F.(9.709).
- ✓ **Anas F.A. Elbarghthi**, S. Mohamed, V.V. Nguyen, V. Dvorak, CFD based design for ejector cooling system using HFOS (1234ze(E) and 1234yf), Energies. 13 (2020). <https://doi.org/10.3390/en13061408>. I.F.(3.004).
- ✓ **Anas F. A. Elbarghthi**, Mohammed Hdaib, Vaclav Dvorak, Novel generator design proposed for compression ejector refrigeration system, Energies (Manuscript number: 1420991, Submitted 29th September 2021, Status: under review). I.F.(3.004).
- ✓ Mohammed Hdaib, **Anas F A Elbarghthi**, Vaclav Dvorak, Johnson Ezenwankwo, Abdelmadjid Boualleg, Introducing Supercritical R744 for Evaporation Process of HFOs in Plate Heat Exchanger, International Journal of thermal science (Submitted 20th October 2021). I.F.(3.744).

Conferences and workshops

- ✓ V. Dvorak, **A. F. A. Elbarghthi**, Influence of number and thickness of blades on the performance of centrifugal fans. Proceedings of the 31st DAAAM International Symposium, 2020;31:724–7. <https://doi.org/10.2507/31st.daaam.proceedings.100>.
- ✓ **A. F. A. Elbarghthi**, Vaclav Dvorak, Ejector-boosted Transcritical CO₂ Refrigeration System, Computational Mechanics, Plzni, 2021. 8-10Nov 2021.

AUTHOR CURRICULUM VITAE

Anas F A Elbarghthi

Address Jestedska 341/103, Liberec 46008 – Czech Republic
Birthday 2nd December 1984 Libya
Email anas.elbarghthi@tul.cz
Phone +420778092554

Education and training

24th Jan 2018 – Present Self-fund Ph.D. student at Technical University of Liberec, Czech Republic.
1st Sep 2015 – 17th Jun 2017 Master degree in Mechanical Engineering (MSc) Szent István University –Hungary, Godollo.
1st Feb 2012 – 4th Apr 2014 Bachelor Degree Faculty of Mechanical Engineering Technology/Benghazi, Libya.
2nd Sep 2004 – 7th Jul 2007 Higher diploma in Mechanical Engineering. Higher Centre of Mechanical Vocation Benghazi, Libya.
14th Oct 1999 – 23th Jun 2002 Diploma in Refrigeration & Air-Conditioning Division. Petroleum Training & Qualifying Institute, Tripoli, Libya.

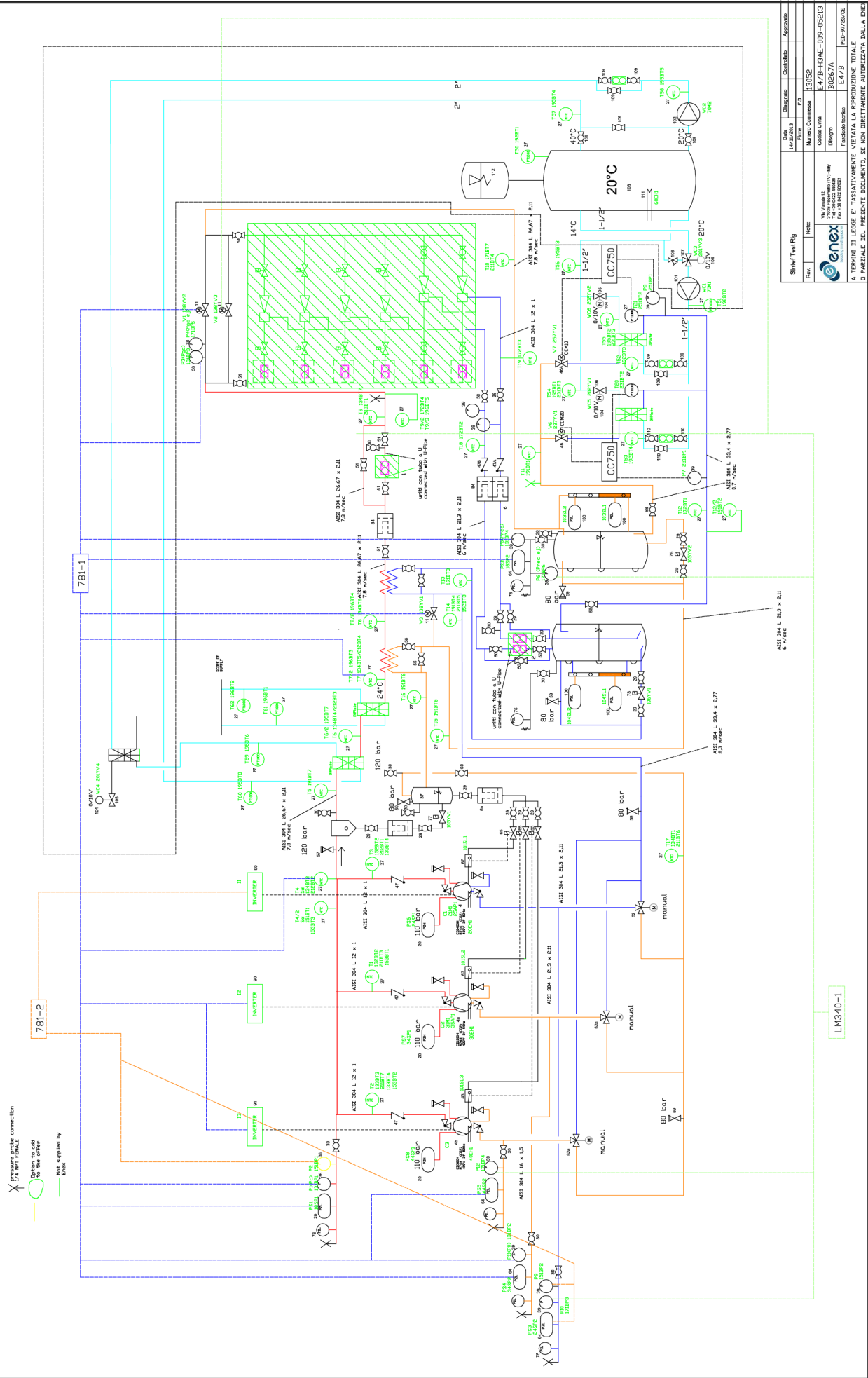
Work experience

1st Jan 2010 – Present Material senior purchaser at Supply Department, Arabian Gulf Oil Company, Benghazi, Libya.
1st Jan 2003 – 31st Dec 2009 Refrigeration and Air Condition technician at Maintenance Department, Arabian Gulf Oil Company, Benghazi, Libya.

Internship and pedagogical activities

6th Jan 2020 – 31st Jul 2020 Internship at the Energy and Process Engineering Department, Norwegian University of Science and Technology (NTNU), Trondheim, Norway.
2018 – 2021 Participating in project number 21226/2220-2019 and leading project No. SGS-2021-5063 at TUL, Liberec, Czech Republic.
2018 – 2019 Participating in teaching in the extent of two lessons per week by leading the exercises of the subject of fluid mechanics at TUL, Liberec, Czech Republic.

Appendix 1. Process and instrumentation diagram for R744 test rig



Shihai Test Rig		Data	Disegnato	Coordinato	Approvato
Rev.	1	14/07/2013	F.P.		
Numero Commessa	E478-HGAE-009-05213				
Codice UTM	B2657A				
Disegno	E478				
Intenditore	E478				
Intenditore	E478				
A TERMINI DI LEGGE È TASSATIVAMENTE VIETATA LA RIPRODUZIONE TOTALE O PARZIALE DEL PRESENTE DOCUMENTO, SE NON DIRETTAMENTE AUTORIZZATA DALLA ENX					